
A SURVEY OF DEEP LEARNING-BASED RADIOLOGY REPORT GENERATION USING MULTIMODAL DATA

Xinyi Wang

The University of Nottingham
United Kingdom

Graziela Figueredo

The University of Nottingham
United Kingdom

Ruizhe Li

The University of Nottingham
United Kingdom

Wei Emma Zhang

The University of Adelaide
Australia

Weitong Chen

The University of Adelaide
Australia

Xin Chen *

The University of Nottingham
United Kingdom

ABSTRACT

Automatic radiology report generation can alleviate the workload for physicians and minimize regional disparities in medical resources, therefore becoming an important topic in the medical image analysis field. It is a challenging task, as the computational model needs to mimic physicians to obtain information from multi-modal input data (i.e., medical images, clinical information, medical knowledge, etc.), and produce comprehensive and accurate reports. Recently, numerous works have emerged to address this issue using deep-learning-based methods, such as transformers, contrastive learning, and knowledge-base construction. This survey summarizes the key techniques developed in the most recent works and proposes a general workflow for deep-learning-based report generation with five main components, including multi-modality data acquisition, data preparation, feature learning, feature fusion and interaction, and report generation. The state-of-the-art methods for each of these components are highlighted. Additionally, we summarize the latest developments in large model-based methods and model explainability, along with public datasets, evaluation methods, current challenges, and future directions in this field. We have also conducted a quantitative comparison between different methods in the same experimental setting. This is the most up-to-date survey that focuses on multi-modality inputs and data fusion for radiology report generation. The aim is to provide comprehensive and rich information for researchers interested in automatic clinical report generation and medical image analysis, especially when using multimodal inputs, and to assist them in developing new algorithms to advance the field.

Keywords Report generation · Deep learning · Multimodal · Medical image analysis

1 Introduction

Medical images can offer detailed information about the bodies and help physicians screen, diagnose, and monitor medical conditions without requiring invasive techniques [Beddiar et al., 2023, Liao et al., 2023]. Radiologists summarize the information extracted from medical imaging to radiological reports for clinical decision-making. The manual generation of reports is however labour-intensive, time-consuming, and requires extensive expertise [Beddiar et al., 2023]. The volume of radiological imaging data is growing significantly faster than the number of trained radiologists. In some cases, each radiologist needs to analyze an image every 3 to 4 seconds during an 8-hour workday [Hosny et al., 2018, McDonald et al., 2015]. Rimmer [2017] revealed that 97% of the United Kingdom radiology departments faced challenges in meeting diagnostic reporting requirements. Topol [2019] pointed out that the demand for medical image interpretation greatly surpasses the current capacity of physicians in the United States. This makes it challenging for radiologists to provide high-quality reports within the scheduled time. The current demand extends patient waiting time increases the risk of disease transmission [Beddiar et al., 2023] and compromises patient care. The development of automatic report-generation techniques can help alleviate this problem.

Automatic high-quality report generation is challenging. It is intrinsically a multi-modality problem. [Tu et al., 2024, Yan et al., 2023]. A high-standard report demands clarity, correctness, conciseness, completeness, consistency, and coherence [Kaur et al., 2022, Liao et al.,

*Corresponding author: Xin Chen, xin.chen@nottingham.ac.uk

2023]. To meet these requirements, radiologists need to combine image data with information from other modalities, such as medical knowledge and clinical history, since a single image lacks sufficient diagnostic details. For example, the same image may yield different diagnoses depending on the associated clinical context. Ideally, automated systems should mimic this process, and experiments also show that diverse modalities can enhance report generation performance [Yang et al., 2022, Li et al., 2023b, Zhang et al., 2024a].

Mimicking this process is difficult for automated systems. First, multi-modal data are represented in distinct feature spaces with different sizes, data formats (e.g. discrete vs. continuous), and data structures (e.g. graphs, vectors, etc.) [Li et al., 2023e]. This disparity complicates the alignment and integration of multi-modal data. Second, models need to remove redundant information while identifying and leveraging complementary information from multi-modal inputs. Third, different modalities exhibit various types of noise. Fourth, data from disparate sources contribute unevenly to report generation, necessitating that models assess and appropriately weigh these contributions. Due to these challenges, previously developed techniques mostly considered images as input, while for the past three years, multi-modality deep learning developed very rapidly. An increasing number of research papers endeavoured to emulate physicians by leveraging multi-modal data for the generation of diagnostic reports. Additionally, the recent rise of large models that utilize prompts has made the use of multi-modal inputs a mainstream trend, as shown in Figure 1.

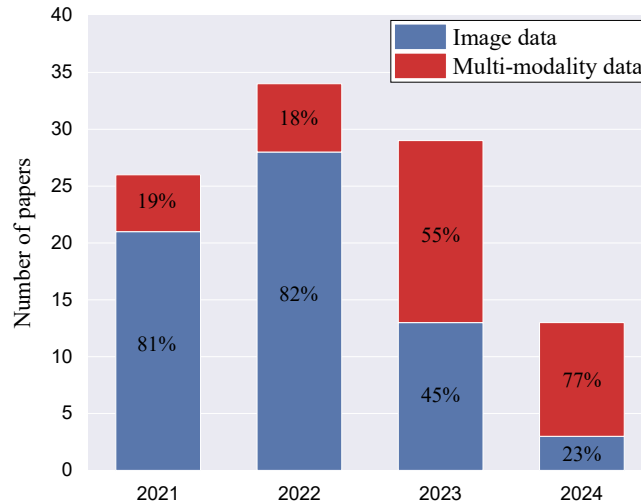


Figure 1: The distributions of reviewed papers using image data and multi-modality data as inputs per year from 2021 to 2024. The percentage denotes the input’s prevalence among articles published within the year.

Most of the previous surveys on this topic [Kaur et al., 2022, Beddiar et al., 2023, Liao et al., 2023, Shamshad et al., 2023, Liu et al., 2023a, Pang et al., 2023] did not include non-imaging inputs. Messina et al. [2022] considered non-imaging inputs but only included 6 papers. In total, the previous surveys included 40 to 66 papers for report generation, primarily focusing on articles published before 2022. In these studies, automated systems typically follow five key steps: multi-modality input acquisition, data preparation, feature learning, feature fusion and interaction, and report generation. Performance-improving techniques are applied at specific stages, making step-wise categorization useful for clarifying their functions. Although earlier surveys have addressed this point, they have not provided sufficient clarity. Additionally, we found that previous surveys have given limited attention to two important issues. While the application of large medical models in report generation has gained increasing recognition, current surveys lack analysis of their usage and fine-tuning. Further, interpretability and uncertainty quantification in clinical decision making remains a concern. While Messina et al. [2022] study on explainable AI is comprehensive, there is limited survey analysis of papers published after 2022.

This survey differs from previous ones in five main contributions:

- We analyse an additional 22 papers that utilize non-image inputs and focus on the acquisition, analysis, and integration of multi-modal inputs. To the best of our knowledge, it is the first review to investigate state-of-the-art multi-modal data processing techniques for report generation.
- Totally, we examine 100 papers published from 2021 to 2024 to provide a comprehensive study on novel techniques in automatic report generation, of which 90 focus on traditional deep learning methods, and 10 are based on large model approaches.
- We propose a general workflow for deep-learning-based report generation with a taxonomy of approaches employed, as shown in Figure 2. Table A1 in Appendix A summarizes all reviewed papers.
- For large model-based approaches, including language models, vision models, and multimodal models, we summarize the acquisition of image-text datasets with prompts, the evolution from large language model to large multimodal model, and how to train large medical models with limited resources.

report generation". Following the searches, the titles and abstracts of each article were read briefly to identify those that met the selection criteria. If there was uncertainty, the article was included to ensure relevant studies were not omitted. The selection criteria were framed around three aspects. First, we included articles published in the years 2021, 2022, 2023, and 2024 due to the significant number of developments using multi-modal technology in recent years. We aim to focus on the latest algorithms not covered in previous surveys. Second, the studies should be original research on the automatic generation of full-text natural language radiology reports. While large model-based methods may generate only parts of reports for specific prompts, they are included in this survey because they have the potential to produce complete reports with different prompts. In contrast, methods that generate short captions of one or two sentences are excluded due to the differing nature of long reports and sentence generation. Third, papers published in journals, conferences, and conference workshop proceedings were included. Additionally, papers from arXiv in 2023 and 2024 with more than 15 citations were selected. Due to the potential impact of emerging medical large models on report generation, relevant articles from arXiv are included regardless of their citation count.

A total of 151 papers were identified using three search engines. In addition, by tracing the ancestry and descendants of papers, we identified another 30 papers. After removing duplicates, 110 publications were retained. We thoroughly read these works and applied exclusion criteria. First, at least one of the generated languages should be English because it is the common language of academia, which ensures broader accessibility, easier evaluation, and more accurate comparisons of algorithm performance. Second, at least one of the input data should be images. Finally, 102 works were included in the following analysis.

3 Methods

Deep-learning-based radiology report generation typically follows a standard workflow summarized in Figure 2 a. Overall, a basic radiology report generation framework consists of 5 steps: (1) multi-modality data acquisition (Section 3.1); (2) data preparation (Section 3.2); (3) feature learning (Section 3.3); (4) feature fusion and interaction (Section 3.4); and (5) report generation (Section 3.5). Although traditional deep learning methods and large model-based approaches prioritize different aspects of research for automatic report generation, both adhere to the workflow shown in Figure 2 a. Traditional deep learning methods focus on enhancing the effectiveness of each step, while the exploration of large models is in its early stages. Large models focus on large-scale data acquisition, the transition from large language models to large multimodal models, and effective training. This section analyzes the techniques in the 100 works based on the workflow, and the next section discusses the details of large models. We believe that effective techniques from traditional methods can inspire the future development of large models due to their similar workflows.

Typically, medical images, when analyzed with or without other types of data, are first prepared, including image normalization, resizing, etc. (step 2). Subsequently, they are inputted into feature extractors to perform feature learning (step 3), predominantly implemented using a Convolutional Neural Network (CNN) or Transformer architectures, along with auxiliary loss functions or enhancement modules. The feature extractors aim at extracting features relevant to report generation, and additional techniques are utilized to improve the expressiveness of the features. For certain approaches, a feature fusion and interaction module (step 4) is subsequently applied to align cross-modal data and mitigate the negative effects caused by differences between the visual and textual domains. After fusion and interaction, the features are input into the generator to generate the report (step 5). Throughout this process, the network parameters are generally trainable. In some cases, a frozen pre-trained encoder can be used to enhance training stability. For instance, the visual encoder in large-model-based methods [Li et al., 2024, Lee et al., 2023]. Table A1 in Appendix A presents detailed information for each paper across the five steps and training strategies.

3.1 Multi-modality inputs acquisition

The input data refers to the data received by the report generation system. During model training and inference, the data can vary; for example, both images and real reports are used as inputs during training, while only images are used during inference [Shetty et al., 2023]. However, the model learns from the distribution and features of the training data. If the testing data changes the model will likely struggle to generalize, resulting in decreased performance. Therefore, in this section, we define and explain the acquisition of input data used consistently in both the training and testing phases of the reviewed papers.

Input data includes images, medical terminology, medical knowledge base, real text reports, clinical information, questionnaires, and medical descriptions. Figure 3 illustrates the types, examples and sources of these data. The following provides a detailed description:

- *Image data* includes X-ray, magnetic resonance imaging (MRI), computed tomography (CT), ultrasound, gastrointestinal endoscope image, retinal image, and dermoscopy image. Most papers we reviewed focus on generating medical reports for chest X-ray images (82 works). Other than chest diagnosis, retinal image is the second most prevalent image modality (6 works). The retinal image includes lots of categories, e.g., fundus fluorescein angiography and color fundus photography. Other works focus on chest CT (5 works), gastrointestinal endoscope image (2 works), spine MRI (1 work), dermoscopy image (1 work), and breast ultrasound images (1 work). Although some images are non-radiological, such as ophthalmic images, we still include their report-generation techniques in this survey.

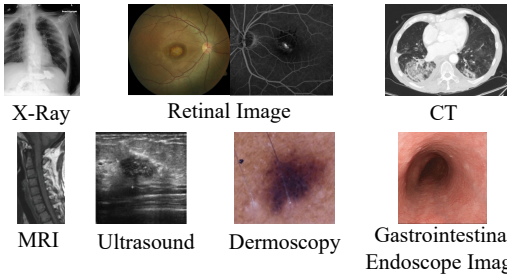
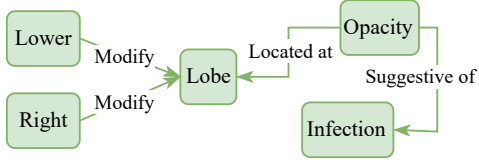
Inputs	Type	Example	Data Acquisition
Image	Image	 <p>X-Ray Retinal Image CT MRI Ultrasound Dermoscopy Gastrointestinal Endoscope Image</p>	<ul style="list-style-type: none"> Public/private datasets:  Collected from hospital
Instructions	Text	<p>“Generate a comprehensive and detailed diagnosis report for this chest x-ray image” or “Are there any disease in the lung?”</p>	<ul style="list-style-type: none"> Prompts. Public structural report template - Defined based on keywords labels
Medical terminology	Text	<p>"cardiomegaly", "scoliosis", "fractures", "effusion", "thickening", "pneumothorax", "hernia", "calcinosis", etc.</p>	<ul style="list-style-type: none"> Keyword labels of image:  Annotated by physicians Common abnormality findings:  Authoritative medical standards
Real texts report	Text	<p>"Findings: Frontal and lateral radiographs of the chest demonstrate normal heart size. The mediastinal and hilar contours are normal. No pleural effusion or pneumothorax. Clear lungs. Impression: Normal chest radiograph."</p>	<ul style="list-style-type: none"> Reports in training dataset:  Annotated by physicians
Medical knowledge base	Graph		<ul style="list-style-type: none"> Public datasets:  Derived from real reports Self-designed knowledge base:  Authoritative medical standards Or  Derived from real reports
Clinical information	Text/ Number	<p>Age:32, Gender: "Female", Medical history: "Acute liver injury and abdominal pain..." Technique: "Chest PA and lateral" Comparison: "No prior radiographs..."</p>	<ul style="list-style-type: none"> Indication, technique, and comparison sections in radiology reports.

Figure 3: A summary of the types, examples, and sources of multi-modal input data.

- *Instructions* refer to the explanations provided for completing a task or carrying out an operation. It comprises prompts and questionnaires. Prompts like “Generate a comprehensive and detailed diagnosis report for this chest x-ray image” are commonly used with large models for report generation [Tanwani et al., 2022, Pellegrini et al., 2023b, Lee et al., 2023, Wang et al., 2023e, Hyland et al., 2023, Bannur et al., 2024, Chen et al., 2024, Guo et al., 2024, Zhang et al., 2024a, Li et al., 2024, Alkhaldi et al., 2024]. Questionnaires are sets of questions designed for report generation [Tanwani et al., 2022, Pellegrini et al., 2023a]. Pellegrini et al. [2023a] developed a structured report dataset for Chest X-rays, containing hundreds of questions, in which reports are generated by answering a series of questions, similar to the process of hierarchical visual question answering.
- *Medical terminology* refers to medical terms and expressions, which are from keyword labels of images [Huang et al., 2021a,b, 2022, Liu et al., 2023c], or self-built corpora [Liu et al., 2021b, Cao et al., 2022, 2023, Xue et al., 2024, Gu et al., 2024, Li et al., 2023d], storing common descriptions found in medical reports. Incorporating medical terminologies can assist the model in generating descriptions that are relevant to medical terminology. Liu et al. [2023c] further developed a concepts library for medical descriptions based on various terminologies, providing detailed information on symptoms and health status. For example, the term “Cardiomegaly” corresponds to “The heart size is enlarged”.
- *Real texts report* refers to radiology reports written by physicians. In the reviewed papers, two methods are used to obtain these reports. The first retrieves them from the training dataset to avoid overlap with the test set, as detailed in Section 3.2. It mimics the behaviour of radiologists referencing similar prior cases when writing reports. The second uses prior reports, referring to the

patient’s historical data [Bannur et al., 2024]. As described in Section 3.2, utilizing this data enables monitoring of temporal changes, which is essential for clinical applications.

- *Medical knowledge base* mostly records the connections between different organs and diseases, and is presented in a graph format. A graph is a fundamental data structure consisting of a set of nodes and edges, which can easily represent a set of subjects and their connections. A knowledge graph can primarily be obtained in two ways: (1) public datasets such as the RadGraph [Jain et al., 2021] used by two works [Yang et al., 2022, Li et al., 2023b]. Recently, an enhanced version of RadGraph, termed RadGraph-XL [Delbrouck et al., 2024], was introduced, offering improved performance. This update extends its applicability to a broader range of medical imaging modalities (i.e., chest CT, abdomen/pelvis CT, brain MRI, and chest X-ray), anatomical regions, and data sources; (2) self-designed knowledge bases according to authoritative medical standards [Huang et al., 2023, Xu et al., 2023] or real reports in training dataset [Jia et al., 2022]. Utilizing a knowledge base allows the model to learn medical knowledge akin to a physician.
- *Clinical information* encompasses patient demographics (e.g., age and gender), clinical observations, and medical histories. By incorporating clinical information, the model can obtain rich clinical context, which helps it better understand the specific situation and background of the patient. Clinical information is embedded in the indication, technique, and comparison sections of radiology reports (see Figure 7). While most studies utilize only the indication section [Zhou et al., 2021, Dalla Serra et al., 2022, 2023a,b, Hyland et al., 2023], MAIRA-2 [Bannur et al., 2024] leverages all three sections, stating that the technique and comparison sections provide additional information, and demonstrates their positive impact through experiments.

3.2 Data preparation

Data preparation endeavours to enhance data quality and prepare it for model deployment, typically encompassing data cleansing, transformation, and organization. Conventional data preparation techniques primarily target images and text. Image processing typically involves resizing and cropping, while text processing includes case normalization, removal of non-alphabetic tokens, and tokenization. The methods utilized in each paper are outlined in Table A1 in Appendix A, but it is worth noting that conventional preparation methods are so ubiquitous that some papers do not mention them. While the information is not recorded in the table, it does not mean the absence of a data preparation process.

Novel data preparation methods in the reviewed papers can be categorized into filtering [Ramesh et al., 2022], grouping [Wang et al., 2022b], and case-specific information extraction. Ramesh et al. [2022] argued that writing a radiology report necessitates referencing historical information, which inevitably included descriptors such as ‘again’ and ‘decrease’. However, these terms cannot be inferred from a single image, therefore Ramesh et al. [2022] filtered such descriptions in the reports. This exclusion was found to facilitate the model’s learning process; however, simply modifying ground truth reports does not accurately reflect clinical practice. In some clinical settings, monitoring temporal changes is essential for the effective diagnosis and management of various diseases, such as pneumonia [Kalil et al., 2016, Wu et al., 2021a]. At the same time, follow-up reports are often shorter than those for the initial image, focusing only on changes or new findings (e.g., “Otherwise, little change.”). Without historical context can result in incomplete image descriptions. Current publicly available datasets are typically organized by subject identifiers and study identifiers, representing different examinations for the same patient and arranging them chronologically [Johnson et al., 2019a, Wu et al., 2021a, Chambon et al., 2024]. Analyzing a sequence of images or inputting prior reports into the model might be more appropriate [Bannur et al., 2024, Dalla Serra et al., 2023a]. Another approach is to train using only the initial image-report pairs to maintain data validity, though this would limit the model’s applicability and significantly reduce the amount of available training data.

Grouping refers to organizing sentences from ground truth reports into distinct sections, typically relying on keywords from pre-defined knowledge graphs and filtering rules. Each section describes a specific anatomical structure. Grouping aims to enable the generation system to process various types of sentences differently. For instance, Wang et al. [2022b] employed different decoders to generate descriptions for different anatomical structures. Alongside the reviewed papers, a recently released public dataset named ImaGenome [Wu et al., 2021a] also includes grouping results in their annotation files (see Section 6). The grouping result becomes more easily accessible.

When using medical knowledge bases and real text reports, inputting the entire knowledge base or all reports from the training dataset often leads to information redundancy, making it difficult for the network to extract relevant information. Extracting case-specific information can alleviate this problem. Figure 4 illustrates three highly effective methods in reviewed papers.

The first method is the retrieval of related real text reports [Liu et al., 2021b, Song et al., 2022, Yang et al., 2022, Li et al., 2023b, Liu et al., 2023c, Li et al., 2023d, Jin et al., 2024]. This process mimics radiologists consulting previous medical case reports when drafting their own. By calculating the similarity between the input image and the images in the training set, we select the reports corresponding to the top N most similar images and use these reports as inputs. The second method is the retrieval of related medical descriptions. Liu et al. [2023c] obtained medical description from a pre-defined concepts library based on input terminologies. However, this method still depends on disease tags from radiologists for high performance, increasing their workload.

The third method combines retrieved reports in the first method with a medical knowledge base (e.g., RadGraph) to extract case-related medical knowledge [Yang et al., 2022, Li et al., 2023b]. An automated tool first extracts entities from the reports, and then all related

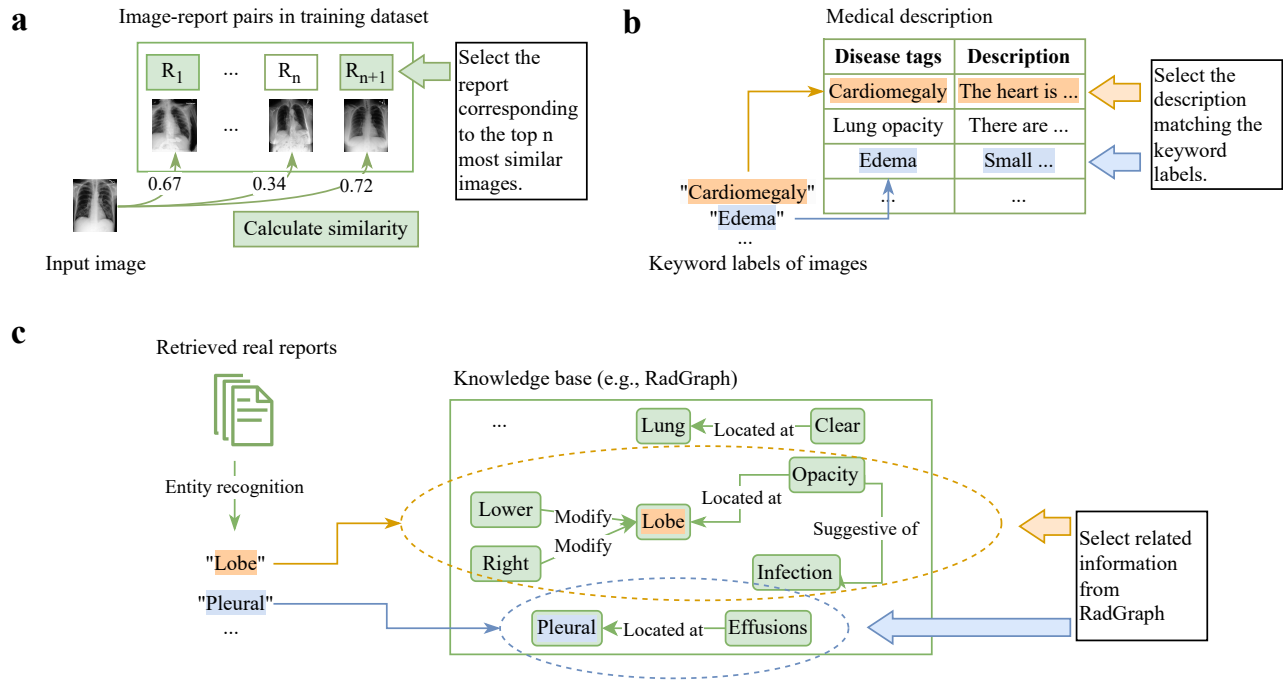


Figure 4: Three typical methods for extracting case-related information. (a) Extracting relevant textual reports from the training set by comparing the similarity between the input image and images in the training set. (b) Extracting relevant medical descriptions from a concepts library based on the image’s annotated keywords. (c) Automatically extracting entities (e.g., anatomy) from the reports retrieved in (a) and using these entities to search the knowledge base for related knowledge graphs. “...” refers to concepts such as these. The figure only lists a few examples from the training dataset, keyword labels of images, medical descriptions, recognized entities in the report, and knowledge base.

information from the knowledge base is retrieved as input. Alternatively, Li et al. [2023d] use the annotation tool in RadGraph to extract entities and positional information from retrieved reports.

Additionally, two studies [Xu et al., 2023, Huang et al., 2023] used image classification results to process self-built graphs and extract case-related information. This method is less effective than the three mentioned above, partly due to inherent classification errors. Improving classifier performance could enhance the quality of report generation.

3.3 Feature learning

3.3.1 Image-based feature learning

Previous research primarily utilized CNNs as architectures for extracting image features, however, recently, an increasing number of researchers have opted for the use of Transformers due to their improved performance. Simultaneously, numerous studies proposed novel modules to enhance the model capability. In this section, the model architectures are first introduced and subsequently enhancement modules are described. These modules include auxiliary tasks, contrastive learning, and memory metrics. The architecture and modules utilized in each paper are outlined in Table A1 in Appendix A.

Architectures for image feature extraction The statistics of the architectures used as image feature extractors are shown in Figure 5. It shows a clear trend of more studies adopting Transformer-based architectures for image feature extraction. However, unlike the decoder architecture in Section 3.5.1, where the Transformer has entirely replaced the Long Short-Term Memory (LSTM), many studies combine CNNs with Transformers, using CNNs for image processing and feeding the extracted features into the Transformer encoder. However, there is a lack of research comparing this approach with using only CNNs or only Transformers for report generation.

Most studies developed CNN architectures based on classical models, such as the Residual Nets (ResNet) [He et al., 2016] (42 papers) and the Dense Convolutional Network (DenseNet) [Huang et al., 2017] (22 papers). To improve model performance, ten works modified the CNN structure by attention modules, which assigned varying degrees of importance (weights) to different parts of the input by learnable parameters, allowing the model to selectively focus on specific regions of an image, such as small localized lesions. Specifically, the core

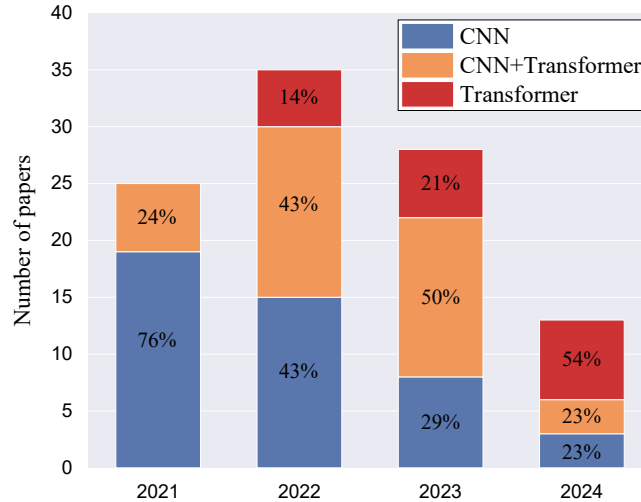


Figure 5: The statistics of the reviewed papers using different architectures to extract image features per year from 2021 to 2024. The percentage denotes the method’s prevalence among articles published within the year.

of CNNs lies in the convolutional kernels, which extracts informative features by processing spatial and channel information within local receptive fields. The introduction of attention mechanisms is based on the assumption that the model requires a mechanism (i.e., attention) to adaptively recalibrate channel or spatial features by explicitly modeling their interdependencies. This enables the model to focus more effectively on the most relevant features. Traditional attention mechanisms can be classified into channel-wise [Du et al., 2022, Wang et al., 2022e, Gajbhiye et al., 2022, Pahwa et al., 2021] and spatial-wise [Pahwa et al., 2021, Jia et al., 2021], which allocate different weights to the various channels and spatial positions of the inputs respectively. In addition, Li et al. [2023c] and Wang et al. [2024a] utilized the idea of the class activation map [Zhou et al., 2016] to obtain weights. Yan et al. [2022] initially extracted image patch features, clustered them using an unsupervised method, and then weighted the cluster results. Experimental results show that the attention mechanism allows models to pay more attention to the lesions than to irrelevant backgrounds. With the rise of the Transformers [Vaswani et al., 2017], multi-head attention has become a potent method for information interaction. In clinical practice, it is widely acknowledged that radiologists report with varying granularity in radiology reports to reflect different degrees of pathological changes [Wang et al., 2023c]. Therefore, both global and local information are essential for report generation, with varying importance when generating different content. Dynamic interactions between these elements can facilitate adjustments in their significance, thereby enhancing outcomes. Wang et al. [2023c] extracted regions of interest from the frontal view and then employed multi-head attention to fuse information between the frontal and lateral views with the regions.

For Transformer architectures, most of them leverage a standard Transformer encoder, while two studies [Li et al., 2023e, Lee et al., 2023] noted that aligning images with text is challenging due to the continuous nature of images and the discrete nature of text. To address this, they used pre-trained models [Ramesh et al., 2021, Esser et al., 2021] to generate discrete visual tokens. However, despite the ablation study validation [Li et al., 2023e], the results were still inferior to other report generation methods, likely due to information loss during discretization. Additionally, the pre-trained models were trained on non-medical images, and this domain gap can also impact performance. Other works improved the model performance by modifying the self-attention module. Three works [Wang et al., 2022e, Lin et al., 2023, Wang et al., 2023d] added high-order interactions among the query, key, and value of the Transformer attention module to enhance their interactions for extracting more complex information. Two works [Miura et al., 2021, Wang et al., 2022e] were inspired by the memory-augmented attention [Cornia et al., 2020] and extended the keys and values with additional plain learnable vectors to record more information. Wang et al. [2023d] modified the encoder by including additional input tokens. These tokens were named ‘expert tokens’ to emulate the “multi-expert joint diagnosis” methodology. Ablation studies indicate that these designs enhance the results significantly.

In conclusion, while an increasing number of studies employ Transformer-based architectures for feature extraction, direct comparisons with CNNs remain absent. Most architectural enhancements focus on modifications to attention mechanisms, which have demonstrated effective improvements. Some research explored the discretization of visual features to align with text features; however, it yielded limited success.

Auxiliary loss functions for image feature extraction Auxiliary loss functions aim to provide additional supervision signals to the feature extractor, enabling it to extract information relevant to report generation from images. Generally, the model optimizes the main and auxiliary loss functions simultaneously through a weighted sum, with the weights reflecting the relative importance of each task. The auxiliary loss functions described in this section are used to constrain the features extracted by the visual encoder. Additionally in this

section, we include losses that are contributed to the pre-training phase, such as those from contrastive learning. Although these losses do not work directly with the main loss function, they still serve as auxiliary losses to help build a more effective visual encoder. These tasks mainly include classification (22 papers), graph construction (10 papers), embedding comparison (10 papers), contrastive learning (8 papers), and detection/segmentation (7 papers). Each of them is introduced in detail below.

Classification loss function: The most common auxiliary task used in the reviewed papers is classification referring to assigning images to predefined categories. Ensuring the generated radiology reports contain essential medical facts is crucial. Introducing an auxiliary classification loss helps the model focus on extracting features relevant to these facts during feature extraction. Predefined categories are usually disease labels [Liu et al., 2021e, Zhou et al., 2021, Wang et al., 2022d, Yang et al., 2023, Zhang et al., 2023b, Wang et al., 2024a, Jin et al., 2024, Hou et al., 2021b, 2023], which are provided by auto annotation tools (e.g., CheXpert [Irvin et al., 2019] and CheXbert [Smit et al., 2020a]), typically covering 14 categories of diseases (e.g., atelectasis). For instance, Yang et al. [2023] utilized the CheXpert labeling tool to annotate 14 common chest radiological findings and integrated a classification layer following the visual encoder to predict diseases. The model was optimized by minimizing the binary cross-entropy loss between the true labels and the predicted disease outcomes. Some researchers argue that these categories are insufficient to capture all necessary medical facts for report generation, and thus extend them to include other medical tags [Gajbhiye et al., 2022, Kaur and Mittal, 2022b, Wang et al., 2022e, Hou et al., 2021b, Du et al., 2022, You et al., 2022, Alfarghaly et al., 2021], such as anatomical structures (e.g., abdominal) and pathological signs (e.g., cicatrix). The medical tags are provided by manual annotations, e.g., the Medical Subject Headings annotation (MeSH) for IU-Xray dataset, or auto annotation tools, e.g., the Medical Text Indexer web Application Programming Interface ² and RadGraph [Jain et al., 2021]. Compared to disease labels, medical tags offer a more comprehensive range of information. However, to the best of our knowledge, no literature supports the superiority of medical tags over disease labels. Perhaps due to the extensive scope covered by medical tags, deep learning models face challenges in acquiring such rich knowledge. Zhou et al. [2021] incorporated 32 additional labels for lesion location, size, and shape (e.g., “upper/lower” and “patchy”) into the disease label set, observing a slight improvement in model performance.

Other notable categories used in the reviewed papers include matching status [Li et al., 2023b], local properties [Yang et al., 2021a], report cluster results [Li et al., 2022a], and fix answer categories [Tanwani et al., 2022]. Li et al. [2023b] proposed a binary classification task to predict the image-report matching status. The image features, extracted by the image encoder, are input into a cross-attention mechanism alongside the reports. The output then passes through a linear layer to predict the matching probability, which is supervised with a cross-entropy loss. The objective of this task is to align the visual features more closely with the text representation. Yang et al. [2021a] devised localized property labels for breast ultrasound images, such as tumor morphology, to facilitate the identification of properties that are challenging to be discerned in low-resolution images. Li et al. [2022a] first conducted unsupervised clustering on the ground truth report, subsequently utilizing the resultant clusters as labels. The study validated the independence of the clustering results to ensure the diversity of the generated themes. The ablation study confirmed the effectiveness of these methods, yet the final results were inferior to those achieved using more direct additional supervisory information, such as disease labels and image-text matching. Tanwani et al. [2022] considered the report generation as a question-answer task, and the classifier was designed for fixed answer categories.

In conclusion, the classification loss function helps the model focus on extracting medically relevant features by providing additional supervision based on medical facts. Other classification tasks include image-text matching, which aligns textual and visual features; local property classification, which aids in identifying details in low-resolution images; and question-answering tasks. Providing more direct disease-related supervision is beneficial for improving results, however, experimental results revealed that overly abundant information may complicate the network’s learning and information extraction, potentially diminishing its effectiveness. In addition, for a detection auxiliary task, classifiers need to be applied to identify attributes of detected regions (e.g., ‘right lung’). This paragraph eschews such cases to circumvent redundancy.

Graph construction loss function: Graph construction aims to integrate prior knowledge into the report generation process, encompassing key organs, diseases, and their interrelations. It enables the network to extract nodes’ features from the image and defines their relationships (i.e., edges) as parameters in graph convolutional networks. A classical method was proposed by Zhang et al. [2020] and yielded promising outcomes. A knowledge graph was constructed firstly based on insights provided by domain experts, where nodes represented major abnormalities and major organs, and bidirectional connections linked nodes that were related to each other. To initialize node features, a spatial attention module was introduced after the CNN backbone using 1×1 convolution layers and softmax layers. The number of channels matched the number of nodes. The nodes’ initial embedding was derived as attention-weighted feature maps. Then graph convolution layers were employed to disseminate information throughout the graph, followed by two branches for classification and report generation. First, the classification branch was trained, and subsequently, parameters in both the CNN backbone and the graph convolution layers were frozen, only the report generation decoder was trained. Six works [Liu et al., 2021b,d, Cao et al., 2022, Wang et al., 2022c, Yan, 2022, Zhang et al., 2023b] utilized this method [Zhang et al., 2020]. Wang et al. [2022c] expanded the graph [Zhang et al., 2020] by incorporating information from a radiology terms corpus named Radiology Lexicon (RadLex)³ [Langlotz, 2006]. As the number of graph nodes increased, the model performance initially improved, peaked at 40 nodes, and then declined, with a noticeable decrease at 60 nodes. Liu et al. [2021d] constructed a large graph based on the Medical Information Mart for Intensive Care Chest X-ray (MIMIC-CXR) dataset. The nodes represented frequent clinical abnormalities and the edges represented the co-occurrence situation

²<https://ii.nlm.nih.gov/MTI/index.shtml>

³<http://www.radlex.org/>

of different abnormalities. In addition, Li et al. [2023c] used the disease prediction results to obtain the node features. The nodes were classification probabilities, with learnable edge weights.

Another graph reconstruction method aims at reconstructing triplets that are in the form of (entity1, relationship, entity2), such as (opacity, suggestive of, infection). Dalla Serra et al. [2022] proposed a triplet extraction method for chest X-rays, where entities were first extracted using RadGraph [Jain et al., 2021] and then merged via ScispaCy [Neumann et al., 2019] for simplified annotation. Li et al. [2022b] used an AI-accelerated human-in-the-loop method for entity recognition and relation linking in ophthalmic images [Wu et al., 2021b]. Three works [Dalla Serra et al., 2022, 2023b, Li et al., 2022b] firstly predicted the triplets and then generated reports based on them. Triplet prediction is supervised by cross-entropy loss in token prediction. The experimental results indicate that integrating the extracted triplet with image features in the subsequent network significantly enhances performance [Li et al., 2022b, Dalla Serra et al., 2023b]. The manually constructed graphs mentioned above are highly accurate and pre-defined, allowing the model to mimic human learning from textbooks. However, these graphs are specific to particular diseases; for instance, a graph constructed for chest X-rays cannot be directly applied to retinal diagnostics. Furthermore, the need for manual annotations increases physicians' workload. To address these limitations, Yang et al. [2023] propose replacing pre-defined graphs with a learnable memory metric (see Section 3.4).

In conclusion, utilizing graph convolutional networks is a mainstream approach for knowledge integration during training, whereas triplet generation is infrequently utilized. Both methods depend on pre-defined information, leading to limited scalability.

Embedding comparison loss function: Embedding comparison refers to constraining the consistency of different features in intermediate layers, thereby guiding the learning process. The comparison in reviewed papers is mainly applied between features extracted from images and real reports [Najdenkoska et al., 2021, 2022, Zhou et al., 2021, Yang et al., 2021b, Chen et al., 2022, Wang et al., 2021, 2022d, Yang et al., 2023], aligning learned visual features with supervised textual features in the same space to facilitate subsequent report generation. Experimental results show that the supervision signals from real text enable the extracted visual features to carry richer semantic information, facilitating more effective translation into radiology reports. Four works [Wang et al., 2021, Zhou et al., 2021, Wang et al., 2022d, Yang et al., 2023] utilized a triple loss function to compel the image-text paired features to be closer to a latent space than the unpaired ones. Najdenkoska et al. [2021, 2022] inspired by the Auto-Encoding Variational Bayes [Kingma and Welling, 2013]. They used real reports to obtain a latent space during training and generated reports based on this space. The image extractors were enabled to capture features from images that closely resemble those found in real reports. Other two works [Yang et al., 2021b, Chen et al., 2022] used the Term Frequency and Inverse Document Frequency (TF-IDF) to extract important information from real reports as supervision signals. TF-IDF is a statistical measure assessing a word's importance by considering its frequency in a specific document and its rarity across the entire document set.

In addition, to produce reports for abnormalities not seen during training, Sun et al. [2022] initially linearly projected visual features to semantic features, and extracted semantic features of labels by the pre-trained Bidirectional Encoder Representations from Transformers for Biomedical Text Mining (BioBert) model [Lee et al., 2020]. Consistent constrain was applied between two similarities: 1) the similarity between pairwise elements in the semantic features from visual features; and 2) the similarity between the semantic features from visual features and the semantic features from labels. This operation ensures the similarity between visual features and label features, aligning them while preserving medical facts within the visual features. Zhang et al. [2023b] integrated semi-supervised learning into report generation using teacher-student networks. They first applied different types of noise to an input image to create two variations, which were then fed into the two networks. An auxiliary loss function was employed to ensure consistency in the extracted visual features.

In conclusion, using information from real text reports as supervision signals is highly effective for feature extraction. Visual features that are aligned with the text and rich in semantic content can enhance subsequent report generation. Additionally, embedding-based approaches can inspire future research. For example, if large models demonstrate superior performance, a teacher-student framework could enable smaller models to replicate similar learning outcomes.

Contrastive learning loss function: Contrastive learning is a self-supervised learning method, which allows models to minimize the distance among positive pairs and maximize it for negative ones. Contrastive learning mainly leverages the similarities and differences between samples other than annotations, facilitating the extraction of stronger feature representations. It can be used for image extractor pretraining [Wang et al., 2022e, Lin et al., 2023, Wu et al., 2022, Wang et al., 2023b] or to optimize the model in conjunction with the main loss (i.e., report generation) [Tanwani et al., 2022, Wang et al., 2022a, Li et al., 2023b, Liu et al., 2023c]. For pretraining, Lin et al. [2023] utilized a classical contrastive learning method named Momentum Contrast [He et al., 2020], where different views or augmented versions of the same image were considered as positive pairs. Another representative contrastive learning work is the Contrastive Language-Image Pre-training (CLIP) model [Radford et al., 2021]. It connects textual and visual information by directly training on a vast dataset consisting of image-text pairs. Wang et al. [2022e] directly employed it for image feature extraction and Wu et al. [2022] applied the idea of CLIP to train the feature extractors on the training dataset. Wang et al. [2023b] however argued that previous works treated the entire report as input, overlooking the distinct information contained within individual sentences. This oversight could result in incorrect matching of image-text pairs. Therefore, they proposed phenotype-based contrastive learning. This method involved randomly initializing a set of vectors as phenotypes, allowing sentences and visual embeddings to interact with them, and finally conducting contrastive learning between the processed embeddings. The results outperformed previous contrastive learning methods in report generation.

When contrastive learning be part of the training loss, it can be applied between visual and textual features (i.e. image-text pairs) [Tanwani et al., 2022, Li et al., 2023b, Liu et al., 2023c], or be applied based on labels, treating samples with shared labels as positives and those without any common labels as negatives [Wang et al., 2022a]. Ablation studies showed a significant improvement when using contrastive learning as an auxiliary loss function.

In conclusion, the additional supervisory signal from contrastive learning arises from variations and similarities among distinct samples. It can be employed for both pre-training and training phases. Given the rich information in medical images and reports, an image pair (or an image-text pair) can form positive pairs for one medical fact while serving as negative pairs for another. Thus, the effective design of positive and negative samples is crucial. Currently, sentence-level matching has demonstrated strong performance for image-text pairs, and utilizing image labels is an effective approach for image pairs.

Detection/segmentation loss function: Object detection locates and identifies objects or patterns within an image, focusing on determining their presence and position. Segmentation divides an image into meaningful regions by identifying and separating objects based on specific characteristics. Both processes improve the model’s comprehension of medical images through object recognition and region extraction. Abnormalities in medical images are often confined to small, localized regions. Supervision by detection or segmentation auxiliary loss enables backbones to yield dense features specific to these regions, rather than the sparse features typically extracted. The detected or segmented regions can be anatomical regions [Tanida et al., 2023, Dalla Serra et al., 2023b,a, Wang et al., 2023c, Han et al., 2021, Gu et al., 2024] and abnormal regions [Sun et al., 2022]. Detection is commonly applied to X-ray imaging using the public Chest ImaGenome dataset, while segmentation is only used for spine MRI on a private dataset. The ImaGenome provides atlas-based detection annotations, which offer bounding box labels for anatomical structures (see Section 6). This makes them easier to acquire than segmentation annotations.

Overall, auxiliary loss functions operate in three ways. The primary approach provides disease-related supervisory signals (e.g., classification, graph construction, and detection) to facilitate the model’s identification of specific lesions. The second approach aligns image data with relevant textual information (e.g., embedding comparison), enriching image features with semantic information to make decoding into a report easier. The third approach is contrastive learning, which leverages image similarities and differences to extract more robust features. The careful design of the sample pairs is crucial. In addition, the outputs of auxiliary tasks supervised by auxiliary loss function can provide valuable information such as disease labels, therefore, entering them into the following generation network is a common choice [Alfarghaly et al., 2021, Hou et al., 2021b, Singh et al., 2021, Yang et al., 2021a, You et al., 2021, Zhou et al., 2021, Du et al., 2022, Jia et al., 2022, Kaur and Mittal, 2022b, Sun et al., 2022, Wang et al., 2022a,e, Yan et al., 2022, You et al., 2022, Tanida et al., 2023, Li et al., 2022b, Jin et al., 2024]. For example, Zhou et al. [2021] sent the semantic word embeddings of the predicted findings from the classifier to the report generation decoder.

Enhancement modules for image feature extraction Designing enhancement modules involves creating components to improve the interaction of specific information, thereby enhancing feature extraction efficiency. In the reviewed papers, two main types of modules are employed. Firstly, contrastive attention guides the model’s focus on specific regions. Liu et al. [2021c] designed a contrastive attention model to extract abnormal region features by comparing input samples with normal cases. Similar features shared between the input and normal cases were subtracted from the input image feature, and the remaining feature was then concatenated with the original feature. Song et al. [2022] argued that Liu et al. [2021c] did not consider historical similar cases; therefore, they proposed a module based on similarity retrieval technique to obtain similar images from the training dataset. Unique information in the image is emphasized by enlarging different features between inputs and the retrieved images.

The second is memory metric. Using a memory metric for image feature extraction assumes the presence of similar features in various medical images. Memory metrics are employed to record and transmit the similarity information during training [Chen et al., 2022, Yan, 2022]. Typically, an $n \times n$ matrix is randomly initialized, where n represents the number of metric rows. Then, at each training step, the matrix is updated based on the visual features and the previous metrics.

3.3.2 Non-imaging-based feature learning

The types of non-image data include text, graph, and numerical data (see Figure 3). Numerical data is typically fed into the network in the next step after one-hot encoding, without a specifically designed encoder. Therefore, in this section, we focus on feature extraction for text and graph inputs.

After tokenization mentioned in Section 3.2, text data is divided into basic units (such as words, subwords, or characters). Then the general embedding technique (e.g., lookup table) is applied to convert these tokens into continuous vector representations. Next, many studies directly fuse these vectors with image features, while others incorporate a text encoder to enhance the representational capabilities of textual features. Transformer-based models and their variants are mainstream methods, widely applied to terminology [Liu et al., 2021e, Cao et al., 2022, 2023, Liu et al., 2021b, Xue et al., 2024, Liu et al., 2023c, Li et al., 2023d], real text reports [Liu et al., 2021b, 2023c, Li et al., 2023d, Jin et al., 2024], and questionnaires [Tanwani et al., 2022, Pellegrini et al., 2023a]. These models are typically trainable, and some studies also utilize frozen models that are pre-trained on medical datasets to extract clinical features more effectively. For example, Li et al. [2023d] utilized the Clinical Bidirectional Encoder Representations from Transformers (ClinicalBERT) [Alsentzer et al., 2019] to extract clinical concept features. There is no experimental evidence proving that the introduction of pre-trained models enhances

performance; however, reducing the number of trainable parameters can accelerate convergence and facilitate training. In addition, in medical reports, there is an imbalance between normal and abnormal descriptions, which may cause the model to prioritize normal descriptions. To address this issue, Li et al. [2023d] employed TF-IDF to re-weight the input terminology embeddings. During training, the weights are derived from ground truth reports, while during inference, they are obtained from the reports of similar training images.

In knowledge graph feature extraction, extracting node embeddings with pre-trained transformer models is common [Huang et al., 2023, Li et al., 2023b, Xu et al., 2023]; the critical challenge lies in effectively utilizing edge information (i.e., relationships). The pre-defined graph connecting organs and diseases indicates their association but does not specify the relationships. Traditional graph convolutional networks utilize fixed weights, such as the adjacency matrix, to represent the association and update the node features by averaging the features of neighboring nodes. However, this approach fails to capture the importance of different neighbors to the node. To address this, the graph attention mechanism is introduced and computes the attention weights between the node and its neighbors, then performs a weighted aggregation of the neighbors' features to update the node's feature [Huang et al., 2023, Xu et al., 2023, Li et al., 2023b]. In addition, Li et al. [2023b] added identifiers to indicate node levels (i.e., root, organ, and disease). Combined with the case-specific extraction method (see Section 3.2), this approach yields significant performance improvements.

Yang et al. [2022] aims to represent more complex relationships between medical entities, utilizing a general graph embedding model called RotatE [Sun et al., 2019]. Relationships are represented as rotations from entity1 to entity2 within a complex vector space. In this way, four common relationships (i.e., symmetry, antisymmetry, inversion, and composition) can be represented. However, these four relationships are not practical for medical data. Relationships can be more specified in the medical field; for instance, RadGraph defines relationships between medical entities as "suggestive of", "located at", and "modify". Yang et al. [2022] transformed it into sentences (e.g., "pneumothorax suggestive of bleeding") to extract semantic features using a pre-trained transformer model.

In conclusion, feature extraction from text data typically relies on transformer models, which lack distinctive designs. For graph data, leveraging relationships is a crucial topic. Exploring ways to incorporate more specific relationships presents a promising research direction.

3.4 Multi-modal feature fusion and interaction

Feature fusion and interaction refer to the integration of multi-modal data from inputs or auxiliary tasks. It is important for report generation using multi-modal inputs. As discussed in Section 1, aligning multimodal data involves four main challenges: distinct feature spaces, identifying complementary and redundant information, various types of noise, and uneven contributions. Fusion and interaction methods can help alleviate the above problems. Additionally, the correspondence between image regions and report sentences can be learned during this process.

The most straightforward approach is feature-level operation including the concatenation, summation, or multiplication of multimodal features (14 works). However, the feature-level operation could be too simple to enable sufficient interaction. Therefore, neural network-based methods are leveraged. Huang et al. [2021a] used an LSTM network to integrate keywords and image features, starting with image features as input and sequentially introducing keywords at each time step. This method is relatively cumbersome and less effective than attention mechanisms. The multi-head attention mechanism is a widely adopted method for feature fusion (28 works), involving three inputs: query, key, and value. Its core idea is to compute the similarity between the query and key, and use this correlation to weight the value, enabling the identification of alignable features across different modalities while filtering out irrelevant information. The attention mechanism can be applied to concatenated feature data through self-attention, allowing for an arbitrary number of input modalities. For example, Dalla Serra et al. [2022] concatenated clinical information tokens with visual features and used the combined features as the query, key, and value. Pellegrini et al. [2023a] merged question features with image features, feeding the concatenated features into the BERT model. However, it does not differentiate between specific modalities. Alternatively, another approach is that one modality (e.g., images) can act as the query, while another modality (e.g., textual keywords) serves as keys and values, allowing the query modality to guide the model in learning to identify relevant information from other modalities. For instance, Yang et al. [2022] proposed a Knowledge-enhanced multi-head attention mechanism, using visual features as queries and knowledge graph entity embeddings as keys and values for feature fusion, with relation embeddings incorporated. Ablation studies showed that including relation embeddings improves performance. However, there is no detailed experimental analysis of the difference between concatenating features as Q, K, V inputs in attention and using one as Q and the others as K and V.

We would like to highlight the memory metric-based method proposed by Chen et al. [2021] to facilitate feature interaction. Theoretically, certain parts of the textual and visual features should convey the same information. However, differences in feature spaces make direct mapping between text and image features challenging, requiring an intermediate medium to facilitate the process. Chen et al. [2021] employed a $N \times D$ metric for this purpose, where N refers to the number of memory vectors, and D refers to the dimension of each memory vector. First, the metric was initialized randomly. Image features, text features from generated tokens, and memory metric features then underwent linear transformation to align their feature spaces. Subsequently, distances between the image features and memory metric features, as well as text features and memory metric features, were calculated. The top K metric features with the closest distances to the image or text were selected, respectively. These selected features were then weighted based on these distances and were fed back into an encoder-decoder structure. This metric, serving as a medium, ensured that the selected visual and textual features belong

to the same feature space (i.e., memory metric), loosely aligning the visual and textual features and reducing the problems arising from distinct feature spaces. Additionally, the authors tested separate textual and visual memory metrics, which also improved performance. This suggests that regularity patterns may exist within radiology images and reports, and using the memory metric can better capture these patterns to enhance model performance. This point is further supported by Yang et al. [2023], who introduce a memory metric that dynamically captures knowledge during training. This metric is then used as a knowledge base during inference to address the limitation of manually constructing knowledge graphs, as discussed in Section 3.3.1. The memory metric is updated at each step by incorporating textual and visual features, as well as metrics from the previous step, using an attention mechanism.

Two studies [Qin and Song, 2022, You et al., 2022] followed Chen et al. [2021]. Wang et al. [2022a] modified it in two ways: 1) they initialized the memory metric by visual and textual features; 2) the cross-modal interaction occurred only among cases with the same label. These two modifications resulted in a notable improvement. Li et al. [2023e] contended that the methods mentioned lack explicit constraints for cross-modal alignments. They considered orthonormal bases as the memory metric and input them along with visual or textual features, into multi-head attention modules. Then the outputs of attention modules were processed by a self-defined gate mechanism. A triplet matching loss was utilized to align the processed visual and textual features. This method slightly improved the results.

Overall, the multimodal fusion and interaction methods reviewed primarily focus on addressing challenges associated with distinct feature spaces. To balance the contributions of different modalities, a common strategy involves automatically learning the weights of contributions during training. However, regarding the other two challenges, many approaches rely heavily on similarity calculations between inputs to identify informative features. This reliance limits their ability to capture complementary information that is critical for maximizing the strengths of each modality. Furthermore, there is often a lack of specialized mechanisms to effectively address various types of noise.

3.5 Report generation

The last step is report generation, which utilizes extracted features from earlier steps to produce the final reports. The generation methods mainly include decoder-based techniques (Section 3.5.1), retrieval-based techniques (Section 3.5.2), and template-based techniques (Section 3.5.2).

3.5.1 Decoder-based techniques for report generation

A typical method for training decoder-based report generation is autoregressive training. In this process, image (or fused) features and generated tokens (or real text preceding the token awaiting generation) are input into the model to compute the probability distribution for the next token. New tokens are generated by sampling from this distribution, and a loss function is applied between the output distribution and the ground truth. Two main challenges arise in this process: first, how to mitigate information forgetting and extract useful information from long texts to generate new tokens. Second, designing an effective loss function is crucial for guiding text generation and avoiding biases, such as favouring high-frequency words over important medical keywords. The approaches to these two challenges are primarily discussed in Sections 3.5.1 and 3.5.1. Additionally, this section presents two other training strategies: reinforcement learning (Section 3.5.1) and curriculum learning (Section 3.5.1).

Architectures for decoder-based techniques The decoder decodes the extracted representation of inputs and generates a descriptive report. The mainstream architectures include LSTM [Hochreiter and Schmidhuber, 1997] and Transformer. Compared to LSTM, the Transformer processes the entire sequence simultaneously rather than sequentially. Therefore, the Transformer allows for more efficient parallelization during training and can capture long-range dependencies. In the 100 reviewed papers, the Transformer tends to replace LSTM. Sixty-six works utilized the Transformer as a decoder and only 23 of them utilized LSTMs (12 works) or hierarchical LSTMs (11 works). For the papers published in 2023 and 2024, all encoder-decoder structures used the Transformer as their decoders. There are two ways to modify the decoder and improve model performance by more effectively capturing the information within the text: shortcut connections and memory-driven transformer.

Shortcut connections: Connecting different layers in networks can be considered as a promising way to enhance the flow of information in both forward and backward propagation [Mirikharaji et al., 2023]. The U-connection [Huang et al., 2023] and meshed connection [Miura et al., 2021, Lee et al., 2022, Cornia et al., 2020] are added between encoder and decoder, resulting in a similar performance enhancement [Huang et al., 2023].

Memory-driven Transformer: We would like to highlight the Memory-driven Transformer (R2Gen) proposed by Chen et al. [2020]. It has been increasingly popular in recent years. The R2Gen introduces a memory module and a memory-driven conditional layer normalization module into the Transformer decoder architecture. The design of the memory module hypothesizes that diverse images exhibit similar patterns in their radiological reports, thereby serving as valuable references for each other. Building a memory matrix can capture this pattern and transfer it during training. Specifically, similar to that in Section 3.3.1, a matrix is randomly initialized and is updated using the gate mechanism based on the matrix from the last step and generated reports. The layer normalization is designed to integrate the outputs of the memory module into the decoder.

Eight works directly utilized the R2Gen as their decoder. In addition, the design of the memory module and layer normalization inspired subsequent works [Xue et al., 2024, Jia et al., 2021, Zhang et al., 2023a]. It is noted that the novel utilization of the memory module by Zhang et al. [2023a] integrates ground truth reports into the training process, leading to successful outcomes.

Loss functions for decoder-based techniques The mainstream loss function for report generation is the cross-entropy loss based on the generated sentences and the ground-truth sentences. Cross-entropy loss can be re-weighted based on term frequency [Gajbhiye et al., 2022], TF-IDF [Wang et al., 2022d] or uncertainty [Wang et al., 2024b] to mitigate model bias or handle challenging cases. In addition, Pandey et al. [2021] utilized cycle-consistency loss [Zhu et al., 2017] to generate reports. The core idea is that a report and its corresponding image share the same information, hence they can be used to generate each other.

The application of an auxiliary loss function can provide additional supervision signals, further enhancing model performance. Two works Wang et al. [2021], Li et al. [2022a] applied an additional constraint between features extracted from the generated and real reports. Wu et al. [2023b] applied a penalty to the predicted probabilities of frequent tokens. Zhang et al. [2023b] created two different versions of an input image by adding noise and feeding them into two networks. An auxiliary loss function ensures the consistency of the outputs produced by the two generators. Wang et al. [2024a] obtained two discriminative regions in an image from the generated words and visual classifier separately, then enforced the consistency between them.

Reinforcement learning for decoder-based techniques Reinforcement learning offers a method to update the model parameters based on non-differentiable reward functions [Messina et al., 2022]. In report generation, the model is typically viewed as an agent interacting with a generation environment. Input features and previously generated tokens are considered as the states of the environment. The parameters of the model define a policy for generating actions (i.e., next token generation) based on the states, with a reward computed at each step based on the action [Qin and Song, 2022]. The model is trained to maximize the reward using various strategies such as the policy gradients-based REINFORCE algorithm [Williams, 1992]. This reward-based training is often combined with loss-based approaches, either by alternating between them [Kaur and Mittal, 2022b] or first training with loss, followed by rewards [Qin and Song, 2022]. Improvement in the specified evaluation metric (see Section 7) can be considered as the basis for designing rewards, such as the Consensus-based Image Description Evaluation (CIDEr) [Kaur and Mittal, 2022b], the Bilingual Evaluation Understudy (BLEU) [Qin and Song, 2022, Gu et al., 2024], the Metric for Evaluation of Translation with Explicit ORDERing (METEOR) [Qin and Song, 2022], the Recall-Oriented Understudy for Gisting Evaluation (ROUGE) [Qin and Song, 2022], BERTScore [Miura et al., 2021], F1 score [Miura et al., 2021, Wu et al., 2023b], and accuracy [Hou et al., 2021b]. In addition, Hou et al. [2021b] trained a language fluency discriminator using the ground truth and generated reports, and then utilized the discriminator to provide rewards.

Curriculum learning for decoder-based techniques Data-level curriculum learning is a strategy that organizes training samples in the order of difficulties, allowing the model to learn in a progressive manner [Soviany et al., 2022]. Unlike traditional methods, where training data is shuffled and indiscriminately fed into the model, this approach typically involves: (1) ranking the training data based on a predefined strategy; (2) starting the training process with simpler samples and progressively introducing more complex ones; and (3) training the model on the full dataset to reinforce its learning. The key element of this approach is data ranking (i.e., the first step), which mimics the human learning progression. This prevents the model from being overwhelmed by complex samples early in training, thereby reducing the risk of getting stuck in suboptimal solutions. Moreover, the strategy is applicable to both loss-based and reward-based training methods. Liu et al. [2021a] introduced curriculum learning to the field of report generation by designing specific metrics to evaluate the difficulty of image-report training data. They proposed four metrics named image heuristics, image confidence, text heuristics, and text confidence. Image heuristic evaluates the similarity between input images and normal images. Image confidence indicates the confidence of a classification model. The report heuristic was related to the number of abnormal sentences, and report confidence is evaluated by the negative log-likelihood loss [Xu et al., 2020]. Instead of directly summing the four metrics, they adaptively select the most suitable metric using dynamic feedback for each training step, and use the selected metric to choose an appropriate training batch. Experimental results show that incorporating this training strategy into various methods leads to improved outcomes.

In conclusion, the Transformer has replaced LSTM as the dominant architecture. Structural enhancements, such as short connections, improve information flow and alleviate gradient vanishing, though they also increase model complexity. The memory matrix allows cross-referencing between cases, but attention must be paid to memory size, as an excessively large memory can introduce redundancy and degrade performance. Another improvement lies in the loss function. It involves either assigning different weights to words or incorporating auxiliary loss functions; however, these additional supervision signals provide limited information compared to those used in image feature extraction. Reinforcement learning offers a method for optimizing non-differentiable objectives, but focusing on specific rewards (e.g., ROUGE-L) may negatively impact performance on other metrics, making reward function design critical. Additionally, curriculum learning presents a promising approach to organizing training data.

3.5.2 Retrieval-based and template-based techniques for report generation

Retrieval-based techniques generate reports by selecting existing sentences from a large corpus and the selection is typically based on similarity comparison [Endo et al., 2021, Ramesh et al., 2022, Jeong et al., 2024]. Initially, text and image encoders are trained using a contrastive method, such as the CLIP [Radford et al., 2021]. The textual features of sentences in a corpus and the visual features of

an input image are extracted by the encoders. The visual features are then compared with all textual features in the corpus. The top K sentences with the maximum similarity score are selected for the predicted report. In addition, Jeong et al. [2024] added a multimodal encoder after the retrieval process to calculate the image-text matching scores between the input image and the retrieved sentences. A filter was applied based on the score to remove entailed or contradicted sentences.

Other retrieval-based techniques do not follow the above process. Kong et al. [2022] treated the report generation in two steps sentence retrieval and selection. They first retrieved a candidate sentence set from the training datasets with far more sentences than a standard medical report and then selected the sentences by a classifier. Zhang et al. [2022] proposed a retrieval method based on a hashing technique, which mapped multi-modal data with the same label into a shared space.

Template-based methods typically start with the diagnosis of diseases, and then pre-defined sentences are selected based on the diagnosis results. These selected sentences are concatenated to produce reports [Pino et al., 2021]. Abela et al. [2022] argued that this method was limited by exact labels, therefore they retrieved template sentences by class probabilities and different thresholds corresponding to different descriptions.

In conclusion, retrieval-based and template-based techniques utilize existing data or predefined templates, theoretically enhancing performance, particularly in linguistic fluency. However, challenges such as inadequate feature representation and immature similarity measurement often lead to inferior outcomes. For instance, while inadequate feature representation may only affect specific generated words in decoder-based models, it can result in entirely irrelevant sentence selections in retrieval-based and template-based approaches. Furthermore, these techniques generally exhibit lower flexibility and limited content generation, negatively impacting human-computer interaction.

4 Large Models in Report Generation

Large models, including language models, vision models and multi-modal models, have revolutionized the field of deep learning. Particularly for large language models, their human-like conversational capabilities and ability to respond to free-text queries without task-specific training have been profoundly impactful. However, deploying general large language models in clinical settings remains unfeasible due to insufficient response accuracy and safety concerns [Yan et al., 2023, Saab et al., 2024], which has led to significant attention on their application to medical tasks such as report generation.

In the initial phases, rather than directly generating reports from imaging data, researchers focus on using general large language models to revise reports produced by traditional methods [Selivanov et al., 2023, Wang et al., 2023a]. Traditional deep learning methods were applied to predict report-related information (e.g., lesion regions) and generate preliminary reports from images. Subsequently, pre-trained models (e.g., ChatGPT [Wang et al., 2023a] and GPT-3 [Brown et al., 2020, Selivanov et al., 2023, Wang et al., 2023a]) were employed to improve these reports based on the predicted information, leading to moderate improvements.

Training a large model on a large medical dataset is a more straightforward solution to achieve better performance. An overview of these models is presented in Table 1. We have provided the GitHub repository link for the open-source model. Some links provide only inference APIs [Alkhalidi et al., 2024, Chen et al., 2024], while others include training code [Zhang et al., 2024a, Li et al., 2024, Wang et al., 2023e, Pellegrini et al., 2023b, Wu et al., 2023a]. This process generally comprises two main phases. The first phase is pre-training, where the model learns general feature representations through unsupervised or self-supervised learning on a large, unlabeled medical dataset. This phase enables the model to acquire broad generalization capabilities and adjust its weights to be more aligned with the target medical tasks. The second phase is fine-tuning, which involves refining the model for a specific task (e.g., medical report generation) using a relatively small, high-quality labeled dataset. The common monitoring tool is wandb⁴, tracking metrics like loss or validation set results, similar to traditional training. Understanding this process requires grasping three key components:

- Acquisition of medical image-text datasets with prompts designed for training.
- Except for BiomedGPT [Zhang et al., 2024a], the other reviewed papers are based on large language models. Thus, understanding the transition from large language models to large multimodal models, particularly regarding the integration of image data, is essential.
- Training large models demands substantial computational resources. For instance, Touvron et al. [2023] reported that training the famous large language model named LLaMA with 65B-parameter required 2,048 A100 GPUs with 80GB of RAM over approximately 21 days. Such resource demands are beyond the reach of most researchers. Therefore, it is crucial to explore methods for training large medical models with limited resources.

We discussed the aforementioned issues in Sections 4.1, 4.2, and 4.3, respectively. It is untenable to fully separate large models for generating medical reports from foundational medical models. Thus, in these sections, foundational model methods are introduced first, followed by their application in report generation.

⁴<https://wandb.ai/home>

Table 1: Comparison of vision–language models for medical tasks. “Params” describes the parameter scale, roughly indicating the size of LLMs. “Foud” indicates if the model can be used for other medical tasks besides report generation. “RG” shows if it is trained or tested for report generation. “OS” refers to its open-source status.

Name	Params	Visual Encoder	Adapter	LLM	Foud	RG	OS
RaDialog [Pellegrini et al., 2023b]	7B/13B/33B	BioViL-T	Q-Former	Vicuna-7B/13B/33B	✗	✓	https://github.com/ChantalMP/RaDialog
R2GenGPT [Wang et al., 2023e]	7B	Swin Transformer	Linear	LLaMA2-7B	✗	✓	https://github.com/wang-zhanyu/R2GenGPT
LLM-CXR [Lee et al., 2023]	13B	VQ-GAN	–	LLaMA2-13B	✗	✓	✗
MAIRA-1 [Hyland et al., 2023]	7B	RAD-DINO	MLP-4	Vicuna-7B	✗	✓	✗
MAIRA-2 [Bannur et al., 2024]	7B/13B	RAD-DINO	MLP-4	Vicuna-7B/13B v1.5	✗	✓	✗
CheXagent [Chen et al., 2024]	7B	EVA-CLIP	Q-Former	Mistral-7B-v0.1	✓	✓	https://github.com/Stanford-AIMI/CheXagent
LLava-Med [Li et al., 2024]	7B	BioMedCLIP	Linear	LLaMA-7B	✓	✗	https://github.com/microsoft/LLaVA-Med
MiniGPT-Med [Alkhalidi et al., 2024]	7B	EVA-CLIP	Linear	LLaMA2-7B	✓	✓	https://github.com/Vision-CAIR/MiniGPT-Med
LLaVA-Ultra [Guo et al., 2024]	13B	CLIP-ViT-L/14 and SAM-ViT-L	Linear	LLaMA-13B	✓	✗	✗
BiomedGPT-B [Zhang et al., 2024a]	182M	ResNet-101	–	BERT-style encoder + GPT-style decoder	✓	✓	https://github.com/taokz/BiomedGPT
RadFM [Wu et al., 2023a]	14B	3D ViT	Transformer +linear	MedLLaMA-13B	✓	✓	https://github.com/chaoyi-wu/RadFM
MedVersa [Zhou et al., 2024]	–	Swin Transformer /3D UNet	Linear	Llama-2	✓	✓	✗

4.1 Acquisition of medical image-text datasets with prompts

A large dataset is required during the pre-training phase. PMC-15M [Zhang et al., 2023c] is a dataset comprising 15 million biomedical image-text pairs, each consisting of an image and its corresponding caption from biomedical papers. In addition to medical images, it also includes other types of data, such as general biomedical illustrations and microscopy images, without any prompts provided. Therefore, it is impractical to directly utilize the entire dataset for medical image analysis. Li et al. [2024] derived two sub-datasets from PMC-15M for large model training. The first dataset, consisting of 600K image-text pairs, was selected based on caption length. Corresponding prompts were randomly chosen from a predefined list, such as “Describe the image concisely”. The second dataset consists of multi-round questions and answers for 60K filtered images from the PMC-15M dataset. The image types include X-rays, CT scans,

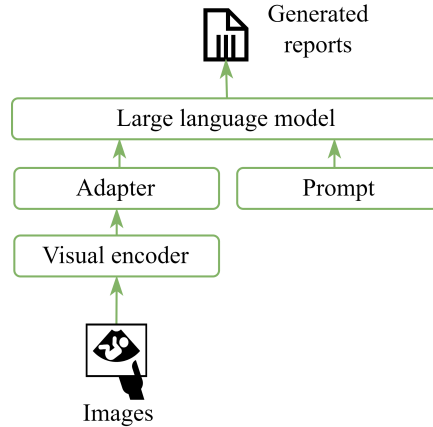


Figure 6: A typical process for transitioning from language models to multimodal models.

MRIs, histopathology slides, and gross pathology images. In addition to the original text associated with each image, sentences referring to these images were extracted from the original papers to provide extra context. Image, original text, and additional descriptions were then provided to GPT-4, which was tasked with generating multi-round questions and answers as if it could see the images. This novel dataset design enables the Large Language and Vision Assistant for BioMedicine (LLaVa-Med) [Li et al., 2024] to perform well through pre-training on it and also inspired subsequent works [Guo et al., 2024].

A 60k medical image dataset is relatively small for large model training, and the image-text pair format limits its utility for diverse medical tasks such as disease diagnosis. Consequently, efforts have been made to compile a comprehensive radiology-focused dataset, with the most straightforward approach being the integration of multiple public datasets [Alkhalidi et al., 2024, Zhang et al., 2024a, Chen et al., 2024, Wu et al., 2023a]. For example, Zhang et al. [2024a] aggregated 14 public datasets and Chen et al. [2024] derived a large-scale instruction-tuning dataset about Chest X-rays from 28 publicly available datasets. Distinct prompt templates were designed for each type of task. For report generation, most studies incorporate MIMIC-CXR into the training set [Alkhalidi et al., 2024], with a few also utilizing the Indiana University Chest X-Ray Collection (IU-Xray) [Zhang et al., 2024a]. In addition, most datasets contained only 2D images. Wu et al. [2023a] integrated 18 public datasets to construct a radiology image dataset called the Medical Multi-modal Dataset (MedMD), which includes 15.5M 2D scans and 500k 3D scans. They also filtered MedMD, retaining only radiology images. However, no studies have yet conducted ablation experiments to assess how pre-training on different datasets affects model performance. For example, whether using the MIMIC-CXR dataset in both the pre-training and fine-tuning phases improves report generation compared to using it only in fine-tuning.

For the fine-tuning phase, prompts need to be designed based on the existing report generation dataset (e.g., MIMIC-CXR). Most reviewed papers rely on fixed prompts, such as “Generate a comprehensive and detailed diagnosis report for this chest X-ray image” [Wang et al., 2023e], or use prompts based on the other sections in the report (i.e., indication, technique, and comparison) to provide the model with additional patient-related information [Hyland et al., 2023, Bannur et al., 2024]. Pellegrini et al. [2023b] integrated disease classification results into the prompt. However, the classifier’s low accuracy yields minimal improvement. Given that prompt design is critical for optimizing model performance [Liu et al., 2023b], further research into developing effective prompts for report-generation tasks is necessary.

4.2 Evolution from large language models to large multimodal models

A common approach for evolving from a large language model to a large multimodal model is to add an adapter between the visual encoder and the language model to align image features with the language model’s input, as shown in Figure 6. Table 1 lists the adapter designs, which are usually linear projections or multilayer perceptrons (MLP). Hyland et al. [2023] found that a 4-layer MLP outperforms a 2-layer MLP on report generation tasks, due to the increased non-linearity enhancing the model’s expressive power. Additionally, Pellegrini et al. [2023b] introduced a more sophisticated adapter (i.e., Q-Former) from Bilp-2 [Li et al., 2023a], but it yielded no significant improvement.

When training large foundational medical models, task-specific prompts are designed, such as “Does the patient have disease X?” for disease diagnosis, “Is this image from modality X?” for modality recognition, and “Generate a detailed diagnosis report for this chest x-ray image.” for report generation. Typically, cross-entropy loss is applied between the predicted and ground-truth text sequences, helping to standardize the training process across different tasks.

Based on the architecture, the evolution can be achieved in one step by training the visual encoder, adapter, or large language model directly with the target dataset [Wang et al., 2023e, Hyland et al., 2023]. The model’s initial weights come from general large language models (e.g., Vicuna [Chiang et al., 2023], LLaMA [Touvron et al., 2023], Mistral [Jiang et al., 2023]), general visual encoder (e.g., EVA-CLIP [Sun et al., 2023]), and domain-specific visual encoders (e.g., BioMedCLIP [Zhang et al., 2023c], BioViL [Bannur et al., 2023], RAD-DINO [Pérez-García et al., 2024]). Wang et al. [2023e] found that for report generation, training only the adapter was ineffective compared to training both the adapter and the visual encoder. Hyland et al. [2023] observed that when the visual encoder is frozen and only the adapter and LLM are trained, the choice of a radiology-specific visual encoder can significantly improve model performance. Guo et al. [2024] argued that the size imbalance between the visual encoder and the language model causes a bottleneck in feature extraction. To address this, they use two large visual encoders, CLIP and the Segment Anything Model (SAM) [Kirillov et al., 2023], and combine their features through weighted addition, which outperforms the use of a single encoder.

The one-step approach is highly convenient; however, training the entire visual encoder or LLM on large datasets is costly. To address this, two-step approaches have been proposed for scenarios that require training on larger datasets to achieve better generalization. Inspired by LLaVA [Liu et al., 2024], LLaVa-Med [Li et al., 2024] presents a feasible solution. In the initial phase, the 600K dataset from PMC-15M is used to train the adapter for image captioning, with the visual encoder and language model parameters kept frozen. In the subsequent phase, the model is trained on the 60K instruction set from PMC-15M. The visual encoder weights remain fixed, and the projection layer and language model parameters are updated.

Lee et al. [2023] argued that using adapters hinders the interaction between visual and semantic information. To address this, they proposed using frozen Vector Quantised Variational Autoencoder (VQ-GAN) [Esser et al., 2021] to represent image information in a discrete form, incorporating these image tokens as special tokens into the vocabulary of large language models. While experimental results have yet to show improvements in report generation tasks using this method compared to adapters, the VQ-GAN approach remains notable. It introduces a learnable codebook that maps encoded image features to the nearest discrete variable, enabling discretization. This technique is well-established in natural image generation for capturing high-quality discrete image representations but remains underexplored in report generation.

Most medical foundation models are trained directly on multi-task datasets, enabling them to perform a variety of tasks. In contrast, Zhou et al. [2024] treat the large model as a planner, predicting specific tokens that activate the corresponding vision modules (e.g., detection and segmentation), which allows it to handle an even wider array of tasks. For instance, when the <DET> token is predicted, the detection module is triggered to generate bounding box information. However, this approach increases the number of models involved, making the pipeline non-end-to-end.

Integrating image features into large language models while preserving their conversational abilities is crucial. However, the current report-generation large models do not achieve this. General medical models are only capable of handling simple conversations. Nonetheless, as shown in Section 8, with accessing to sufficient data, large models demonstrate advantages on natural language-based evaluation metric, highlighting their potential.

4.3 Training large medical models with limited resources

Directly applying a general-purpose LLM into a highly specialized task (e.g. radiology report generation) can not achieve an optimal performance, therefore normally requires LLM fine-tuning using a task-specific dataset. However, fine-tuning the entire LLM is extremely resources demanding. Employing adapters, frozen layers, and training only a subset of the LLM parameters can conserve training resources; however, these techniques often involve a trade-off between efficiency and model performance. Additionally, incorporating extra adapters increases the overall model parameters, further burdening the computational resources required during the inference stage and prolonging the inference time. This section presents two more direct approaches for conserving training resources: Low-Rank Adaptation (LoRA) [Hu et al., 2021], a classic large model fine-tuning technique widely utilized in report generation task [Wang et al., 2023e, Alkhaldi et al., 2024, Pellegrini et al., 2023b, Guo et al., 2024], and a lightweight medical foundation model for medical tasks, including report generation.

When fine-tuning large models, the weights W update can be expressed as $W + \Delta W$, where ΔW denotes the change in W during training. The core idea of LoRA⁵ is that not all parameters need to be changed for a specific target task (e.g., report generation) during fine-tuning. The update weights ΔW can be efficiently represented using a low-rank matrix and computed via low-rank decomposition. Specifically, given model weights $W \in \mathbb{R}^{d \times k}$, the weight update is assumed to be of low rank r , i.e., $W + \Delta W = W + BA$, where $B \in \mathbb{R}^{d \times r}$ and $A \in \mathbb{R}^{r \times k}$, with $r \ll \min(d, k)$. Thus, only the low-rank matrices A and B are trained, and their product BA is added to the original weights. This approach substantially reduces the computational resources required, as only the delta weights ΔW need to be stored for each new model, thereby conserving disk space. Moreover, experiments conducted on large models (such as GPT-3 175B) have demonstrated that models fine-tuned with LoRA can achieve performance comparable to, or even surpassing, that of full model fine-tuning. However, Wang et al. [2023e] observed that when applying this approach to fine-tune the adapter and visual encoder (with 90.9M parameters) for report generation, the performance was inferior to that of full model fine-tuning. This discrepancy arises because, as the model size decreases, the proportion of effective parameters increases, thereby diminishing the advantage of using low-rank matrices

⁵<https://github.com/microsoft/LoRA>

to approximate ΔW . The LoRA has been integrated into the State-of-the-art Parameter-Efficient Fine-Tuning (PEFT) library ⁶ and can be directly accessed via its interface. PEFT is designed to efficiently fine-tune large pre-trained models.

A straightforward strategy to conserve training resources is to reduce the model’s trainable parameters. However, due to the performance improvements [Bannur et al., 2024] and enhanced generalization ability with larger models, most reviewed studies still employ models exceeding 7B parameters (see Table 1). Recently, Zhang et al. [2024a] developed lightweight medical foundation models of 33M/93M/182M parameters, with the 182M BiomedGPT-B achieving state-of-the-art results in 16 out of 25 medical tasks compared to 7B models. Although it has not been compared with other models on the standard report generation benchmark, it offers a valuable insight that relatively lightweight large models can be trained to accomplish report generation. BiomedGPT mainly differs from traditional models by curating a large-scale pretraining corpus and specifically developing instruction-tuning data, emphasizing the importance of a high-quality labeled large training dataset. Although for the report generation task, BiomedGPT-B was tested on only 30 image-report pairs and evaluated manually rather than using natural language or medical correctness metrics, it is still regarded as a significant advancement for lightweight foundation models in medical report generation.

It is noteworthy that there remains no definitive consensus on the optimal model size and data quantity requirements for training large models for report generation tasks. Pellegrini et al. [2023b] fine-tuned models with 7B, 13B, and 33B parameters on the MIMIC dataset, finding no significant performance differences. In contrast, Bannur et al. [2024] merged four datasets as training datasets, introducing more diverse inputs and outputs rich in information (as described in Section 5.2). They trained both 7B and 13B models, observing performance improvements as model size increased (see Table 4). Similarly, Zhang et al. [2024a] noted consistent performance enhancements with models of 33M, 92M, and 182M parameters. Despite differences in architecture, these findings suggest a bottleneck effect of model size and data usage on model performance, underscoring the need for systematic investigation.

5 Explainability

Explainability of a deep learning model is defined as the ability to justify an outcome in understandable terms for a human [Doshi-Velez and Kim, 2017, Messina et al., 2022]. This is especially critical in medical contexts, where model outputs can directly or indirectly influence clinical decision-making. However, most current research focuses on improving report generation model performance, with relatively few studies considering explainability. This section summarizes recent advancements in this area, including visualization, auxiliary tasks, and uncertainty quantification.

5.1 Visualization for explainability

Aligned with previous surveys [Messina et al., 2022], visualization remains the dominant method for interpreting model outputs. It highlights the most crucial part of the inputs relevant to report generation, such as specific areas in images, keywords in text, and certain nodes in knowledge graphs. Visualization allows radiologists to assess whether the model accurately targets the relevant information, thereby fostering greater confidence in the system. The reviewed report generation methods mainly employ two approaches to performing visualization.

The first approach is a gradient-based method named Gradient-weighted Class Activation Mapping (Grad-CAM) [Selvaraju et al., 2017]. It calculates the importance of each image feature map for a particular prediction by weighting them with the gradients and then performing a weighted sum. Report generation methods often use Grad-CAM in auxiliary classification tasks to identify image regions that influence model decisions [Alfarghaly et al., 2021, Huang et al., 2021b, Pino et al., 2021, Kaur and Mittal, 2022b], with some methods applying it directly to report generation tasks to determine the image regions relevant to report generation [Najdenkoska et al., 2021, 2022].

The second approach utilizes the attention weights. Compared to Grad-CAM, which is limited to images, attention-based visualization is more applicable across various input data modalities, including images [Liu et al., 2021b, Chen et al., 2021, Wang et al., 2023d, Zhang et al., 2023b, Li et al., 2022a, Qin and Song, 2022, Zhang et al., 2023a, Moon et al., 2022, Hou et al., 2021a, Cao et al., 2023, Lin et al., 2023, You et al., 2022, Li et al., 2023e, Kong et al., 2022, Xue et al., 2024], medical terminology [Liu et al., 2021b], retrieved real reports [Liu et al., 2021b], and medical knowledge base [Liu et al., 2021b]. Typically, attention weights are derived from the Scaled Dot-Product Attention mechanism [Vaswani et al., 2017], which accepts query (Q), key (K), and value (V) vectors as inputs. The formulation is expressed as $Attention(Q, K, V) = softmax(\frac{QK^T}{\sqrt{d_k}})V$, where $\sqrt{d_k}$ is a scaling factor related to the input dimension. The expression $softmax(\frac{QK^T}{\sqrt{d_k}})$ is interpreted as the attention weights.

Regardless of visualization methods, studies typically provide limited image examples to illustrate that their models can accurately identify relevant regions; however, they are deficient in the systematic evaluation of large-scale datasets. Moreover, there is a lack of quantitative metrics to assess visualization results, possibly due to the absence of ground truth. Non-image-based ground truth can be obtained through text comparisons, while image-based ground truth can be established by collecting physicians’ eye-tracking data or using bounding boxes for lesions or anatomical structures.

⁶<https://github.com/huggingface/peft>

5.2 Auxiliary tasks for explainability

Auxiliary tasks can provide valuable information for image classification or detection (see Section 3.3.1), thus enhancing system interpretability by offering radiologists additional insights. However, the potential of auxiliary tasks in improving interpretability has been largely underutilized in previous works [Messina et al., 2022]. Tanida et al. [2023] addressed this gap by linking output results to specific image regions via object detection, enabling users to select areas of interest and receive corresponding explanations. Dalla Serra et al. [2023b] introduced a multi-label classification head that classifies findings for each detected anatomical region. This model outputs both the bounding box locations and findings as intermediate results, which increases model transparency. Bannur et al. [2024] outputs the corresponding bounding box while generating each lesion-containing description.

5.3 Uncertainty quantification for explainability

The uncertainty discussed in this section quantifies the model’s confidence in the quality of the generated outputs. Wang et al. [2024b] measured the uncertainty based on Monte Carlo dropout variational inference [Gal and Ghahramani, 2016]. When dropout is applied in the network, performing T stochastic forward passes for a given input allows the variance of the outputs to reflect the model’s uncertainty. Greater variance implies greater uncertainty. They defined report-level textual uncertainty and sentence-level textual uncertainty. Report-level uncertainty is measured by the variance of similarities between the T generated reports. For sentence-level uncertainty, they first identify the report with the minimum similarity distance to other reports from the T outputs, termed the average reference report. The uncertainty of each sentence is then represented by the variance of the similarities between the sentences in the average reference report and their corresponding sentences in the T generated reports. Compared to report-level uncertainty, sentence-level uncertainty enables physicians and patients to assign varying trust levels to individual sentences rather than fully affirming or rejecting the entire report, warranting further study.

6 Datasets

Datasets play a crucial role in the development of report-generation models. Abundant and diverse training data can improve the model’s accuracy and generalizability. Moreover, a suitable test dataset makes it realistic to test the model’s performance in a practical scenario. In this section, we selected 11 public medical image-report datasets utilized in the reviewed articles to provide a comprehensive introduction to popular and newly collected datasets, see Table 2. The usage of datasets in each article is shown in Table A1 in Appendix A. The datasets primarily focus on the lung, including X-ray [Demner-Fushman et al., 2016, Johnson et al., 2019a,b] and CT [Li et al., 2020, Liu et al., 2021e]. In addition, there are also publicly available datasets on eye scans [Huang et al., 2021b, Lin et al., 2023, Li et al., 2021] and breast scans [Yang et al., 2021a]. The concentration of medical report generation efforts on chest X-rays can be attributed, in part, to the accessibility of large-scale publicly available datasets.

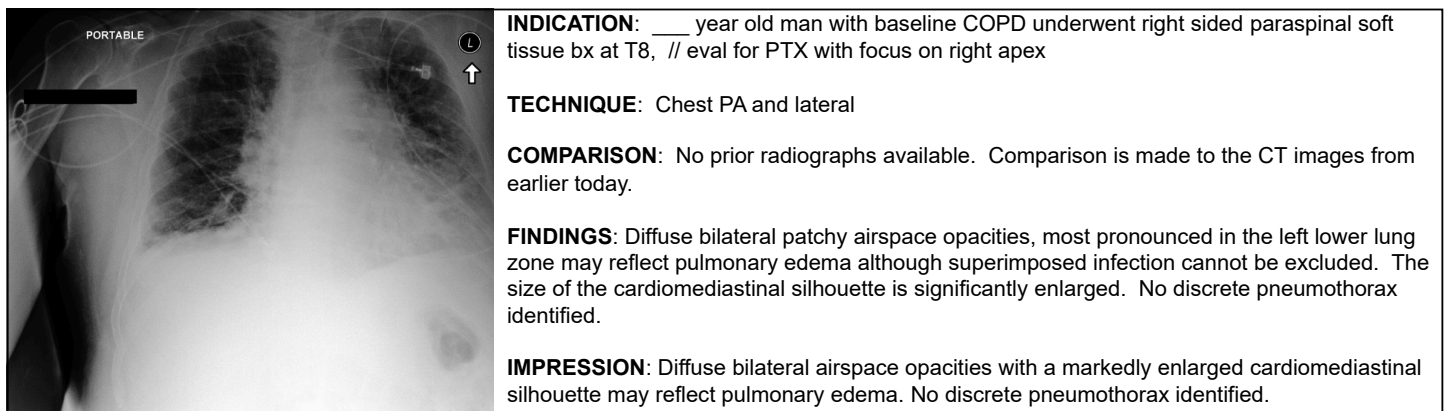


Figure 7: A sample from the MIMIC-CXR dataset. The left is the Chest X-ray image and the right is its corresponding radiology report.

The most popular datasets are the IU-Xray [Demner-Fushman et al., 2016] and the MIMIC-CXR [Johnson et al., 2019a,b]. The IU-Xray contains 7470 images of frontal and lateral X-rays and 3955 reports with manual annotation based on the MeSH codes⁷ and the RadLex codes. These codes encompass standard medical terminology, such as anatomical structures, diseases, pathological signs, foreign objects, and attributes, as defined by authoritative institutions. Manual keyword annotation is invaluable because it helps standardize synonym expressions and clarify linguistic ambiguities, which facilitates the structuring of information in free-text reports [Pellegrini et al., 2023a].

⁷<https://www.nlm.nih.gov/mesh/meshhome.html>

However, IU-Xray annotations are designed to improve retrieval efficiency rather than to structure information, which may result in the overlooking of speculative details when converting free-text reports into a structured format. For example, the annotation for “Focal airspace disease in the right middle lobe. This is most concerning for pneumonia” is annotated as “Airspace Disease/lung/middle lobe/right/focal”, which omits the concern for pneumonia. Additionally, the IU-Xray dataset does not provide an official split strategy. Most reviewed studies use a 7:1:2 ratio for training, validation, and test sets. For deep learning methods, the size of the IU-Xray is insufficient, while the collection of MIMIC-CXR alleviates this problem [Messina et al., 2022]. Chen et al. [2020] also noted that compared to IU-Xray, MIMIC-CXR may exhibit a greater diversity in report patterns. This is more conducive to training a model with strong generalization performance. MIMIC-CXR consists of 377,110 images and 227,827 reports and has been multi-labeled by automatic tools into 14 categories, including lung-related diseases (e.g., pneumonia), heart-related diseases (e.g., cardiomegaly), pleural-related diseases (e.g., pleural effusion), bone-related conditions (e.g., fracture), support devices, and cases where no abnormal finding is detected. The F1 scores for consolidation, pneumonia, atelectasis, pneumothorax, pleural effusion, and fracture annotation all exceed 0.9, indicating the reliability of these automatically annotated labels. An image-report sample from the MIMIC-CXR dataset is shown in Figure 7. The indication, technique, and comparison provide fundamental information for a Chest X-ray test. The automation of radiology report generation targets the findings and impressions sections. The findings section provides a detailed description of the entire image, while the impressions section summarizes these observations. The MIMIC-CXR dataset provides an official data split strategy, consisting of 368,960 training images with 222,758 reports, 2,991 validation images with 1,808 reports, and 5,159 test images with 3,269 reports. To facilitate different methods, many studies have preprocessed this dataset. The most well-known version, introduced by R2Gen [Chen et al., 2020], consists of 270,790 training images, 2,130 validation images, and 3,858 test images, and has been widely used in subsequent approaches. However, Chen et al. [2020] paired each report with only one image, treating multiple images for the same report (e.g., frontal and lateral views) as distinct cases. This can introduce errors, particularly in contrastive learning, as different views might be seen as negative pairs. Moreover, if a report references findings only visible in the lateral view but is matched with a frontal image, this misalignment could negatively impact the model training. Thus, while this data version is popular, careful selection is necessary when using it. Research on the role of frontal and lateral views in automated report generation has been a focus of previous studies. For instance, Bertrand et al. [2019] found that the lateral view alone is less effective than the frontal view, which provides more comprehensive information. However, combining both views can enhance the diagnosis of certain diseases, as they offer complementary data [Laserson et al., 2018]. As discussed in Section 3.3.1.1, Wang et al. [2023c] demonstrated how this combination can be achieved using transformer attention. Nonetheless, utilizing both views increases computational costs and demands more processing power from devices.

The follow-up work provides MIMIC-CXR with richer label information. The Chest ImaGenome dataset [Wu et al., 2021a] is based on the anteroposterior and posteroanterior view Chest X-ray images in the MIMIC-CXR dataset. It provides an anatomy-centered scene graph for each image based on sentence-level annotation. The graph includes objects (e.g., lung), attributes (e.g., opacity), and their relationships. Bounding box locations are specified for key anatomical structures. The annotations are generated through two automated pipelines, and a separate dataset of 500 manually annotated cases is also provided for testing. Additionally, using timestamps from MIMIC-CXR, anatomical annotations are compared across sequential exams based on descriptive changes (e.g., decrease). Dalla Serra et al. [2023a] incorporated the anatomy information from prior reports into model training, improving most metrics. It should be noted that the ImaGenome dataset uses only frontal images, likely because lateral images have less influence on automatic report generation. Frontal images are generally sufficient for annotating most anatomical structures, and even in the presence of partial obstructions (e.g., up to 15% of the lung obscured by the heart or diaphragm [Raouf et al., 2012]), the annotation boxes remain largely unaffected. A new dataset, CheXpert Plus, comparable to MIMIC-CXR, was recently released by Stanford University [Chambon et al., 2024], containing 223,462 images and 187,711 reports. The studies for each patient are also arranged in chronological order. As an extension of the widely used chest X-ray classification dataset named CheXpert [Irvin et al., 2019], it adds corresponding reports, demographic information, automated labels for 14 disease categories, automated graph-based annotations, and a collection of pre-trained models built on this dataset. Although CheXpert Plus has fewer reports than MIMIC, the reports are longer, particularly in the impression section. CheXpert Plus is the largest available dataset for tasks related to the impression section. Additionally, it has been de-identified without altering the structure of the reports, making them more representative of real-world radiology text.

The above datasets contain X-ray images. Besides X-rays, CT is another important imaging modality for the chest. Publicly available datasets for CT report generation were primarily collected for COVID-19 research. The COV-CTR dataset [Li et al., 2020] includes 349 COVID and 379 Non-COVID images, sourced from published papers. One limitation of this dataset is its relatively low image quality. In contrast, the COVID-19 CT dataset [Liu et al., 2021e] contains higher-quality images, which were directly collected from hospitals, offering clearer diagnostic details.

Increasing attention has been paid to the collection of ophthalmic image-report pairs [Huang et al., 2021b, Li et al., 2021, Lin et al., 2023]. Ophthalmic image has lots of modalities, such as Fluorescein Angiography (FA), Fundus Fluorescein Angiography (FFA), Color Fundus photography (CFP), fundus photograph (FP), optical coherence tomography (OCT), fundus autofluorescence (FAF), Indocyanine Green Chorioangiography (ICG), and red-free filtered fundus images. Most retinal datasets are based on one or two modalities and the last released Retina ImBank dataset is the first multi-modality retinal image-text dataset [Lin et al., 2023]. Some datasets provide additional labels for each image, such as lesion boundary [Li et al., 2021], lesion category [Huang et al., 2021b, Li et al., 2021], and keywords [Huang et al., 2021b].

The findings and impressions section of the reports in the aforementioned datasets is in free-text format, which may exhibit expression ambiguity and complicate the assessment of clinical accuracy. Structured reporting presents a potential solution by employing standardized formats for documenting radiological findings and interpretations through predefined templates or checklists, such as “heart size: normal” [Nobel et al., 2022]. In clinical practice, generating structured reports typically requires doctors to answer a sequence of questions [Pellegrini et al., 2023a]. Pellegrini et al. [2023a] released a structured report dataset named Rad-ReStruct based on the IU-Xray. They designed a structured report template with a series of single- or multi-choice questions based on topic existence (e.g., Are there any diseases in the lung?), element existence (e.g., Is there an opacity in the lung?), and attributes (e.g., What is the degree?). They then integrated the IU-Xray report data into the template using its annotated MeSH and RadLex codes.

The training data exhibits a long-tail distribution. For example, in the IU-Xray dataset, “normal” appears 2152 times, while “degenerated” appears only once [Yang et al., 2021b]. In MIMIC-CXR and CheXpert Plus, seven out of 14 diseases have positive occurrence rates below 10%, with one as low as 0.9% (pleural other in MIMIC-CXR). As a result, the model tends to favor more common words or options from the training set. Overcoming this data imbalance issue is essential.

The training and testing data for most reviewed traditional deep learning models come from the same dataset, which overlooks the importance of testing model generalization — a critical factor for clinical applications. Given the limited size of the IU-Xray dataset, several studies trained their models using other datasets and then used the entire IU-Xray dataset as an external validation set to assess the model’s generalization performance [Miura et al., 2021, Bannur et al., 2024]. Moreover, clinical data exists in dynamic environments where patient populations, clinical practices, and operational processes evolve over time [Kelly et al., 2019]. Therefore, for a model to be truly applicable in clinical settings, dynamic test datasets and comprehensive calibration processes are necessary to ensure the model can continue to meet requirements as data evolves.

7 Evaluation

Accurate assessment of the quality of generated reports is crucial for measuring model performance. The quality of generated reports can be evaluated both quantitatively and qualitatively. Quantitative methods check the text quality and medical correctness of the generated report by natural language evaluation metrics (Section 7.1) and medical correctness metrics (Section 7.2), respectively. Qualitative evaluation is normally performed by human experts and they provide overall evaluation for the generated reports (Section 7.3). Table 3 summarizes the description of evaluation methods introduced in this section. The usage of evaluation methods in each article is shown in Table A1 in Appendix A.

7.1 Natural language-based evaluation metrics

Natural language evaluation metrics are from natural language processing tasks and measure the general text quality of generated reports. In the reviewed papers, the most popular metrics are BLEU [Papineni et al., 2002], ROUGE-L [Lin, 2004], METEOR [Banerjee and Lavie, 2005], and CIDEr [Vedantam et al., 2015], which are based on n-gram matching between reference reports and generated reports. The model is deemed superior with an increased number of matches. Among them, the BLEU is the earliest and proposed a modified precision method. When evaluating the quality of radiology report generation, we typically opt for BLEU-1, BLEU-2, BLEU-3, and BLEU-4 metrics. The n in BLEU-n means the calculation is based on n-gram. The METEOR is an extension of BLEU-1 and introduces recall into evaluation. The ROUGE-L also considers precision and recall based on the longest common subsequence between reference and generated text. The CIDEr adopts the TF-IDF. The TF-IDF vectors weigh each n-gram in a sentence, and then the cosine similarity is calculated between the TF-IDF vectors of reference and generated text. When the model consistently produces the most common sentences, it can achieve notable BLEU scores. However, CIDEr can evaluate generated outputs by encouraging the appearance of important terms and punishing high-frequency vocabulary [Li et al., 2023b]. CIDEr has a popular variant CIDEr-D, which introduces penalties to generate desired sentence length and remove stemming to ensure the proper usage of word forms.

Other than n-gram matching, Endo et al. [2021] proposed a new metric S_{emb} . A pre-trained feature extractor is applied on both the ground truth and the generated reports, and the cosine similarity between extracted embeddings is calculated. This approach is used to assess whether the semantic information contained in two sentences is consistent. Another natural language metric %Novel [Van Miltenburg et al., 2018] is introduced to evaluate the diversity in image captioning.

7.2 Medical correctness metrics

Natural language evaluation metrics evaluate the similarity between produced reports and the ground truth, but cannot accurately measure whether the generated reports contain the required medical facts [Babar et al., 2021b, Messina et al., 2022]. Hence, medical correctness metrics are proposed to pay attention to the prediction of important medical facts. Generally, an automatic labeler is applied to extract medical facts from generated and reference reports. Then different metrics are applied to these. The mainstream metric is clinical efficacy [Liu et al., 2019, Chen et al., 2020], which initially calculates precision, recall, and F1 score, and subsequently extends to accuracy [Babar et al., 2021a, Miura et al., 2021, Moon et al., 2022, Yan, 2022, Yang et al., 2022, Selivanov et al., 2023, Yang et al., 2023] and AUC [Li et al., 2023b]. Most of the works utilized CheXpert [Irvin et al., 2019] as a labeler to extract chest diseases information from ground

Table 2: Public datasets for medical report generation. The report format described (either free-text or structured) refers to the description of the medical condition.

Name	Image type	Label type	Images	Reports	Patients	Used by	Featured use cases
IU-Xray [Demner-Fushman et al., 2016]	Frontal and lateral chest X-rays	Free text report, manual/automatic keywords annotation	7,470	3,955	3,955	71 works	Structured report construction
MIMIC-CXR [Johnson et al., 2019a,b]	Frontal and lateral chest X-rays	Free text report, automatic 14 diseases annotation	377,110	227,827	65,379	68 works	Large-scale dataset, diagnosis, knowledge base
Chest ImaGenome [Wu et al., 2021a]	Frontal chest X-ray	Free text report, automatic objects (with locations), attributes, and relations annotation	242,072	217,013	–	4 works	Detection, anatomy-based sentence generation, explainability, temporal change assessment
COV-CTR [Li et al., 2020]	Lung CT	Free text report	728	728	–	4 works	COVID-related scenarios
DeepEyeNet [Huang et al., 2021b]	FA, CFP	Free text report, manual 265 diseases, and keywords annotation	15,709	15,709	–	3 works	Diagnosis
FFA-IR [Li et al., 2021]	FFA	Free text report, manual retinal lesion boundary and category annotation	1,048,584	10,790	–	2 works	Detection, explainability
COVID-19 CT [Liu et al., 2021e]	Chest CT	Free text report	1,104	368	96	1 work	COVID-related scenarios
BCD2018 [Yang et al., 2021a]	Breast Ultrasound	Free text report	5,349	5,349	–	1 work	–
Retina ImBank [Lin et al., 2023]	FP, OCT, FFA, FAF, ICG, and red-free filtered fundus images	Free text report	18,788	18,788	–	1 work	Diverse image modalities
Retina Chinese [Lin et al., 2023]	FP, FFA, and ICG	Free text report	57,498	57,498	–	1 work	–
Rad-ReStruct [Pellegrini et al., 2023a]	Frontal and lateral chest X-rays	Structured reports	3,720	3,597	3,597	1 work	Structural report generation
CheXpert Plus [Chambon et al., 2024]	Frontal and lateral chest X-rays	Free text report, demographics, automatic 14 diseases annotation, RadGraph annotations	223,462	187,711	64,725	0 work	Large-scale dataset, diagnosis, knowledge base

truth reports, while seven of them [Miura et al., 2021, Yan, 2022, Wang et al., 2023a, 2024a, Dalla Serra et al., 2023b,a, Jin et al., 2024, Pellegrini et al., 2023b, Hyland et al., 2023] utilized a newer labeler CheXbert [Smit et al., 2020a], which has a higher performance. Another popular annotation tool named RadGraph extracts knowledge graphs (i.e., entities and relations) from the reports. It has an upgraded version called RadGraph-XL as mentioned in Section 3.1. Most works employed RadGraphF1 and calculated the overlap of entities and relations independently before averaging the results [Ramesh et al., 2022, Jeong et al., 2024, Hyland et al., 2023, Bannur et al., 2024]. In addition, Pellegrini et al. [2023a] generated structured reports by predicting a series of questions. They utilized macro precision, recall, and F1 score to assess all questions, along with evaluating report-level accuracy. Other metrics calculate the Hamming distance [Zhou et al., 2021] or perform graph comparison [Zhang et al., 2020] based on the extracted results.

Table 3: The quantitative and qualitative evaluation methods for medical report generation.

Metrics	Description	Used by
Natural language-based metrics		
BLEU [Papineni et al., 2002]	A precision-based metric that measures the n-gram overlapping of the generated text and ground truth text.	90 works
ROUGE-L [Lin, 2004]	A F1-like metric that computes a weighted harmonic mean of precision and recall based on the longest common subsequence.	81 works
METEOR [Banerjee and Lavie, 2005]	A F1-like metric that computes a weighted harmonic mean of unigram precision and recall. It is an extension of BLEU-1.	63 works
CIDEr [Vedantam et al., 2015]	The cosine similarity between generated text and ground truth text based on the TF-IDF.	41 works
S_{emb} [Endo et al., 2021]	Sending ground truth report and generated report into a textual feature extractor and calculating the cosine similarity between their embeddings from the last layer.	2 works
%Novel [Van Miltenburg et al., 2018]	The percentage of generated descriptions that are not present in the training data.	1 work
Medical correctness-based metrics		
Clinical Efficacy [Chen et al., 2020, Liu et al., 2019]	Calculate accuracy, precision, recall, and F1 score based on observations extracted from reference reports and generated reports by automated system.	40 works
RadGraph-based metrics [Jain et al., 2021, Delbrouck et al., 2022]	Calculate precision, recall, and F1 score based on knowledge graphs extracted from reference reports and generated reports by RadGraph series models.	5 works
MIRQI [Zhang et al., 2020]	Calculate precision, recall, and F1 score based on graph comparison. The ground truth and generated reports are automatically analysed to construct a sub-graph from a defined abnormality graph.	2 works
nKTD [Zhou et al., 2021]	Calculate the Hamming distance based on observations extracted from reference reports and generated reports by the CheXpert Labeller.	1 work
Human-based evaluation		
Comparison	Generate reports by two different models and allow senior radiologists to find which report is better.	12 works
Classification	Radiologists categorize the produced reports as accurate, missing details, and false reports.	1 work
Error scoring	Radiologists assess the error severity of baseline, model generated, and reference reports.	1 work
Grading	Radiologists need to assign a 5-point scale grade to two types of generated reports, in accordance with clinical standards.	2 works
Large language model-based evaluation		
GREEN [Ostmeier et al., 2024]	A large model takes a reference report and a generated report as input, identifies six types of clinically significant errors, and calculates an overall score.	0 work

7.3 Human-based evaluation

For qualitative assessment, the most common human-based evaluation method is comparison. In general, a set number of samples (i.e., 100/200/300) are selected from the test dataset and subsequently processed by different generated models. More than one professional clinician is responsible to compare and sort the generated reports. Five works utilized ground truth reports in this process. Two works [Miura et al., 2021, Cao et al., 2022] considered the ground truth reports as a reference. Reports were generated by different generators and the radiologists need to select which report is more similar to the reference. Dalla Serra et al. [2022] allowed experts to find 5 types of errors (i.e., hallucination, omission, attribute error, impression error, and grammatical error) in different generated reports according to the reference reports. Xu et al. [2023] asked radiologists to rank the ground truth reports and the generated reports. Qin and Song [2022] invited experts to select the most suitable report from the generated and the ground truth reports according to correctness, language fluency, and content coverage. Other expert evaluation methods are classification [Alfarghaly et al., 2021], grading [Wang et al., 2024b], and error scoring [Jeong et al., 2024].

7.4 Large language model-based evaluation

Recently, the human-like language comprehension abilities of large language models have achieved impressive performance, leading to their application in evaluation. For instance, LLaVA-Med utilizes GPT-4 to assess the helpfulness, relevance, accuracy, and level

of detail of generated responses while assigning an overall score. Similarly, CheXagent provides GPT-4 with a reference report and two generated reports, enabling it to identify the superior report. However, Ostmeier et al. [2024] found that GPT-4 exhibited a low correlation with expert preferences. To address this issue, they developed a specialized model, Generative Radiology Report Evaluation and Error Notation (GREEN), to evaluate report generation. This model takes a reference report and a generated report as input, allowing it to identify and categorize errors into six categories while calculating a score. The strong correlation between this score and expert evaluations underscores its effectiveness.

8 Benchmark Comparison

For model comparison, it is essential to select a benchmark for an impartial evaluation. We choose the MIMIC-CXR [Johnson et al., 2019b,a](see Table 4) dataset as a benchmark to compare the model performance for two reasons. First, according to Table 2, IU-Xray and MIMIC-CXR are the most popular datasets, but IU-Xray lacks standard training-validation-test splits, leading to less comparable results [Messina et al., 2022], while MIMIC-CXR has official training-validation-test splits. Second, MIMIC-CXR is the largest image-report dataset, which provides a broader distribution of data, facilitating testing across diverse scenarios, and reducing biases commonly encountered in smaller datasets. This section first introduces the process of paper selection and discusses issues related to benchmark usage. We then review the techniques employed by the top two methods at each step. Finally, we summarize the performance of large model-based approaches and compare them with traditional deep learning methods.

We endeavour to ensure equitable comparisons, but it’s important to consider the following three problems when analysing these results. First, we select the methods leveraged the original official splits of the MIMIC-CXR dataset [Johnson et al., 2019b], as described in Section 6. Several methodologies highlighted in Section 3 are excluded due to their differing data utilization strategies. Given the importance of large model methods, we include their results in the comparison despite minor differences from the official test set [Wang et al., 2023e]. Second, we choose BLEU, ROUGE, METEOR, CIDEr-D, precision, recall, and F1 score metrics as the evaluation metrics. Similar to the previous survey [Messina et al., 2022], we found that although some metrics have variants, many papers do not specify the particular version used. In that case, we assume they are consistent. Third, the generated report sections vary among different methodologies. Most articles do not explicitly specify the generated report sections, making it challenging to conduct comparative analysis.

We separate the comparison results based on the generated report section. The completed comparison tables are provided in Table A2 in Appendix A. Table 4 presents the top two performances for each evaluation metric. For input acquisition, three of them [Song et al., 2022, Liu et al., 2023c, Jin et al., 2024] utilized multi-modality inputs. While the ablation studies in these papers demonstrate that leveraging multi-modal data yields significant performance enhancements, particularly when real reports are retrieved and used as input (as detailed in Section 3.2) [Song et al., 2022, Jin et al., 2024], the improvements are less pronounced compared to the methods that do not employ multi-modal data. Only [Liu et al., 2023c] achieved an increase of 0.003 on METEOR, and [Jin et al., 2024] improved precision by 0.02. Thus, the utilization of multi-modal data warrants further enhancement.

At the feature learning stage, for the architecture of image feature learning, four works utilized a pure Transformer model [Wang et al., 2022e, Kong et al., 2022, Liu et al., 2023c, Wang et al., 2022d], another five works employed the CNN-based model [Pino et al., 2021, Song et al., 2022, Wu et al., 2022, Jia et al., 2022, Jin et al., 2024], and four works combined CNN and Transformer [Chen et al., 2021, Wang et al., 2023c, 2024a, Wu et al., 2023b]. None of the reviewed studies compared the impact of Transformer and CNN architectures on report generation tasks. In terms of training strategy and enhancement module, eight works [Wang et al., 2022e, Jin et al., 2024, Wu et al., 2023b, Wang et al., 2024a, 2022d, Wu et al., 2022, Liu et al., 2023c] leveraged auxiliary tasks and Song et al. [2022] designed contrastive attention. The ablation experiments demonstrated their effectiveness. It is apparent that using auxiliary loss for additional supervision is a widely adopted approach for enhancing report generation efficacy during the visual encoder phase. For non-image feature learning, there is a consensus on using transformer-based architectures, and for feature fusion, feature-level operations or attention are employed before inputting them into subsequent networks, lacking specific design considerations.

At the generation stage, the majority of studies employ a decoder, with only Pino et al. [2021] utilizing template-based approaches and Kong et al. [2022] adopting retrieval-based techniques. The method proposed by Kong et al. [2022] demonstrates superior performance, especially in lesion detection. It initially retrieves a substantial set of sentence candidates for subsequent selection. However, the lack of ablation studies prevents us from assessing the effectiveness of this design. Among the decoder-based methods, only two employed LSTM architecture [Wu et al., 2022, Jia et al., 2022], while the remaining methods all utilize Transformer architecture. In comparison to transformer-based approaches, LSTM-based methods exhibited inferior performance, selected primarily due to the limited number of models explicitly designed for generating the “impression” and “finding” sections. Two works utilized the modified Transformer R2Gen [Wang et al., 2023c, 2024a], and there is no significant advantage. Three studies enhanced cross-entropy loss by re-weighting [Wang et al., 2022d] or adding auxiliary loss [Wang et al., 2024a, Wu et al., 2023b], but did not yield significantly improved results. Notably, the outstanding performance of Wu et al. [2023b]’s work on the F1 metric stems from utilizing F1-based rewards in reinforcement learning, but their results on other metrics were subpar.

For large model-based methods, R2GenGPT [Wang et al., 2023e] achieved competitive results by fine-tuning only the visual encoder and adapter on the MIMIC-CXR dataset, underscoring the potential of large models in this domain. At the same time, the usage of a rich training dataset and carefully designed input-output settings enabled MAIRA-2 13B [Bannur et al., 2024] to achieve the best results in

Table 4: Comparisons of the model performance on the MIMIC-CXR Dataset. B1, B2, B3, B4, R-L, C-D, P, R, and F represent BLEU-1, BLEU-2, BLEU-3, BLEU-4, ROUGE-L, CIDEr-D, precision, recall, and F1 score, respectively. **The best** and **second best** results are highlighted. All values were extracted from their papers. \uparrow indicates that a higher value for this metric is better. * means large model-based methods.

Paper	B1 \uparrow	B2 \uparrow	B3 \uparrow	B4 \uparrow	R-L \uparrow	METEOR \uparrow	C-D \uparrow	P \uparrow	R \uparrow	F \uparrow
Findings Section										
Chen et al. [2021]	0.353	0.218	0.148	0.106	0.278	0.142	-	0.334	0.275	0.278
Pino et al. [2021]	-	-	-	-	0.185	-	0.238	0.381	0.531	0.428
Song et al. [2022]	0.360	0.227	0.156	0.117	0.287	0.148	-	0.444	0.297	0.356
Bannur et al. [2024] 7B*	0.465	-	-	0.234	0.384	0.419	-	-	-	0.427
Bannur et al. [2024] 13B*	0.479	-	-	0.243	0.391	0.430	-	-	-	0.439
Impression + Findings Section										
Wu et al. [2022]	0.340	0.212	0.145	0.103	0.270	0.139	0.109	-	-	-
Wang et al. [2022d]	0.351	0.223	0.157	0.118	0.287	-	0.281	-	-	-
Jia et al. [2022]	0.363	0.228	0.156	0.130	0.300	-	-	-	-	-
Wang et al. [2023e]*	0.411	0.267	0.186	0.134	0.297	0.160	0.269	0.392	0.387	0.389
Zhou et al. [2024]*	-	-	-	0.160	-	-	-	-	-	-
Unspecified generated sections										
Lee et al. [2023]*	0.092	0.046	0.026	0.015	0.162	0.069	0.525	-	-	0.211
Wang et al. [2023c]	0.363	0.235	0.164	0.118	0.301	0.136	-	-	-	-
Wang et al. [2024a]	0.374	0.230	0.155	0.112	0.279	0.145	0.161	0.483	0.323	0.387
Wu et al. [2023b]	0.383	0.224	0.146	0.104	0.280	0.147	-	-	-	0.758
Liu et al. [2023c]	0.391	0.249	0.172	0.125	0.304	0.160	-	-	-	-
Jin et al. [2024]	0.398	-	-	0.112	0.268	0.157	-	0.501	0.509	0.476
Wang et al. [2022e]	0.413	0.266	0.186	0.136	0.298	0.170	0.429	-	-	-
Kong et al. [2022]	0.423	0.261	0.171	0.116	0.286	0.168	-	0.482	0.563	0.519

finding section generation. In addition, LLM-CXR [Lee et al., 2023] presents contrasting results on natural language metrics, with a low BLEU score (BLEU-1: 0.092) and a high CIDEr score (0.525). Disregarding differences in metric versions (e.g., CIDEr and CIDEr-D), this may suggest the model excels in keyword generation, making CIDEr a more reliable metric than BLEU due to its emphasis on keyword importance. Overall, compared with traditional deep learning-based methods, large model-based methods have significantly improved report generation performance on natural language-based metrics, achieving an improvement of more than 10% in nearly all metrics. This highlights the superior language generation capabilities of large models. However, claiming a clear advantage of large model-based methods over traditional models is difficult. First, large model-based methods typically require extensive training data. For instance, MAIRA-2 7B/13B was trained on a combination of four image-report datasets, resulting in unfair comparisons. It is essential to train traditional models on large-scale data to assess performance improvements from large model architecture or data volume. Second, advancements in medical correctness metrics are less significant, likely due to the current lack of specialized models for lesion detection in large model-based methodologies. Finally, compared to traditional models, a key advantage of large models lies in their ability to engage in interactive dialogues, which is crucial for applications such as telehealth, virtual medical consultations, and medical education [Johri et al., 2025]. However, current methods fail to incorporate interactive data in large model training and lack clear evaluation protocols to assess this capability, preventing the advantage of interactive dialogue from being fully realized.

The ability of some general large models to generate reports has not been evaluated on standard benchmarks, and thus these models are not included in the table. For instance, BiomedGPT evaluated its report generation capability by randomly selecting 30 samples from the MIMIC-CXR test set using human-based evaluation. Overall, the evaluation process for large models in report generation remains inconsistent. Variations in evaluation metrics prevent a clear performance hierarchy between general and domain-specific large models. For example, miniGPT-Med outperforms the domain-specific CheXagent on BERT-Sim metric [Zhang et al., 2019] and CheXbert-Sim metric [Smit et al., 2020b], while the domain-specific MAIRA-2 surpasses the general Med-PaLM M on most metrics (e.g., ROUGE-L). However, it is difficult to compare the performance of miniGPT-Med and MAIRA-2. Recently, Zhang et al. [2024b] proposed ReXrank⁸, a public leaderboard designed to evaluate AI-based report generation for chest X-ray images. This platform is essential for standardizing chest X-ray report generation benchmarks and serves as a framework for constructing benchmarks for other types of radiological images. Furthermore, an interface has been made available for users to upload their models.

In conclusion, due to the inconsistent usage of benchmarks, this section can only compare a subset of the reviewed papers. In the five stages, the integration of multimodal inputs has not demonstrated clear advantages and lacks unique designs. Current effective designs focus mainly on image feature extraction, especially through auxiliary loss. During the report generation phase, reinforcement learning effectively enhances specific metrics. However, there are currently no effective designs for loss function. Additionally, large models

⁸<https://reXrank.ai/>

have shown considerable language-related capabilities, but improvements are needed to generate results with higher medical correctness. Further experiments are required to validate their superiority over traditional methods in report generation when using comparable training datasets.

9 Challenges and Future Works

Although automated systems offer promising efficiency for clinical workflows, current methods have not produced very high-quality reports. This section evaluates the current progress in automated report generation development and identifies potential areas for improvement.

9.1 Constructing and utilizing multi-modal data

Considering report generation as a multi-modal problem is more aligned with clinical practice [Tu et al., 2024, Yan et al., 2023]. Babar et al. [2021a] have proven the ineffectiveness of simple encoder-decoder report generation models and mentioned that adding prior knowledge can be a promising method. However, the current utilization of multi-modal data remains under-explored. Firstly, the methods for non-image feature extraction and the fusion of multi-modality data are often limited and simplistic, such as using graph encoding for the knowledge base and attention mechanisms for feature fusion. Additionally, there is a lack of comparative analysis on the effectiveness of these methods. For instance, the reviewed papers do not compare two attention fusion approaches: one where concatenated features from different modalities are used as the input for Q, K, and V, and another where one modality is used for Q, and the other modality for K and V. Secondly, there is inadequate utilization of complementary information across input modalities and a lack of targeted design for filtering different types of noise. Thirdly, the construction of the knowledge base is imperfect. The pre-defined graph [Zhang et al., 2020] is overly simplistic. Despite Radgraph being a vast knowledge base, it is solely derived from reports, lacking the relationship between images and reports, such as organ recognition or understanding of typical radiological scenarios, which radiologists possess. The Chest Imagenome dataset [Wu et al., 2021a] provides organ recognition annotations, alleviating the problem. Additionally, these publicly available knowledge bases only concentrate on chest X-rays. RadGraph-XL addresses this by expanding knowledge graph construction to other medical imaging modalities and anatomies. This expansion facilitates the development of general medical knowledge databases.

9.2 Evaluation of medical correctness

Evaluating the medical correctness of generated reports is crucial for clinical applications. Compared to previous works [Messina et al., 2022, Liao et al., 2023], recent works have paid more attention to it, but still have two shortcomings. First, in the reviewed articles, medical correctness evaluation has only been applied to chest X-ray reports. Second, the evaluation is based on the automatic labeler of radiology reports, resulting in a limited scope and reliability of the labels. For instance, the labeler in the medical efficacy metric only targeted 14 types of diseases and the average F1 score is around 0.798 [Smit et al., 2020a]. Improving the accuracy and scale of automatic labeling tools can help optimize the evaluation process.

9.3 Large public datasets and unified benchmark comparison

As shown in Table 2, most public datasets are limited in size. Deep learning-based techniques require a large amount of data. The contemporary prevalence of large models underscores this need for large data volumes. Among the datasets, the MIMIC dataset and recently released CheXpert Plus are relatively large, but only include chest X-ray data. Large datasets targeting other image modalities and diseases need to be constructed. In addition, while MIMIC-CXR is a well-established benchmark compared to IU-Xray, dataset utilization lacks standardization, complicating comparisons. We urge papers using the MIMIC dataset to define their training, validation, and testing partitions, with explicit disclosure of the filtration method, particularly for the testing dataset. Open-sourcing the code can also facilitate the comparison of different methods on a unified test set. The recently introduced ReXrank leaderboard significantly addresses benchmark inconsistency, marking a milestone contribution despite focusing only on chest X-rays.

9.4 Human-AI interaction and explainability

Effective human-computer interaction can improve the explainability of models. Recent studies have increasingly prioritized human-computer interaction. For traditional deep learning-based methods, Tanwani et al. [2022] constructed a visual question-answering system for the generation of medical reports, and Tanida et al. [2023] linked the output results to image regions using object detection, allowing users to select areas of interest and receive the corresponding language explanations. However, these systems lack comprehensive language understanding, limiting meaningful interaction with users. The advent of large models with advanced language comprehension presents new opportunities. General dialogue systems, such as GPT-4, have demonstrated the ability to articulate their thought processes and provide rigorous logical answers. In contrast, specialized large models for report generation have yet to achieve comparable advancements. Eight recent studies have explored report-generation tasks using large models. One of these studies produces additional bounding boxes to indicate the areas targeted by the generated descriptions [Bannur et al., 2024]. However, the design of prompts is still relatively uniform,

and none have tested whether these models can articulate their thought processes by responding to queries such as “How did you determine the location of the lesion?” Additionally, while some research has incorporated patient clinical histories at the input stage, there has been no exploration of scenarios where users might wish to provide medical history in queries, for example “I previously had tuberculosis. What impact would that have?”

Providing quantitative results can also improve the explainability of the system and increase user trust. Although measuring uncertainty is prevalent in medical image analysis [Lambert et al., 2024], only one reviewed paper [Wang et al., 2024b] offered quantitative assessments of system uncertainty, suggesting a promising avenue for future research.

9.5 Standardized report generation

Most existing methods primarily address unstructured report generation. In contrast, structured reporting offers several advantages, including time savings [Hong and Kahn, 2013, Nobel et al., 2022], error reduction, lower communication costs associated with ambiguous language, and improved data consistency and comparability for the development of data records and research. Pellegrini et al. [2023a] developed a structured template and released a related dataset. This promising start could pave the way for further exploration in this direction. It is noteworthy that effective template design is essential for structural reporting; poorly designed templates can fragment related processes into subcategories, disrupt cohesive synthesis, and hinder comprehensive understanding, especially in multi-compartmental pathological conditions. Currently, research on designing effective structured report templates is limited, making it a valuable area for investigation.

10 Conclusions

In this study, we have conducted a detailed technical review of 100 papers on automatic medical report generation published in the years 2021, 2022, 2023, and 2024 to showcase both mainstream and novel techniques. Our particular focus lies on the utilization and fusion of multi-modality data. The analysis of methods is structured based on the components of the report generation pipeline, presenting the key techniques for each component. Moreover, we examine recent advancements in large model applications and model explainability and summarize current publicly available datasets and evaluation methods, including both quantitative and qualitative assessments. Subsequently, we compare the results of a subset of the reviewed articles under the same experimental setting. Finally, we outline the current challenges and propose future directions for the generation of medical reports. In general, sustained progress is needed to produce high-quality reports. This survey aims to offer a comprehensive overview of report generation techniques, emphasize critical issues, and assist researchers in quickly grasping recent advances in the field to build stronger systems for clinical practice.

References

- Brandon Abela, Jumana Abu-Khalaf, Chi-Wei Robin Yang, Martin Masek, and Ashu Gupta. Automated radiology report generation using a transformer-template system: Improved clinical accuracy and an assessment of clinical safety. In *AI 2022: Advances in Artificial Intelligence: 35th Australasian Joint Conference, AI 2022, Perth, WA, Australia, December 5–8, 2022, Proceedings*, pages 530–543. Springer, 2022.
- Omar Alfarghaly, Rana Khaled, Abeer Elkorany, Maha Helal, and Aly Fahmy. Automated radiology report generation using conditioned transformers. *Informatics in Medicine Unlocked*, 24:100557, 2021.
- Asma Alkhalidi, Raneem Alnajim, Layan Alabdullatef, Rawan Alyahya, Jun Chen, Deyao Zhu, Ahmed Alsinan, and Mohamed Elhoseiny. Minigt-med: Large language model as a general interface for radiology diagnosis. *arXiv preprint arXiv:2407.04106*, 2024.
- Emily Alsentzer, John Murphy, William Boag, Wei-Hung Weng, Di Jindi, Tristan Naumann, and Matthew McDermott. Publicly available clinical bert embeddings. In *Proceedings of the 2nd Clinical Natural Language Processing Workshop*, pages 72–78, 2019.
- Zaheer Babar, Twan van Laarhoven, and Elena Marchiori. Encoder-decoder models for chest x-ray report generation perform no better than unconditioned baselines. *Plos one*, 16(11):e0259639, 2021a.
- Zaheer Babar, Twan van Laarhoven, Fabio Massimo Zanzotto, and Elena Marchiori. Evaluating diagnostic content of ai-generated radiology reports of chest x-rays. *Artificial Intelligence in Medicine*, 116:102075, 2021b.
- Satanjeev Banerjee and Alon Lavie. Meteor: An automatic metric for mt evaluation with improved correlation with human judgments. In *Proceedings of the acl workshop on intrinsic and extrinsic evaluation measures for machine translation and/or summarization*, pages 65–72, 2005.
- Shruthi Bannur, Stephanie Hyland, Qianchu Liu, Fernando Perez-Garcia, Maximilian Ilse, Daniel C Castro, Benedikt Boecking, Harshita Sharma, Kenza Bouzid, Anja Thieme, et al. Learning to exploit temporal structure for biomedical vision-language processing. In *Proceedings of the IEEE/CVF Conference on Computer Vision and Pattern Recognition*, pages 15016–15027, 2023.
- Shruthi Bannur, Kenza Bouzid, Daniel C Castro, Anton Schwaighofer, Sam Bond-Taylor, Maximilian Ilse, Fernando Pérez-García, Valentina Salvatelli, Harshita Sharma, Felix Meissen, et al. Maira-2: Grounded radiology report generation. *arXiv preprint arXiv:2406.04449*, 2024.

- Djamila-Romaissa Beddiar, Mourad Oussalah, and Tapio Seppänen. Automatic captioning for medical imaging (mic): a rapid review of literature. *Artificial Intelligence Review*, 56(5):4019–4076, 2023.
- Hadrien Bertrand, Mohammad Hashir, and Joseph Paul Cohen. Do lateral views help automated chest x-ray predictions? *arXiv preprint arXiv:1904.08534*, 2019.
- Tom Brown, Benjamin Mann, Nick Ryder, Melanie Subbiah, Jared D Kaplan, Prafulla Dhariwal, Arvind Neelakantan, Pranav Shyam, Girish Sastry, Amanda Askell, et al. Language models are few-shot learners. *Advances in neural information processing systems*, 33: 1877–1901, 2020.
- Yiming Cao, Lizhen Cui, Fuqiang Yu, Lei Zhang, Zhen Li, Ning Liu, and Yonghui Xu. Kdtnet: medical image report generation via knowledge-driven transformer. In *Database Systems for Advanced Applications: 27th International Conference, DASFAA 2022, Virtual Event, April 11–14, 2022, Proceedings, Part III*, pages 117–132. Springer, 2022.
- Yiming Cao, Lizhen Cui, Lei Zhang, Fuqiang Yu, Ziheng Cheng, Zhen Li, Yonghui Xu, and Chunyan Miao. Cmt: Cross-modal memory transformer for medical image report generation. In *International Conference on Database Systems for Advanced Applications*, pages 415–424. Springer, 2023.
- Pierre Chambon, Jean-Benoit Delbrouck, Thomas Sounack, Shih-Cheng Huang, Zhihong Chen, Maya Varma, Steven QH Truong, Chu The Chuong, and Curtis P. Langlotz. Chexpert plus: Augmenting a large chest x-ray dataset with text radiology reports, patient demographics and additional image formats, 2024. URL <https://arxiv.org/abs/2405.19538>.
- Weipeng Chen, Haiwei Pan, Kejia Zhang, Xin Du, and Qianna Cui. Vmeknet: Visual memory and external knowledge based network for medical report generation. In *PRICAI 2022: Trends in Artificial Intelligence: 19th Pacific Rim International Conference on Artificial Intelligence, PRICAI 2022, Shanghai, China, November 10–13, 2022, Proceedings, Part I*, pages 188–201. Springer, 2022.
- Zhihong Chen, Yan Song, Tsung-Hui Chang, and Xiang Wan. Generating radiology reports via memory-driven transformer. In *Proceedings of the 2020 Conference on Empirical Methods in Natural Language Processing (EMNLP)*, pages 1439–1449, 2020.
- Zhihong Chen, Yaling Shen, Yan Song, and Xiang Wan. Cross-modal memory networks for radiology report generation. In *Proceedings of the 59th Annual Meeting of the Association for Computational Linguistics and the 11th International Joint Conference on Natural Language Processing (Volume 1: Long Papers)*, pages 5904–5914, 2021.
- Zhihong Chen, Maya Varma, Jean-Benoit Delbrouck, Magdalini Paschali, Louis Blankemeier, Dave Van Veen, Jeya Maria Jose Valanarasu, Alaa Youssef, Joseph Paul Cohen, Eduardo Pontes Reis, et al. Chexagent: Towards a foundation model for chest x-ray interpretation. *arXiv preprint arXiv:2401.12208*, 2024.
- Wei-Lin Chiang, Zhuohan Li, Zi Lin, Ying Sheng, Zhanghao Wu, Hao Zhang, Lianmin Zheng, Siyuan Zhuang, Yonghao Zhuang, Joseph E Gonzalez, et al. Vicuna: An open-source chatbot impressing gpt-4 with 90%* chatgpt quality. See <https://vicuna.lmsys.org> (accessed 14 April 2023), 2(3):6, 2023.
- Marcella Cornia, Matteo Stefanini, Lorenzo Baraldi, and Rita Cucchiara. Meshed-memory transformer for image captioning. In *Proceedings of the IEEE/CVF conference on computer vision and pattern recognition*, pages 10578–10587, 2020.
- Francesco Dalla Serra, William Clackett, Hamish MacKinnon, Chaoyang Wang, Fani Deligianni, Jeff Dalton, and Alison Q O’Neil. Multimodal generation of radiology reports using knowledge-grounded extraction of entities and relations. In *Proceedings of the 2nd Conference of the Asia-Pacific Chapter of the Association for Computational Linguistics and the 12th International Joint Conference on Natural Language Processing*, pages 615–624, 2022.
- Francesco Dalla Serra, Chaoyang Wang, Fani Deligianni, Jeff Dalton, and Alison Q O’Neil. Controllable chest x-ray report generation from longitudinal representations. In *The 2023 Conference on Empirical Methods in Natural Language Processing*, 2023a.
- Francesco Dalla Serra, Chaoyang Wang, Fani Deligianni, Jeffrey Dalton, and Alison Q O’Neil. Finding-aware anatomical tokens for chest x-ray automated reporting. In *International Workshop on Machine Learning in Medical Imaging*, pages 413–423. Springer, 2023b.
- Jean-Benoit Delbrouck, Pierre Chambon, Christian Bluethgen, Emily Tsai, Omar Almusa, and Curtis Langlotz. Improving the factual correctness of radiology report generation with semantic rewards. In *Findings of the Association for Computational Linguistics: EMNLP 2022*, pages 4348–4360, 2022.
- Jean-Benoit Delbrouck, Pierre Chambon, Zhihong Chen, Maya Varma, Andrew Johnston, Louis Blankemeier, Dave Van Veen, Tan Bui, Steven Truong, and Curtis Langlotz. Radgraph-xl: A large-scale expert-annotated dataset for entity and relation extraction from radiology reports. In *Findings of the Association for Computational Linguistics ACL 2024*, pages 12902–12915, 2024.
- Dina Demner-Fushman, Marc D Kohli, Marc B Rosenman, Sonya E Shooshan, Laritza Rodriguez, Sameer Antani, George R Thoma, and Clement J McDonald. Preparing a collection of radiology examinations for distribution and retrieval. *Journal of the American Medical Informatics Association*, 23(2):304–310, 2016.
- Finale Doshi-Velez and Been Kim. Towards a rigorous science of interpretable machine learning. *arXiv preprint arXiv:1702.08608*, 2017.
- Xin Du, Haiwei Pan, Kejia Zhang, Shuning He, Xiaofei Bian, and Weipeng Chen. Automatic report generation method based on multiscale feature extraction and word attention network. In *Asia-Pacific Web (APWeb) and Web-Age Information Management (WAIM) Joint International Conference on Web and Big Data*, pages 520–528. Springer, 2022.

- Mark Endo, Rayan Krishnan, Viswesh Krishna, Andrew Y Ng, and Pranav Rajpurkar. Retrieval-based chest x-ray report generation using a pre-trained contrastive language-image model. In *Machine Learning for Health*, pages 209–219. PMLR, 2021.
- Patrick Esser, Robin Rombach, and Bjorn Ommer. Taming transformers for high-resolution image synthesis. In *Proceedings of the IEEE/CVF conference on computer vision and pattern recognition*, pages 12873–12883, 2021.
- Gaurav O Gajbhiye, Abhijeet V Nandedkar, and Ibrahima Faye. Translating medical image to radiological report: Adaptive multilevel multi-attention approach. *Computer Methods and Programs in Biomedicine*, 221:106853, 2022.
- Yarin Gal and Zoubin Ghahramani. Dropout as a bayesian approximation: Representing model uncertainty in deep learning. In *international conference on machine learning*, pages 1050–1059. PMLR, 2016.
- Tiancheng Gu, Dongnan Liu, Zhiyuan Li, and Weidong Cai. Complex organ mask guided radiology report generation. In *Proceedings of the IEEE/CVF Winter Conference on Applications of Computer Vision*, pages 7995–8004, 2024.
- Xuechen Guo, Wenhao Chai, Shi-Yan Li, and Gaoang Wang. LLaVA-ultra: Large chinese language and vision assistant for ultrasound. In *ACM Multimedia 2024*, 2024. URL <https://openreview.net/forum?id=7ZYEoB71Vd>.
- Zhongyi Han, Benzhen Wei, Xiaoming Xi, Bo Chen, Yilong Yin, and Shuo Li. Unifying neural learning and symbolic reasoning for spinal medical report generation. *Medical image analysis*, 67:101872, 2021.
- Kaiming He, Xiangyu Zhang, Shaoqing Ren, and Jian Sun. Deep residual learning for image recognition. In *Proceedings of the IEEE conference on computer vision and pattern recognition*, pages 770–778, 2016.
- Kaiming He, Haoqi Fan, Yuxin Wu, Saining Xie, and Ross Girshick. Momentum contrast for unsupervised visual representation learning. In *Proceedings of the IEEE/CVF conference on computer vision and pattern recognition*, pages 9729–9738, 2020.
- Sepp Hochreiter and Jürgen Schmidhuber. Long short-term memory. *Neural computation*, 9(8):1735–1780, 1997.
- Yi Hong and Charles E Kahn. Content analysis of reporting templates and free-text radiology reports. *Journal of digital imaging*, 26: 843–849, 2013.
- Ahmed Hosny, Chintan Parmar, John Quackenbush, Lawrence H Schwartz, and Hugo JWL Aerts. Artificial intelligence in radiology. *Nature Reviews Cancer*, 18(8):500–510, 2018.
- Benjamin Hou, Georgios Kaissis, Ronald M Summers, and Bernhard Kainz. Ratchet: Medical transformer for chest x-ray diagnosis and reporting. In *Medical Image Computing and Computer Assisted Intervention–MICCAI 2021: 24th International Conference, Strasbourg, France, September 27–October 1, 2021, Proceedings, Part VII 24*, pages 293–303. Springer, 2021a.
- Daibing Hou, Zijian Zhao, Yuying Liu, Faliang Chang, and Sanyuan Hu. Automatic report generation for chest x-ray images via adversarial reinforcement learning. *IEEE Access*, 9:21236–21250, 2021b.
- Wenjun Hou, Kaishuai Xu, Yi Cheng, Wenjie Li, and Jiang Liu. Organ: observation-guided radiology report generation via tree reasoning. *arXiv preprint arXiv:2306.06466*, 2023.
- Edward J Hu, Yelong Shen, Phillip Wallis, Zeyuan Allen-Zhu, Yanzhi Li, Shean Wang, Lu Wang, and Weizhu Chen. Lora: Low-rank adaptation of large language models. *arXiv preprint arXiv:2106.09685*, 2021.
- Gao Huang, Zhuang Liu, Laurens Van Der Maaten, and Kilian Q Weinberger. Densely connected convolutional networks. In *Proceedings of the IEEE conference on computer vision and pattern recognition*, pages 4700–4708, 2017.
- Jia-Hong Huang, Ting-Wei Wu, Chao-Han Huck Yang, and Marcel Worring. Deep context-encoding network for retinal image captioning. In *2021 IEEE International Conference on Image Processing (ICIP)*, pages 3762–3766. IEEE, 2021a.
- Jia-Hong Huang, C-H Huck Yang, Fangyu Liu, Meng Tian, Yi-Chieh Liu, Ting-Wei Wu, I Lin, Kang Wang, Hiromasa Morikawa, Henghua Chang, et al. Deepoph: medical report generation for retinal images via deep models and visual explanation. In *Proceedings of the IEEE/CVF winter conference on applications of computer vision*, pages 2442–2452, 2021b.
- Jia-Hong Huang, Ting-Wei Wu, C-H Huck Yang, Zenglin Shi, I Lin, Jesper Tegner, Marcel Worring, et al. Non-local attention improves description generation for retinal images. In *Proceedings of the IEEE/CVF winter conference on applications of computer vision*, pages 1606–1615, 2022.
- Zhongzhen Huang, Xiaofan Zhang, and Shaoting Zhang. Kiut: Knowledge-injected u-transformer for radiology report generation. In *Proceedings of the IEEE/CVF Conference on Computer Vision and Pattern Recognition*, pages 19809–19818, 2023.
- Stephanie L Hyland, Shruthi Bannur, Kenza Bouzid, Daniel C Castro, Mercy Ranjit, Anton Schwaighofer, Fernando Pérez-García, Valentina Salvatelli, Shaury Srivastav, Anja Thieme, et al. Maira-1: A specialised large multimodal model for radiology report generation. *arXiv preprint arXiv:2311.13668*, 2023.
- Jeremy Irvin, Pranav Rajpurkar, Michael Ko, Yifan Yu, Silvana Ciurea-Ilcus, Chris Chute, Henrik Marklund, Behzad Haghgoo, Robyn Ball, Katie Shpanskaya, et al. Chexpert: A large chest radiograph dataset with uncertainty labels and expert comparison. In *Proceedings of the AAAI conference on artificial intelligence*, volume 33, pages 590–597, 2019.

- Saahil Jain, Ashwin Agrawal, Adriel Saporta, Steven QH Truong, Du Nguyen Duong, Tan Bui, Pierre Chambon, Yuhao Zhang, Matthew P Lungren, Andrew Y Ng, et al. Radgraph: Extracting clinical entities and relations from radiology reports. *arXiv preprint arXiv:2106.14463*, 2021.
- Jaehwan Jeong, Katherine Tian, Andrew Li, Sina Hartung, Subathra Adithan, Fardad Behzadi, Juan Calle, David Osayande, Michael Pohlen, and Pranav Rajpurkar. Multimodal image-text matching improves retrieval-based chest x-ray report generation. In *Medical Imaging with Deep Learning*, pages 978–990. PMLR, 2024.
- Xing Jia, Yun Xiong, Jiawei Zhang, Yao Zhang, Blackley Suzanne, Yangyong Zhu, and Chunlei Tang. Radiology report generation for rare diseases via few-shot transformer. In *IEEE International Conference on Bioinformatics and Biomedicine (BIBM)*, pages 1347–1352. IEEE, 2021.
- Xing Jia, Yun Xiong, Jiawei Zhang, Yao Zhang, Yangyong Zhu, and S Yu Philip. Few-shot radiology report generation via knowledge transfer and multi-modal alignment. In *2022 IEEE International Conference on Bioinformatics and Biomedicine (BIBM)*, pages 1574–1579. IEEE, 2022.
- Albert Q Jiang, Alexandre Sablayrolles, Arthur Mensch, Chris Bamford, Devendra Singh Chaplot, Diego de las Casas, Florian Bressand, Gianna Lengyel, Guillaume Lample, Lucile Saulnier, et al. Mistral 7b. *arXiv preprint arXiv:2310.06825*, 2023.
- Haibo Jin, Haoxuan Che, Yi Lin, and Hao Chen. Promptmrg: Diagnosis-driven prompts for medical report generation. In *Proceedings of the AAAI Conference on Artificial Intelligence*, volume 38, pages 2607–2615, 2024.
- Alistair EW Johnson, Tom J Pollard, Seth J Berkowitz, Nathaniel R Greenbaum, Matthew P Lungren, Chih-ying Deng, Roger G Mark, and Steven Horng. Mimic-cxr, a de-identified publicly available database of chest radiographs with free-text reports. *Scientific data*, 6(1):317, 2019a.
- Alistair EW Johnson, Tom J Pollard, Nathaniel R Greenbaum, Matthew P Lungren, Chih-ying Deng, Yifan Peng, Zhiyong Lu, Roger G Mark, Seth J Berkowitz, and Steven Horng. Mimic-cxr-jpg, a large publicly available database of labeled chest radiographs. *arXiv preprint arXiv:1901.07042*, 2019b.
- Shreya Johri, Jaehwan Jeong, Benjamin A Tran, Daniel I Schlessinger, Shannon Wongvibulsin, Leandra A Barnes, Hong-Yu Zhou, Zhuo Ran Cai, Eliezer M Van Allen, David Kim, et al. An evaluation framework for clinical use of large language models in patient interaction tasks. *Nature Medicine*, pages 1–10, 2025.
- Andre C Kalil, Mark L Metersky, Michael Klompas, John Muscedere, Daniel A Sweeney, Lucy B Palmer, Lena M Napolitano, Naomi P O’Grady, John G Bartlett, Jordi Carratalà, et al. Management of adults with hospital-acquired and ventilator-associated pneumonia: 2016 clinical practice guidelines by the infectious diseases society of america and the american thoracic society. *Clinical infectious diseases*, 63(5):e61–e111, 2016.
- Navdeep Kaur and Ajay Mittal. Radiobert: A deep learning-based system for medical report generation from chest x-ray images using contextual embeddings. *Journal of Biomedical Informatics*, 135:104220, 2022a.
- Navdeep Kaur and Ajay Mittal. Cadxreport: Chest x-ray report generation using co-attention mechanism and reinforcement learning. *Computers in Biology and Medicine*, 145:105498, 2022b.
- Navdeep Kaur, Ajay Mittal, and Gurpreem Singh. Methods for automatic generation of radiological reports of chest radiographs: a comprehensive survey. *Multimedia Tools and Applications*, 81(10):13409–13439, 2022.
- Christopher J Kelly, Alan Karthikesalingam, Mustafa Suleyman, Greg Corrado, and Dominic King. Key challenges for delivering clinical impact with artificial intelligence. *BMC medicine*, 17:1–9, 2019.
- Diederik P Kingma and Max Welling. Auto-encoding variational bayes. *arXiv preprint arXiv:1312.6114*, 2013.
- Alexander Kirillov, Eric Mintun, Nikhila Ravi, Hanzi Mao, Chloe Rolland, Laura Gustafson, Tete Xiao, Spencer Whitehead, Alexander C Berg, Wan-Yen Lo, et al. Segment anything. In *Proceedings of the IEEE/CVF International Conference on Computer Vision*, pages 4015–4026, 2023.
- Ming Kong, Zhengxing Huang, Kun Kuang, Qiang Zhu, and Fei Wu. Transq: Transformer-based semantic query for medical report generation. In *Medical Image Computing and Computer Assisted Intervention–MICCAI 2022: 25th International Conference, Singapore, September 18–22, 2022, Proceedings, Part VIII*, pages 610–620. Springer, 2022.
- Benjamin Lambert, Florence Forbes, Senan Doyle, Harmonie Dehaene, and Michel Dojat. Trustworthy clinical ai solutions: a unified review of uncertainty quantification in deep learning models for medical image analysis. *Artificial Intelligence in Medicine*, page 102830, 2024.
- Curtis P Langlotz. Radlex: a new method for indexing online educational materials, 2006.
- Jonathan Laserson, Christine Dan Lantsman, Michal Cohen-Sfady, Itamar Tamir, Eli Goz, Chen Brestel, Shir Bar, Maya Atar, and Eldad Elnekave. Textray: Mining clinical reports to gain a broad understanding of chest x-rays. In *Medical Image Computing and Computer Assisted Intervention–MICCAI 2018: 21st International Conference, Granada, Spain, September 16–20, 2018, Proceedings, Part II 11*, pages 553–561. Springer, 2018.

- Hojun Lee, Hyunjun Cho, Jieun Park, Jinyeong Chae, and Jihie Kim. Cross encoder-decoder transformer with global-local visual extractor for medical image captioning. *Sensors*, 22(4):1429, 2022.
- Jinhyuk Lee, Wonjin Yoon, Sungdong Kim, Donghyeon Kim, Sunkyu Kim, Chan Ho So, and Jaewoo Kang. Biobert: a pre-trained biomedical language representation model for biomedical text mining. *Bioinformatics*, 36(4):1234–1240, 2020.
- Suhyeon Lee, Won Jun Kim, Jinho Chang, and Jong Chul Ye. Llm-cxr: Instruction-finetuned llm for cxr image understanding and generation. *arXiv preprint arXiv:2305.11490*, 2023.
- Chunyu Li, Cliff Wong, Sheng Zhang, Naoto Usuyama, Haotian Liu, Jianwei Yang, Tristan Naumann, Hoifung Poon, and Jianfeng Gao. Llava-med: Training a large language-and-vision assistant for biomedicine in one day. *Advances in Neural Information Processing Systems*, 36, 2024.
- Jun Li, Shibo Li, Ying Hu, and Hui Ren Tao. A self-guided framework for radiology report generation. In *Medical Image Computing and Computer Assisted Intervention—MICCAI 2022: 25th International Conference, Singapore, September 18–22, 2022, Proceedings, Part VIII*, pages 588–598. Springer, 2022a.
- Junnan Li, Dongxu Li, Silvio Savarese, and Steven Hoi. Blip-2: Bootstrapping language-image pre-training with frozen image encoders and large language models. In *International conference on machine learning*, pages 19730–19742. PMLR, 2023a.
- Mingjie Li, Fuyu Wang, Xiaojun Chang, and Xiaodan Liang. Auxiliary signal-guided knowledge encoder-decoder for medical report generation. *arXiv preprint arXiv:2006.03744*, 2020.
- Mingjie Li, Wenjia Cai, Rui Liu, Yuetian Weng, Xiaoyun Zhao, Cong Wang, Xin Chen, Zhong Liu, Caineng Pan, Mengke Li, et al. Ffa-ir: Towards an explainable and reliable medical report generation benchmark. In *Thirty-fifth Conference on Neural Information Processing Systems Datasets and Benchmarks Track (Round 2)*, 2021.
- Mingjie Li, Wenjia Cai, Karin Verspoor, Shirui Pan, Xiaodan Liang, and Xiaojun Chang. Cross-modal clinical graph transformer for ophthalmic report generation. In *Proceedings of the IEEE/CVF Conference on Computer Vision and Pattern Recognition*, pages 20656–20665, 2022b.
- Mingjie Li, Bingqian Lin, Zicong Chen, Haokun Lin, Xiaodan Liang, and Xiaojun Chang. Dynamic graph enhanced contrastive learning for chest x-ray report generation. In *Proceedings of the IEEE/CVF Conference on Computer Vision and Pattern Recognition*, pages 3334–3343, 2023b.
- Mingjie Li, Rui Liu, Fuyu Wang, Xiaojun Chang, and Xiaodan Liang. Auxiliary signal-guided knowledge encoder-decoder for medical report generation. *World Wide Web*, 26(1):253–270, 2023c.
- Qingqiu Li, Jilan Xu, Runtian Yuan, Mohan Chen, Yuejie Zhang, Rui Feng, Xiaobo Zhang, and Shang Gao. Enhanced knowledge injection for radiology report generation. In *2023 IEEE International Conference on Bioinformatics and Biomedicine (BIBM)*, pages 2053–2058. IEEE, 2023d.
- Yaowei Li, Bang Yang, Xuxin Cheng, Zhihong Zhu, Hongxiang Li, and Yuexian Zou. Unify, align and refine: Multi-level semantic alignment for radiology report generation. In *Proceedings of the IEEE/CVF International Conference on Computer Vision*, pages 2863–2874, 2023e.
- Yuxiang Liao, Hantao Liu, and Irena Spasić. Deep learning approaches to automatic radiology report generation: A systematic review. *Informatics in Medicine Unlocked*, page 101273, 2023.
- Chin-Yew Lin. Rouge: A package for automatic evaluation of summaries. In *Text summarization branches out*, pages 74–81, 2004.
- Zhihong Lin, Donghao Zhang, Danli Shi, Renjing Xu, Qingyi Tao, Lin Wu, Mingguang He, and Zongyuan Ge. Contrastive pre-training and linear interaction attention-based transformer for universal medical reports generation. *Journal of Biomedical Informatics*, page 104281, 2023.
- Chang Liu, Yuanhe Tian, and Yan Song. A systematic review of deep learning-based research on radiology report generation. *arXiv preprint arXiv:2311.14199*, 2023a.
- Fenglin Liu, Shen Ge, and Xian Wu. Competence-based multimodal curriculum learning for medical report generation. In *Proceedings of the 59th Annual Meeting of the Association for Computational Linguistics and the 11th International Joint Conference on Natural Language Processing (Volume 1: Long Papers)*, pages 3001–3012, 2021a.
- Fenglin Liu, Xian Wu, Shen Ge, Wei Fan, and Yuexian Zou. Exploring and distilling posterior and prior knowledge for radiology report generation. In *Proceedings of the IEEE/CVF conference on computer vision and pattern recognition*, pages 13753–13762, 2021b.
- Fenglin Liu, Changchang Yin, Xian Wu, Shen Ge, Ping Zhang, and Xu Sun. Contrastive attention for automatic chest x-ray report generation. In *Findings of the Association for Computational Linguistics: ACL-IJCNLP*, page 269–280, 2021c.
- Fenglin Liu, Chenyu You, Xian Wu, Shen Ge, Xu Sun, et al. Auto-encoding knowledge graph for unsupervised medical report generation. *Advances in Neural Information Processing Systems*, 34:16266–16279, 2021d.

- Guangyi Liu, Yinghong Liao, Fuyu Wang, Bin Zhang, Lu Zhang, Xiaodan Liang, Xiang Wan, Shaolin Li, Zhen Li, Shuixing Zhang, et al. Medical-vlbert: Medical visual language bert for covid-19 ct report generation with alternate learning. *IEEE Transactions on Neural Networks and Learning Systems*, 32(9):3786–3797, 2021e.
- Guanxiong Liu, Tzu-Ming Harry Hsu, Matthew McDermott, Willie Boag, Wei-Hung Weng, Peter Szolovits, and Marzyeh Ghassemi. Clinically accurate chest x-ray report generation. In *Machine Learning for Healthcare Conference*, pages 249–269. PMLR, 2019.
- Haotian Liu, Chunyuan Li, Qingyang Wu, and Yong Jae Lee. Visual instruction tuning. *Advances in neural information processing systems*, 36, 2024.
- Pengfei Liu, Weizhe Yuan, Jinlan Fu, Zhengbao Jiang, Hiroaki Hayashi, and Graham Neubig. Pre-train, prompt, and predict: A systematic survey of prompting methods in natural language processing. *ACM Computing Surveys*, 55(9):1–35, 2023b.
- Zhizhe Liu, Zhenfeng Zhu, Shuai Zheng, Yawei Zhao, Kunlun He, and Yao Zhao. From observation to concept: A flexible multi-view paradigm for medical report generation. *IEEE Transactions on Multimedia*, 2023c.
- Robert J McDonald, Kara M Schwartz, Laurence J Eckel, Felix E Diehn, Christopher H Hunt, Brian J Bartholmai, Bradley J Erickson, and David F Kallmes. The effects of changes in utilization and technological advancements of cross-sectional imaging on radiologist workload. *Academic radiology*, 22(9):1191–1198, 2015.
- Pablo Messina, Pablo Pino, Denis Parra, Alvaro Soto, Cecilia Besa, Sergio Uribe, Marcelo Andía, Cristian Tejos, Claudia Prieto, and Daniel Capurro. A survey on deep learning and explainability for automatic report generation from medical images. *ACM Computing Surveys (CSUR)*, 54(10s):1–40, 2022.
- Zahra Mirikharaji, Kumar Abhishek, Alceu Bissoto, Catarina Barata, Sandra Avila, Eduardo Valle, M Emre Celebi, and Ghassan Hamarneh. A survey on deep learning for skin lesion segmentation. *Medical Image Analysis*, page 102863, 2023.
- Yasuhide Miura, Yuhao Zhang, Emily Tsai, Curtis Langlotz, and Dan Jurafsky. Improving factual completeness and consistency of image-to-text radiology report generation. In *Proceedings of the 2021 Conference of the North American Chapter of the Association for Computational Linguistics: Human Language Technologies*, pages 5288–5304, 2021.
- Mashood Mohammad Mohsan, Muhammad Usman Akram, Ghulam Rasool, Norah Saleh Alghamdi, Muhammad Abdullah Aamer Baqai, and Muhammad Abbas. Vision transformer and language model based radiology report generation. *IEEE Access*, 11:1814–1824, 2022.
- Jong Hak Moon, Hyungyung Lee, Woncheol Shin, Young-Hak Kim, and Edward Choi. Multi-modal understanding and generation for medical images and text via vision-language pre-training. *IEEE Journal of Biomedical and Health Informatics*, 26(12):6070–6080, 2022.
- Ivona Najdenkoska, Xiantong Zhen, Marcel Worring, and Ling Shao. Variational topic inference for chest x-ray report generation. In *Medical Image Computing and Computer Assisted Intervention—MICCAI 2021: 24th International Conference, Strasbourg, France, September 27–October 1, 2021, Proceedings, Part III 24*, pages 625–635. Springer, 2021.
- Ivona Najdenkoska, Xiantong Zhen, Marcel Worring, and Ling Shao. Uncertainty-aware report generation for chest x-rays by variational topic inference. *Medical Image Analysis*, 82:102603, 2022.
- Mark Neumann, Daniel King, Iz Beltagy, and Waleed Ammar. Scispace: fast and robust models for biomedical natural language processing. *arXiv preprint arXiv:1902.07669*, 2019.
- J Martijn Nobel, Koos van Geel, and Simon GF Robben. Structured reporting in radiology: a systematic review to explore its potential. *European radiology*, pages 1–18, 2022.
- Sophie Ostmeier, Justin Xu, Zhihong Chen, Maya Varma, Louis Blankemeier, Christian Bluethgen, Arne Edward Michalson, Michael Moseley, Curtis Langlotz, Akshay S Chaudhari, et al. Green: Generative radiology report evaluation and error notation. *arXiv preprint arXiv:2405.03595*, 2024.
- Esha Pahwa, Dwij Mehta, Sanjeet Kapadia, Devansh Jain, and Achleshwar Luthra. Medskip: Medical report generation using skip connections and integrated attention. In *Proceedings of the IEEE/CVF International Conference on Computer Vision*, pages 3409–3415, 2021.
- Abhineet Pandey, Bhawna Paliwal, Abhinav Dhall, Ramanathan Subramanian, and Dwarikanath Mahapatra. This explains that: Congruent image–report generation for explainable medical image analysis with cyclic generative adversarial networks. In *Interpretability of Machine Intelligence in Medical Image Computing, and Topological Data Analysis and Its Applications for Medical Data: 4th International Workshop, iMIMIC 2021, and 1st International Workshop, TDA4MedicalData 2021, Held in Conjunction with MICCAI 2021, Strasbourg, France, September 27, 2021, Proceedings 4*, pages 34–43. Springer, 2021.
- Ting Pang, Peigao Li, and Lijie Zhao. A survey on automatic generation of medical imaging reports based on deep learning. *BioMedical Engineering OnLine*, 22(1):48, 2023.
- Kishore Papineni, Salim Roukos, Todd Ward, and Wei-Jing Zhu. Bleu: a method for automatic evaluation of machine translation. In *Proceedings of the 40th annual meeting of the Association for Computational Linguistics*, pages 311–318, 2002.

- Chantal Pellegrini, Matthias Keicher, Ege Özsoy, and Nassir Navab. Rad-restruct: A novel vqa benchmark and method for structured radiology reporting. In *International Conference on Medical Image Computing and Computer-Assisted Intervention*, pages 409–419. Springer, 2023a.
- Chantal Pellegrini, Ege Özsoy, Benjamin Busam, Nassir Navab, and Matthias Keicher. Radialog: A large vision-language model for radiology report generation and conversational assistance. *arXiv preprint arXiv:2311.18681*, 2023b.
- Fernando Pérez-García, Harshita Sharma, Sam Bond-Taylor, Kenza Bouzid, Valentina Salvatelli, Maximilian Ilse, Shruthi Bannur, Daniel C Castro, Anton Schwaighofer, Matthew P Lungren, et al. Rad-dino: Exploring scalable medical image encoders beyond text supervision. *arXiv preprint arXiv:2401.10815*, 2024.
- Pablo Pino, Denis Parra, Cecilia Besa, and Claudio Lagos. Clinically correct report generation from chest x-rays using templates. In *Machine Learning in Medical Imaging: 12th International Workshop, MLMI 2021, Held in Conjunction with MICCAI 2021, Strasbourg, France, September 27, 2021, Proceedings 12*, pages 654–663. Springer, 2021.
- Han Qin and Yan Song. Reinforced cross-modal alignment for radiology report generation. In *Findings of the Association for Computational Linguistics: ACL 2022*, pages 448–458, 2022.
- Alec Radford, Jong Wook Kim, Chris Hallacy, Aditya Ramesh, Gabriel Goh, Sandhini Agarwal, Girish Sastry, Amanda Askell, Pamela Mishkin, Jack Clark, et al. Learning transferable visual models from natural language supervision. In *International conference on machine learning*, pages 8748–8763. PMLR, 2021.
- Aditya Ramesh, Mikhail Pavlov, Gabriel Goh, Scott Gray, Chelsea Voss, Alec Radford, Mark Chen, and Ilya Sutskever. Zero-shot text-to-image generation. In *International conference on machine learning*, pages 8821–8831. Pmlr, 2021.
- Vignav Ramesh, Nathan A Chi, and Pranav Rajpurkar. Improving radiology report generation systems by removing hallucinated references to non-existent priors. In *Machine Learning for Health*, pages 456–473. PMLR, 2022.
- Suhail Raouf, David Feigin, Arthur Sung, Sabiha Raouf, Lavanya Irugulpati, and Edward C Rosenow III. Interpretation of plain chest roentgenogram. *Chest*, 141(2):545–558, 2012.
- Abi Rimmer. Radiologist shortage leaves patient care at risk, warns royal college. *BMJ: British Medical Journal (Online)*, 359, 2017.
- Khaled Saab, Tao Tu, Wei-Hung Weng, Ryutaro Tanno, David Stutz, Ellery Wulczyn, Fan Zhang, Tim Strother, Chunjong Park, Elahe Vedadi, et al. Capabilities of gemini models in medicine. *arXiv preprint arXiv:2404.18416*, 2024.
- Alexander Selivanov, Oleg Y Rogov, Daniil Chesakov, Artem Shelmanov, Irina Fedulova, and Dmitry V Dylov. Medical image captioning via generative pretrained transformers. *Scientific Reports*, 13(1):4171, 2023.
- Ramprasaath R Selvaraju, Michael Cogswell, Abhishek Das, Ramakrishna Vedantam, Devi Parikh, and Dhruv Batra. Grad-cam: Visual explanations from deep networks via gradient-based localization. In *Proceedings of the IEEE international conference on computer vision*, pages 618–626, 2017.
- Fahad Shamshad, Salman Khan, Syed Waqas Zamir, Muhammad Haris Khan, Munawar Hayat, Fahad Shahbaz Khan, and Huazhu Fu. Transformers in medical imaging: A survey. *Medical Image Analysis*, page 102802, 2023.
- Shashank Shetty, Ananthanarayana VS, and Ajit Mahale. Cross-modal deep learning-based clinical recommendation system for radiology report generation from chest x-rays. *International Journal of Engineering*, 2023.
- Sonit Singh, Sarvnaz Karimi, Kevin Ho-Shon, and Len Hamey. Show, tell and summarise: learning to generate and summarise radiology findings from medical images. *Neural Computing and Applications*, 33:7441–7465, 2021.
- Mehreen Sirshar, Muhammad Faheem Khalil Paracha, Muhammad Usman Akram, Norah Saleh Alghamdi, Syeda Zainab Yousuf Zaidi, and Tatheer Fatima. Attention based automated radiology report generation using cnn and lstm. *Plos one*, 17(1):e0262209, 2022.
- Akshay Smit, Saahil Jain, Pranav Rajpurkar, Anuj Pareek, Andrew Y Ng, and Matthew Lungren. Combining automatic labelers and expert annotations for accurate radiology report labeling using bert. In *Proceedings of the 2020 Conference on Empirical Methods in Natural Language Processing (EMNLP)*, pages 1500–1519, 2020a.
- Akshay Smit, Saahil Jain, Pranav Rajpurkar, Anuj Pareek, Andrew Y Ng, and Matthew P Lungren. Chexbert: combining automatic labelers and expert annotations for accurate radiology report labeling using bert. *arXiv preprint arXiv:2004.09167*, 2020b.
- Xiao Song, Xiaodan Zhang, Junzhong Ji, Ying Liu, and Pengxu Wei. Cross-modal contrastive attention model for medical report generation. In *Proceedings of the 29th International Conference on Computational Linguistics*, pages 2388–2397, 2022.
- Petru Soviany, Radu Tudor Ionescu, Paolo Rota, and Nicu Sebe. Curriculum learning: A survey. *International Journal of Computer Vision*, 130(6):1526–1565, 2022.
- Jinghan Sun, Dong Wei, Liansheng Wang, and Yefeng Zheng. Lesion guided explainable few weak-shot medical report generation. In *Medical Image Computing and Computer Assisted Intervention–MICCAI 2022: 25th International Conference, Singapore, September 18–22, 2022, Proceedings, Part V*, pages 615–625. Springer, 2022.
- Quan Sun, Yuxin Fang, Ledell Wu, Xinlong Wang, and Yue Cao. Eva-clip: Improved training techniques for clip at scale. *arXiv preprint arXiv:2303.15389*, 2023.

- Zhiqing Sun, Zhi-Hong Deng, Jian-Yun Nie, and Jian Tang. Rotate: Knowledge graph embedding by relational rotation in complex space. *arXiv preprint arXiv:1902.10197*, 2019.
- Tim Tanida, Philip Müller, Georgios Kaissis, and Daniel Rueckert. Interactive and explainable region-guided radiology report generation. In *Proceedings of the IEEE/CVF Conference on Computer Vision and Pattern Recognition*, pages 7433–7442, 2023.
- Ajay K Tanwani, Joelle Barral, and Daniel Freedman. Reptsnet: Combining vision with language for automated medical reports. In *Medical Image Computing and Computer Assisted Intervention–MICCAI 2022: 25th International Conference, Singapore, September 18–22, 2022, Proceedings, Part V*, pages 714–724. Springer, 2022.
- Eric Topol. *Deep medicine: how artificial intelligence can make healthcare human again*. Hachette UK, 2019.
- Hugo Touvron, Louis Martin, Kevin Stone, Peter Albert, Amjad Almahairi, Yasmine Babaei, Nikolay Bashlykov, Soumya Batra, Prajjwal Bhargava, Shrubti Bhosale, et al. Llama 2: Open foundation and fine-tuned chat models. *arXiv preprint arXiv:2307.09288*, 2023.
- Tao Tu, Shekoofeh Azizi, Danny Driess, Mike Schaeckermann, Mohamed Amin, Pi-Chuan Chang, Andrew Carroll, Charles Lau, Ryutaro Tanno, Ira Ktena, et al. Towards generalist biomedical ai. *NEJM AI*, 1(3):A10a2300138, 2024.
- Emiel Van Miltenburg, Desmond Elliott, and Piek Vossen. Measuring the diversity of automatic image descriptions. In *Proceedings of the 27th International Conference on Computational Linguistics*, pages 1730–1741, 2018.
- Ashish Vaswani, Noam Shazeer, Niki Parmar, Jakob Uszkoreit, Llion Jones, Aidan N Gomez, Łukasz Kaiser, and Illia Polosukhin. Attention is all you need. *Advances in neural information processing systems*, 30, 2017.
- Ramakrishna Vedantam, C Lawrence Zitnick, and Devi Parikh. Cider: Consensus-based image description evaluation. In *Proceedings of the IEEE conference on computer vision and pattern recognition*, pages 4566–4575, 2015.
- Jun Wang, Abhir Bhalerao, and Yulan He. Cross-modal prototype driven network for radiology report generation. In *Computer Vision–ECCV 2022: 17th European Conference, Tel Aviv, Israel, October 23–27, 2022, Proceedings, Part XXXV*, pages 563–579. Springer, 2022a.
- Jun Wang, Abhir Bhalerao, Terry Yin, Simon See, and Yulan He. Camanet: class activation map guided attention network for radiology report generation. *IEEE Journal of Biomedical and Health Informatics*, 2024a.
- Lin Wang, Munan Ning, Donghuan Lu, Dong Wei, Yefeng Zheng, and Jie Chen. An inclusive task-aware framework for radiology report generation. In *Medical Image Computing and Computer Assisted Intervention–MICCAI 2022: 25th International Conference, Singapore, September 18–22, 2022, Proceedings, Part VIII*, pages 568–577. Springer, 2022b.
- Sheng Wang, Zihao Zhao, Xi Ouyang, Qian Wang, and Dinggang Shen. Chatcad: Interactive computer-aided diagnosis on medical image using large language models. *arXiv preprint arXiv:2302.07257*, 2023a.
- Siyuan Wang, Bo Peng, Yichao Liu, and Qi Peng. Fine-grained medical vision-language representation learning for radiology report generation. In *Proceedings of the 2023 Conference on Empirical Methods in Natural Language Processing*, pages 15949–15956, 2023b.
- Song Wang, Liyan Tang, Mingquan Lin, George Shih, Ying Ding, and Yifan Peng. Prior knowledge enhances radiology report generation. In *AMIA Annual Symposium Proceedings*, volume 2022, page 486. American Medical Informatics Association, 2022c.
- Yixin Wang, Zihao Lin, Zhe Xu, Haoyu Dong, Jie Luo, Jiang Tian, Zhongchao Shi, Lifu Huang, Yang Zhang, Jianping Fan, et al. Trust it or not: Confidence-guided automatic radiology report generation. *Neurocomputing*, page 127374, 2024b.
- Yuhao Wang, Kai Wang, Xiaohong Liu, Tianrun Gao, Jingyue Zhang, and Guangyu Wang. Self adaptive global-local feature enhancement for radiology report generation. In *2023 IEEE International Conference on Image Processing (ICIP)*, pages 2275–2279. IEEE, 2023c.
- Zhanyu Wang, Luping Zhou, Lei Wang, and Xiu Li. A self-boosting framework for automated radiographic report generation. In *Proceedings of the IEEE/CVF Conference on Computer Vision and Pattern Recognition*, pages 2433–2442, 2021.
- Zhanyu Wang, Hongwei Han, Lei Wang, Xiu Li, and Luping Zhou. Automated radiographic report generation purely on transformer: A multicriteria supervised approach. *IEEE Transactions on Medical Imaging*, 41(10):2803–2813, 2022d.
- Zhanyu Wang, Mingkang Tang, Lei Wang, Xiu Li, and Luping Zhou. A medical semantic-assisted transformer for radiographic report generation. In *Medical Image Computing and Computer Assisted Intervention–MICCAI 2022: 25th International Conference, Singapore, September 18–22, 2022, Proceedings, Part III*, pages 655–664. Springer, 2022e.
- Zhanyu Wang, Lingqiao Liu, Lei Wang, and Luping Zhou. Metransformer: Radiology report generation by transformer with multiple learnable expert tokens. In *Proceedings of the IEEE/CVF Conference on Computer Vision and Pattern Recognition*, pages 11558–11567, 2023d.
- Zhanyu Wang, Lingqiao Liu, Lei Wang, and Luping Zhou. R2gengpt: Radiology report generation with frozen llms. *Meta-Radiology*, 1(3):100033, 2023e.
- Ronald J Williams. Simple statistical gradient-following algorithms for connectionist reinforcement learning. *Machine learning*, 8: 229–256, 1992.

- Chaoyi Wu, Xiaoman Zhang, Ya Zhang, Yanfeng Wang, and Weidi Xie. Towards generalist foundation model for radiology by leveraging web-scale 2d&3d medical data, 2023a. URL <https://arxiv.org/abs/2308.02463>.
- Joy Wu, Nkechinyere Agu, Ismini Lourentzou, Arjun Sharma, Joseph Paguio, Jasper Seth Yao, Edward Christopher Dee, William Mitchell, Satyananda Kashyap, Andrea Giovannini, et al. Chest imagenome dataset. *Physio Net*, 2021a.
- Joy T Wu, Ali Syed, Hassan Ahmad, Anup Pillai, Yaniv Gur, Ashutosh Jadhav, Daniel Gruhl, Linda Kato, Mehdi Moradi, and Tanveer Syeda-Mahmood. Ai accelerated human-in-the-loop structuring of radiology reports. In *AMIA Annual Symposium Proceedings*, volume 2020, page 1305, 2021b.
- Xing Wu, Jingwen Li, Jianjia Wang, and Quan Qian. Multimodal contrastive learning for radiology report generation. *Journal of Ambient Intelligence and Humanized Computing*, pages 1–10, 2022.
- Yuexin Wu, I-Chan Huang, and Xiaolei Huang. Token imbalance adaptation for radiology report generation. In *Conference on Health, Inference, and Learning*, pages 72–85. PMLR, 2023b.
- Chen Xu, Bojie Hu, Yufan Jiang, Kai Feng, Zeyang Wang, Shen Huang, Qi Ju, Tong Xiao, and Jingbo Zhu. Dynamic curriculum learning for low-resource neural machine translation. In *Proceedings of the 28th International Conference on Computational Linguistics*, pages 3977–3989, 2020.
- Dexuan Xu, Huashi Zhu, Yu Huang, Zhi Jin, Weiping Ding, Hang Li, and Menglong Ran. Vision-knowledge fusion model for multi-domain medical report generation. *Information Fusion*, 97:101817, 2023.
- Youyuan Xue, Yun Tan, Ling Tan, Jiaohua Qin, and Xuyu Xiang. Generating radiology reports via auxiliary signal guidance and a memory-driven network. *Expert Systems with Applications*, 237:121260, 2024.
- Bin Yan, Mingtao Pei, Meng Zhao, Caifeng Shan, and Zhaoxing Tian. Prior guided transformer for accurate radiology reports generation. *IEEE Journal of Biomedical and Health Informatics*, 26(11):5631–5640, 2022.
- Sixing Yan. Memory-aligned knowledge graph for clinically accurate radiology image report generation. In *Proceedings of the 21st Workshop on Biomedical Language Processing*, pages 116–122, 2022.
- Zhiling Yan, Kai Zhang, Rong Zhou, Lifang He, Xiang Li, and Lichao Sun. Multimodal chatgpt for medical applications: an experimental study of gpt-4v. *arXiv preprint arXiv:2310.19061*, 2023.
- Shaokang Yang, Jianwei Niu, Jiyan Wu, Yong Wang, Xuefeng Liu, and Qingfeng Li. Automatic ultrasound image report generation with adaptive multimodal attention mechanism. *Neurocomputing*, 427:40–49, 2021a.
- Shuxin Yang, Xian Wu, Shen Ge, S Kevin Zhou, and Li Xiao. Knowledge matters: Chest radiology report generation with general and specific knowledge. *Medical Image Analysis*, 80:102510, 2022.
- Shuxin Yang, Xian Wu, Shen Ge, Zhuozhao Zheng, S Kevin Zhou, and Li Xiao. Radiology report generation with a learned knowledge base and multi-modal alignment. *Medical Image Analysis*, 86:102798, 2023.
- Yan Yang, Jun Yu, Jian Zhang, Weidong Han, Hanliang Jiang, and Qingming Huang. Joint embedding of deep visual and semantic features for medical image report generation. *IEEE Transactions on Multimedia*, 2021b.
- Di You, Fenglin Liu, Shen Ge, Xiaoxia Xie, Jing Zhang, and Xian Wu. Aligntransformer: Hierarchical alignment of visual regions and disease tags for medical report generation. In *Medical Image Computing and Computer Assisted Intervention–MICCAI 2021: 24th International Conference, Strasbourg, France, September 27–October 1, 2021, Proceedings, Part III 24*, pages 72–82. Springer, 2021.
- Jingyi You, Dongyuan Li, Manabu Okumura, and Kenji Suzuki. Jpg-jointly learn to align: Automated disease prediction and radiology report generation. In *Proceedings of the 29th International Conference on Computational Linguistics*, pages 5989–6001, 2022.
- Junsan Zhang, Xiuxuan Shen, Shaohua Wan, Sotirios K Goudos, Jie Wu, Ming Cheng, and Weishan Zhang. A novel deep learning model for medical report generation by inter-intra information calibration. *IEEE Journal of Biomedical and Health Informatics*, 2023a.
- Kai Zhang, Rong Zhou, Eashan Adhikarla, Zhiling Yan, Yixin Liu, Jun Yu, Zhengliang Liu, Xun Chen, Brian D Davison, Hui Ren, et al. A generalist vision–language foundation model for diverse biomedical tasks. *Nature Medicine*, pages 1–13, 2024a.
- Ke Zhang, Hanliang Jiang, Jian Zhang, Qingming Huang, Jianping Fan, Jun Yu, and Weidong Han. Semi-supervised medical report generation via graph-guided hybrid feature consistency. *IEEE Transactions on Multimedia*, 2023b.
- Sheng Zhang, Yanbo Xu, Naoto Usuyama, Jaspreet Bagga, Robert Tinn, Sam Preston, Rajesh Rao, Mu Wei, Naveen Valluri, Cliff Wong, et al. Large-scale domain-specific pretraining for biomedical vision-language processing. *arXiv preprint arXiv:2303.00915*, 2(3):6, 2023c.
- Tianyi Zhang, Varsha Kishore, Felix Wu, Kilian Q Weinberger, and Yoav Artzi. Bertscore: Evaluating text generation with bert. In *International Conference on Learning Representations*, 2019.
- Xiaoman Zhang, Hong-Yu Zhou, Xiaoli Yang, Oishi Banerjee, Julián N Acosta, Josh Miller, Ouwen Huang, and Pranav Rajpurkar. Rexrank: A public leaderboard for ai-powered radiology report generation. *arXiv preprint arXiv:2411.15122*, 2024b.

- Yixiao Zhang, Xiaosong Wang, Ziyue Xu, Qihang Yu, Alan Yuille, and Daguang Xu. When radiology report generation meets knowledge graph. In *Proceedings of the AAAI Conference on Artificial Intelligence*, volume 34, pages 12910–12917, 2020.
- Yong Zhang, Weihua Ou, Jiacheng Zhang, and Jiaxin Deng. Category supervised cross-modal hashing retrieval for chest x-ray and radiology reports. *Computers & Electrical Engineering*, 98:107673, 2022.
- Bolei Zhou, Aditya Khosla, Agata Lapedriza, Aude Oliva, and Antonio Torralba. Learning deep features for discriminative localization. In *Proceedings of the IEEE conference on computer vision and pattern recognition*, pages 2921–2929, 2016.
- Hong-Yu Zhou, Subathra Adithan, Julián Nicolás Acosta, Eric J. Topol, and Pranav Rajpurkar. A generalist learner for multifaceted medical image interpretation, 2024. URL <https://arxiv.org/abs/2405.07988>.
- Yi Zhou, Lei Huang, Tao Zhou, Huazhu Fu, and Ling Shao. Visual-textual attentive semantic consistency for medical report generation. In *Proceedings of the IEEE/CVF International Conference on Computer Vision*, pages 3985–3994, 2021.
- Jun-Yan Zhu, Taesung Park, Phillip Isola, and Alexei A Efros. Unpaired image-to-image translation using cycle-consistent adversarial networks. In *Proceedings of the IEEE international conference on computer vision*, pages 2223–2232, 2017.

Appendix A

Table A1: Summary of papers in the survey. The overview is based on the findings of the survey. The dataset and metrics section focuses on mainstream datasets and metrics. ‘-’ indicates that the paper either does not detail this process or does not include the key techniques summarized in this survey. The following abbreviations are used: I-Archi: the architecture of image feature learning, I-Module: the enhancement module of image feature learning, NI: the feature learning of non-image data, GEI: gastrointestinal endoscope image, RetiI: retinal image, Term: terminology, KnowB: knowledge base, RealR: real report, ClinicaI: clinical information, InsT: instructions, FreFilter: frequency-based filtering, ConAtoL: converting all tokens to lowercase, RemoNAT: removing non-alphabetic tokens, DenN: DenseNet, IncepV3: InceptionV3, EffNet: EfficientNet, TranF: Transformer, AT: auxiliary task, ContL: Contrastive learning, ContM: Contrastive module, Embed: general embedding techniques, MM: memory metric, GraA: graph attention, AttenT: attention, FeatO: feature-level operation, OptimS: optimization strategies, H-LSTM: hierarchical LSTM, ReLoss: re-weighted loss function, ReinL: reinforcement learning, R-L: Rouge-L, MET: METEOR, C-D: CIDEr-D, CE: clinical efficacy, R&T: retrieval-based and template-based techniques, RGF1: RadGraphF1, Com: comparison, Clas: classification, Escore: error scoring, ECI: extracting case-related information, IU: IU-Xray, MIMIC: MIMIC-CXR, ImaGeno: Chest ImaGenome, COV: COV-CTR, DeepEye: DeepEyeNet, CCT: COVID-19 CT, Ret-I: Retina ImBank, and Ret-C: Retina Chinese. In addition, AT-Graph, AT-Class, AT-EC, and AT-DS mean the graph-based, classification, embedding comparison, and detection/segmentation auxiliary tasks.

Paper	Input Data	Data Preparation	Feature Learning					Feature Fusion	Generation			Datasets	Metrics
			Image			Non-image			Decoder-based method		R&T		
			Archi	A_L	E_M	Archi	E_M		Archi	T_S			
Traditional deep learning methods													
Liu et al. [2021b]	Chest X-ray, Term, RealR	Tokenizing, ConAtoL, RemoNAT, FreFilter	ResNet	AT-Graph	-	Embed, TranF	-	FeatO	TranF	-	-	IU, MIMIC	BLEU, R-L, MET, C-D
Liu et al. [2021d]	Chest X-ray	-	ResNet	AT-Graph	-	-	-	-	TranF	-	-	IU, MIMIC	BLEU, R-L, MET, CE, Com
Liu et al. [2021a]	Chest X-ray	Tokenizing, ConAtoL, RemoNAT	CNNs	-	-	-	-	-	LSTMs	Curriculum learning	-	IU, MIMIC	BLEU, R-L, MET, Com
Chen et al. [2021]	Chest X-ray	-	ResNet+TranF	-	-	-	-	MM	TranF	-	-	IU, MIMIC	BLEU, R-L, MET, CE
You et al. [2021]	Chest X-ray	-	ResNet	-	-	-	-	AttenT	TranF	-	-	IU, MIMIC	BLEU, R-L, MET, Com
Miura et al. [2021]	Chest X-ray	-	DenN+TranF	-	-	-	-	-	TranF	ReinL	-	MIMIC	BLEU, C-D, CE, Com
Alfargha et al. [2021]	Chest X-ray	Resizing	DenN	AT-Class	-	-	-	AttenT	TranF	-	-	IU	BLEU, R-L, MET, C-D, Clas
Yang et al. [2021b]	Chest X-ray	-	ResNet	AT-EC	-	-	-	-	H-LSTM	-	-	IU, MIMIC	BLEU, R-L, C-D
Pahwa et al. [2021]	Chest X-ray	Resizing, Cropping, Flipping	HRNet+TranF	-	-	-	-	-	R2Gen	-	-	IU	BLEU, R-L, MET
Zhou et al. [2021]	Chest X-ray, ClinicaI	Tokenizing, FreFilter	DenN	AT-Class, AT-EC	-	One-hot, Embed	-	AttenT	H-LSTM	-	-	IU, MIMIC	BLEU, R-L, MET, C-D, nKTD

Continued on next page

Table A1 – continued from previous page

Paper	Input Data	Data Preparation	Feature Learning					Feature Fusion	Generation			Datasets	Metrics
			Archi	Image		Non-image			Decoder-based method		R&T		
				A_L	E_M	Archi	E_M		Archi	T_S			
Huang et al. [2021b]	Retil, Term	–	CNNs	–	–	Embed	–	FeatO	LSTM	–	–	DeepEye	BLEU, R-L, C-D
Han et al. [2021]	Spine MRI	–	Self-design	AT-DS	–	–	–	–	Reasoning	–	–	–	–
Liu et al. [2021e]	Chest X-ray, Chest CT, Term	–	DenN	AT-Class	–	Embed, BERT	–	FeatO, AttenT	TranF	AT	–	CCT	BLEU, R-L, C-D, Com
Wang et al. [2021]	Chest X-ray, Chest CT	Tokenizing	ResNet+TranF	AT-EC	–	–	–	–	H-LSTM	AT	–	IU, COV	BLEU, R-L, C-D
Endo et al. [2021]	Chest X-ray	–	ResNet	–	–	–	–	–	–	–	R	MIMIC	BLEU, <i>S_{emb}</i> , CE
Najdenko et al. [2021]	Chest X-ray	Resizing, Tokenizing, ConAtoL, RemoNAT, FreFilter	DenN+TranF	AT-EC	–	–	–	–	LSTM	–	–	IU, MIMIC	BLEU, R-L, MET, CE
Yang et al. [2021a]	Breast ultrasound	Tokenizing, FreFilter	ResNet	AT-Class	–	–	–	FeatO	LSTM	–	–	BCD2018	BLEU, R-L, MET, C-D
Pandey et al. [2021]	Chest X-ray	Resizing	VGG	–	–	–	–	–	H-LSTM	AT	–	IU	BLEU, R-L
Hou et al. [2021b]	Chest X-ray	Resizing, Tokenizing, FreFilter	ResNet	AT-Class	–	–	–	AttenT	H-LSTM	ReinL	–	IU, MIMIC	BLEU, R-L, MET, C-D, CE
Pino et al. [2021]	Chest X-ray	–	DenN	–	–	–	–	–	–	–	T	IU, MIMIC	BLEU, R-L, C-D, CE, MIRQI
Liu et al. [2021c]	Chest X-ray	Tokenizing, ConAtoL, FreFilter	ResNet	–	ContM	–	–	–	H-LSTM	–	–	IU, MIMIC	BLEU, R-L, MET, CE, Com
Jia et al. [2021]	Chest X-ray	–	ResNet+TranF	–	–	–	–	–	TranF	–	–	IU, MIMIC	BLEU, R-L
Hou et al. [2021a]	Chest X-ray	Resizing, Data augmentation	DenN	–	–	–	–	–	TranF	–	–	MIMIC	BLEU, R-L, MET, CE
Huang et al. [2021a]	Retil, Term	Tokenizing, ConAtoL, RemoNAT, FreFilter	CNNs	–	–	Embed	–	LSTM	LSTM	–	–	DeepEye	BLEU, R-L, C-D

Continued on next page

Table A1 – continued from previous page

Paper	Input Data	Data Preparation	Feature Learning					Feature Fusion	Generation			Datasets	Metrics
			Image			Non-image			Decoder-based method		R&T		
			Archi	A_L	E_M	Archi	E_M		Archi	T_S			
Babar et al. [2021a]	Chest X-ray	Tokenizing, ConAtoL, RemoNAT	–	–	–	–	–	–	Unconditional generation			IU, MIMIC	BLEU, R-L, MET, C-D, CE
Singh et al. [2021]	Chest X-ray	Resizing, Tokenizing, ConAtoL, RemoNAT, FreFilter	IncepV3	AT-Class	–	–	–	–	LSTM	–	–	IU, MIMIC	BLEU, R-L, MET, C-D
Yang et al. [2022]	Chest X-ray, KnowB, RealR	Resizing, Tokenizing, ConAtoL, FreFilter, ECI	ResNet	–	–	Embed, RotatE, BERT	–	AttenT	TranF	–	–	IU, MIMIC	BLEU, R-L, C-D, CE
Ramesh et al. [2022]	Chest X-ray	Tokenizing, Filtering	ResNet/TranF	–	–	–	–	–	–	–	R	MIMIC	S_{emb} , RGF1
Sirshar et al. [2022]	Chest X-ray	Tokenizing, RemoNAT, ConAtoL	VGG	–	–	–	–	–	LSTM	–	–	IU, MIMIC	BLEU
Najdenkov et al. [2022]	Chest X-ray	Resizing, RemoNAT, FreFilter	DenN+TranF	AT-EC	–	–	–	–	TranF, LSTM	–	–	IU, MIMIC	BLEU, R-L, MET, %Novel, CE
Wang et al. [2022e]	Chest X-ray	Cropping, Tokenizing, ConAtoL, FreFilter	DenN	AT-Graph	–	–	–	–	H-LSTM	–	–	IU	BLEU, R-L, C-D
Li et al. [2022b]	Retil	Resizing, Tokenizing, ConAtoL, FreFilter	I3D+TranF	AT-Graph	–	–	–	–	TranF	–	–	FFA-IR	BLEU, R-L, MET, C-D, Com
Qin and Song [2022]	Chest X-ray	–	ResNet+TranF	–	–	–	–	MM	TranF	ReinL	–	IU, MIMIC	BLEU, R-L, MET, CE, Com
Wang et al. [2022a]	Chest X-ray	Resizing, Cropping	ResNet+TranF	ContL	–	–	–	MM	TranF	–	–	IU, MIMIC	BLEU, R-L, MET, C-D
Cao et al. [2022]	Chest X-ray, GEI, Term	–	DenN+TranF	AT-Graph	–	Embed, BERT	–	FeatO, AttenT	TranF	–	–	IU	BLEU, R-L, C-D, Com
Mohsan et al. [2022]	Chest X-ray	Tokenizing, ConAtoL	TranF	–	–	–	–	–	TranF	–	–	IU	BLEU, R-L, MET, C-D
Yan [2022]	Chest X-ray	–	DenN+TranF	AT-Graph	MM	–	–	–	TranF	–	–	IU, MIMIC	BLEU, R-L, MET, C-D, CE, MIRQI

Continued on next page

Table A1 – continued from previous page

Paper	Input Data	Data Preparation	Feature Learning					Feature Fusion	Generation			Datasets	Metrics
			Image		Non-image		Decoder-based method		R&T				
			Archi	A_L	E_M	Archi	E_M			Archi	T_S		
Li et al. [2022a]	Chest X-ray	–	ResNet+TranF	AT-Class	–	–	–	–	TranF	AT	–	IU	BLEU, R-L, MET
Sun et al. [2022]	Retil	Resizing	ResNet+ Faster-RCNN	AT-EC, AT-DS	–	–	–	–	TranF	–	–	FFA-IR	BLEU, R-L, MET, C-D
You et al. [2022]	Chest X-ray	Tokenizing, ConAtoL, RemoNAT	ResNet+TranF	AT-Class	–	–	–	AttenT, MM	TranF	–	–	IU	BLEU, R-L, MET
Wang et al. [2022d]	Chest X-ray	Resizing	TranF	AT-Class, AT-EC	–	–	–	–	TranF	ReLoss	–	IU, MIMIC	BLEU, R-L, C-D
Lee et al. [2022]	Chest X-ray	Resizing, Cropping, Flipping	ResNet+TranF	–	–	–	–	–	R2Gen	–	–	IU	BLEU, R-L, MET
Moon et al. [2022]	Chest X-ray	Resizing, Cropping, Tokenizing	ResNet+TranF	AT	–	–	–	–	TranF	–	–	IU, MIMIC	BLEU, CE
Huang et al. [2022]	Retil, Term	Resizing, Tokenizing, ConAtoL, RemoNAT, FreFilter	CNNs	–	–	Embed	–	AttenT	LSTM	–	–	DeepEye	BLEU, R-L, C-D
Kaur and Mittal [2022a]	Chest X-ray	Resizing, Convert image to grayscale, Flipping, Tokenizing, ConAtoL, RemoNAT	VGG	–	–	–	–	–	H-LSTM	–	–	IU	BLEU, R-L, C-D
Song et al. [2022]	Chest X-ray, RealR	–	DenN	–	ContM	–	–	FeatO, AttenT	TranF	–	–	IU, MIMIC	BLEU, R-L, MET, CE
Jia et al. [2022]	Chest X-ray	–	DenN	–	–	–	–	AttenT	H-LSTM	–	–	IU, MIMIC	BLEU, R-L
Zhang et al. [2022]	Chest X-ray	Resizing	VGG	–	–	–	–	–	–	–	R	MIMIC	Precision
Dalla Se et al. [2022]	Chest X-ray, ClinicalI	Tokenizing, Resizing, Flipping, Rotation, Cropping	ResNet+TranF	AT-Graph	–	Embed	–	AttenT	TranF	–	–	MIMIC	BLEU, R-L, MET, CE, Com
Yan et al. [2022]	Chest X-ray	Tokenizing, ConAtoL, FreFilter	ResNet+TranF	AT	–	–	–	AttenT	TranF	–	–	IU, MIMIC	BLEU, R-L, MET, C-D, CE

Continued on next page

Table A1 – continued from previous page

Paper	Input Data	Data Preparation	Feature Learning					Feature Fusion	Generation			Datasets	Metrics
			Image		Non-image		Decoder-based method		R&T				
			Archi	A_L	E_M	Archi	E_M			Archi	T_S		
Gajbhay et al. [2022]	Chest X-ray	Tokenizing, Removing irrelevant elements, ConAtoL, FreFilter	DenN	AT-Class	-	-	-	-	LSTM	ReLoss	-	IU	BLEU, R-L, MET, C-D
Wang et al. [2022b]	Chest X-ray	Grouping	ResNet+TranF	AT-Class	-	-	-	-	R2Gen	-	-	IU, MIMIC	BLEU, R-L, MET
Abela et al. [2022]	Chest X-ray	-	DenN	-	-	-	-	-	-	-	T	MIMIC	BLEU, CE
Wu et al. [2022]	Chest X-ray	-	ResNet	ContL	-	-	-	-	LSTM	-	-	IU, MIMIC	BLEU, R-L, MET, C-D
Tanwani et al. [2022]	Chest X-ray, InsT	Resizing, Image transformations, Tokenizing	ResNet+TranF	AT-Class, ContL	-	Embed, BERT	-	AttenT	TranF	-	-	IU	BLEU
Chen et al. [2022]	Chest X-ray	Resizing, Tokenizing, ConAtoL, RemoNAT	ResNet+TranF	AT-EC	MM	-	-	-	R2Gen	-	-	IU	BLEU, R-L, MET
Kong et al. [2022]	Chest X-ray	Resizing	TranF	-	-	-	-	-	-	-	R	IU, MIMIC	BLEU, R-L, MET, CE
Wang et al. [2022e]	Chest X-ray	Tokenizing, ConAtoL, RemoNAT, FreFilter	TranF	AT-Class, ContL	-	-	-	FeatO	TranF	-	-	MIMIC	BLEU, R-L, MET, C-D
Du et al. [2022]	Chest X-ray	-	ResNet	AT-Class	-	-	-	-	H-LSTM	-	-	IU	BLEU, R-L, MET
Kaur and Mittal [2022b]	Chest X-ray	Resizing, Tokenizing, ConAtoL, RemoNAT, FreFilter	VGG	AT-Class	-	-	-	FeatO	H-LSTM	ReinL	-	IU	BLEU, R-L, C-D
Tanida et al. [2023]	Chest X-ray	Resizing, Removing redundant whitespaces	ResNet+TranF	AT-DS	-	-	-	-	TranF	-	-	MIMIC, ImaGeno	BLEU, R-L, MET, C-D, CE
Wang et al. [2023d]	Chest X-ray	Tokenizing	TranF	AT	-	-	-	-	TranF	-	-	IU, MIMIC	BLEU, R-L, MET, C-D, CE
Li et al. [2023c]	Chest X-ray, Chest CT	Resizing, Tokenizing, FreFilter	DenN	AT-Graph	-	-	-	AttenT	TranF	-	-	IU, COV	BLEU, R-L, C-D, Com

Continued on next page

Table A1 – continued from previous page

Paper	Input Data	Data Preparation	Feature Learning					Feature Fusion	Generation			Datasets	Metrics
			Image		Non-image		Decoder-based method		R&T				
			Archi	A_L	E_M	Archi	E_M			Archi	T_S		
Wu et al. [2023b]	Chest X-ray	Tokenizing, ConAtoL, Removing irrelevant elements, FreFilter	ResNet+TranF	-	-	-	-	-	TranF	ReinL, AT	-	IU, MIMIC	BLEU, R-L, MET
Li et al. [2023b]	Chest X-ray, KnowB, RealR	Tokenizing, ECI	TranF	AT-Class, ContL	-	Embed, BERT	GraA	AttenT	TranF	-	-	IU, MIMIC	BLEU, R-L, MET, C-D, CE
Huang et al. [2023]	Chest X-ray, KnowB	Tokenizing, ConAtoL, RemoNAT, FreFilter, ECI	ResNet+TranF	-	-	Embed, BERT	GraA	FeatO, AttenT	TranF	-	-	IU, MIMIC	BLEU, R-L, MET, CE
Zhang et al. [2023b]	Chest X-ray	-	DenN+TranF	AT-Graph, AT-Class, AT-EC	-	-	-	-	TranF	AT	-	IU, MIMIC	BLEU, R-L, MET, CE
Xu et al. [2023]	Chest X-ray, Dermoscopy, KnowB	ECI	DenN+TranF	AT-Class	-	Embed, BERT	GraA	AttenT	R2Gen	-	-	IU	BLEU, R-L, MET, Com
Yang et al. [2023]	Chest X-ray, KnowB	Resizing, Tokenizing, ConAtoL, FreFilter	ResNet	AT-Class, AT-EC	-	-	-	AttenT	TranF	-	-	IU, MIMIC	BLEU, C-D, CE
Zhang et al. [2023a]	Chest X-ray, Chest CT	Resizing	ResNet+TranF	-	-	-	-	-	TranF+MM	-	-	IU, MIMIC, COV	BLEU, R-L, MET
Wang et al. [2023a]	Chest X-ray	-	ResNet+TranF	AT-Class, AT-DS	-	-	-	-	R2Gen+LLM	-	-	MIMIC	CE
Lin et al. [2023]	Chest X-ray, Retil	Resizing, Tokenizing, FreFilter	ResNet+TranF	ContL	-	-	-	-	TranF	-	-	IU, MIMIC, Ret-I, Ret-C	BLEU, R-L, MET
Selivanov et al. [2023]	Chest X-ray	Resizing, Tokenizing, ConAtoL, RemoNAT	DenN	-	-	-	-	-	TranF	-	-	IU, MIMIC	BLEU, R-L, C-D, CE
Cao et al. [2023]	Chest X-ray, GEI, Term	-	DenN+TranF	-	-	Embed, BERT	-	FeatO, AttenT, MM	TranF	-	-	IU, MIMIC	BLEU, R-L, MET, C-D
Shetty et al. [2023]	Chest X-ray	-	Self-design	-	-	-	-	-	LSTM	-	-	IU	BLEU
Wang et al. [2023c]	Chest X-ray	-	ResNet+ Faster-RCNN+TranF	-	-	-	-	-	R2Gen	-	-	IU, MIMIC, ImaGeno	BLEU, R-L, MET

Continued on next page

Table A1 – continued from previous page

Paper	Input Data	Data Preparation	Feature Learning						Feature Fusion	Generation			Datasets	Metrics
			Image			Non-image				Decoder-based method		R&T		
			Archi	A_L	E_M	Archi	E_M	Archi		T_S				
Li et al. [2023e]	Chest X-ray	Resizing, Cropping, Tokenizing, FreFilter, ConAtoL, RemoNAT	TranF	-	-	-	-	MM +Self-design	TranF	AT	-	IU, MIMIC	BLEU, R-L, MET, C-D	
Liu et al. [2023c]	Chest X-ray, Term, RealR	FreFilter, ConAtoL	DenN	ContL	-	Embed, TranF	-	FeatO, AttenT	TranF	-	-	IU, MIMIC	BLEU, R-L, MET	
Wang et al. [2023b]	Chest X-ray	-	ResNet+TranF	ContL	-	-	-	-	R2Gen	-	-	IU, MIMIC	BLEU, R-L, MET, C-D	
Pellegrin et al. [2023a]	Chest X-ray, InsT	-	EffNet	-	-	Embed, BERT	-	AttenT	Classification for structural report generation			Rad-ReStruct	CE	
Dalla Secchi et al. [2023a]	Chest X-ray, ClinicalI	Resizing, Cropping, Grouping	ResNet+ Faster-RCNN	AT-DS	-	Embed	-	AttenT	TranF	-	-	MIMIC, ImaGeno	BLEU, R-L, MET, CE	
Li et al. [2023d]	Chest X-ray, RealR, Term	Resizing, ECI	ResNet+TranF	-	-	Embed, BERT	Rewei-ghting	AttenT	TranF	-	-	IU, MIMIC	BLEU, R-L, MET, C-D	
Dalla Secchi et al. [2023b]	Chest X-ray, ClinicalI	Resizing, Cropping	ResNet+ Faster-RCNN	AT-DS, AT-Graph	-	Embed	-	AttenT	TranF	-	-	MIMIC, ImaGeno	BLEU, R-L, MET, CE	
Hou et al. [2023]	Chest X-ray	-	ResNet+TranF	AT-Class	-	-	-	-	TranF	-	-	IU, MIMIC	BLEU, R-L, MET, CE	
Jeong et al. [2024]	Chest X-ray	Resizing	TranF	-	-	-	-	-	-	-	R	MIMIC	BLEU, EScore, RGF1	
Gu et al. [2024]	Chest X-ray, Term	Resizing, Cropping, Flipping, FreFilter, RemoNAT	ResNet	AT-DS, AT	-	Embed, TranF	-	FeatO, AttenT	TranF	ReinL	-	IU, MIMIC	BLEU, R-L, MET, CE	
Wang et al. [2024b]	Chest X-ray, Chest CT	-	ResNet+TranF	AT	-	-	-	-	TranF	ReLoss	-	IU, COV	BLEU, R-L, MET, Grading	
Xue et al. [2024]	Chest X-ray, Term	-	ResNet+TranF	-	-	Embed, TranF	-	FeatO, AttenT	TranF	-	-	IU, MIMIC	BLEU, R-L, MET	
Wang et al. [2024a]	Chest X-ray	Resizing, Cropping	DenN+TranF	AT-Class	-	-	-	-	R2Gen	AT	-	IU, MIMIC	BLEU, R-L, MET, C-D, CE	
Jin et al. [2024]	Chest X-ray, RealR	-	ResNet	AT-Class	-	Embed, TranF	-	FeatO, AttenT	TranF	-	-	IU, MIMIC	BLEU, R-L, MET, CE	
Large model-based methods														
Continued on next page														

Table A1 – continued from previous page

Paper	Input Data	Data Preparation	Feature Learning					Feature Fusion	Generation			Datasets	Metrics
			Image			Non-image			Decoder-based method		R&T		
			Archi	A_L	E_M	Archi	E_M		Archi	T_S			
Pellegrini et al. [2023b]	Chest X-ray, InsT	–	ResNet+TranF	–	–	Embed	–	FeatO, AttenT	TranF	–	–	MIMIC	BLEU, R-L, MET, CE
Lee et al. [2023]	Chest X-ray, InsT	–	CNNs	–	–	Embed	–	FeatO, AttenT	TranF	–	–	MIMIC	BLEU, R-L, MET, C-D, CE
Wang et al. [2023e]	Chest X-ray, InsT	–	TranF	–	–	Embed	–	FeatO, AttenT	TranF	–	–	IU, MIMIC	BLEU, R-L, MET, C-D, CE
Hyland et al. [2023]	Chest X-ray, InsT, ClinicalI	–	TranF	–	–	Embed	–	FeatO, AttenT	TranF	–	–	MIMIC	BLEU, R-L, MET, CE, RGF1
Bannur et al. [2024]	Chest X-ray, InsT, ClinicalI, RealR	–	TranF	–	–	Embed	–	FeatO, AttenT	TranF	–	–	IU, MIMIC	BLEU, R-L, MET, CE, RGF1
Chen et al. [2024]	Chest X-ray, InsT	–	TranF	–	–	Embed	–	FeatO, AttenT	TranF	–	–	MIMIC	RG-based, GPT-4-based, Grading
Guo et al. [2024]	Ultrasound, InsT	–	TranF	–	–	Embed	–	FeatO, AttenT	TranF	–	–	–	–
Zhang et al. [2024a]	Chest X-ray, InsT	–	ResNet	–	–	Embed	–	FeatO, AttenT	TranF	–	–	IU, MIMIC	Human-based evaluation
Li et al. [2024]	Chest X-ray, InsT	–	TranF	–	–	Embed	–	FeatO, AttenT	TranF	–	–	–	GPT-4-based
Alkhalidi et al. [2024]	Chest X-ray, InsT	–	TranF	–	–	Embed	–	FeatO, AttenT	TranF	–	–	MIMIC	–
Wu et al. [2023a]	Chest X-ray, InsT	–	TranF	–	–	Embed	–	FeatO, AttenT	TranF	–	–	IU, MIMIC	BLEU, R-L, CE
Zhou et al. [2024]	Chest X-ray, InsT	–	TranF	–	–	Embed	–	FeatO, AttenT	TranF	–	–	IU, MIMIC	BLEU, CE, RGF

Table A2: Comparisons of the model performance on the MIMIC-CXR Dataset. B1, B2, B3, B4, R-L, C-D, P, R, and F represent BLEU-1, BLEU-2, BLEU-3, BLEU-4, ROUGE-L, CIDEr-D, precision, recall, and F1 score, respectively. **The best** and **second best** results are highlighted. All values were extracted from their papers. * means large model-based methods.

Paper	B1↑	B2↑	B3↑	B4↑	R-L↑	METEOR↑	C-D↑	P↑	R↑	F↑
Findings Section										
Chen et al. [2021]	0.353	0.218	0.148	0.106	0.278	0.142	-	0.334	0.275	0.278
Pino et al. [2021]	-	-	-	-	0.185	-	0.238	0.381	0.531	0.428
Song et al. [2022]	0.360	0.227	0.156	0.117	0.287	0.148	-	0.444	0.297	0.356
Pellegrini et al. [2023b]*	0.346	-	-	0.095	0.271	0.140	-	-	-	0.394
Hyland et al. [2023]*	0.392	-	-	0.142	0.289	0.333	-	-	-	0.386
Zhou et al. [2024]*	-	-	-	0.178	-	-	-	-	-	-
Bannur et al. [2024] 7B*	0.465	-	-	0.234	0.384	0.419	-	-	-	0.427
Bannur et al. [2024] 13B*	0.479	-	-	0.243	0.391	0.430	-	-	-	0.439
Impression + Findings Section										
Wu et al. [2022]	0.340	0.212	0.145	0.103	0.270	0.139	0.109	-	-	-
Wang et al. [2022d]	0.351	0.223	0.157	0.118	0.287	-	0.281	-	-	-
Jia et al. [2022]	0.363	0.228	0.156	0.130	0.300	-	-	-	-	-
Wang et al. [2023e]*	0.411	0.267	0.186	0.134	0.297	0.160	0.269	0.392	0.387	0.389
Zhou et al. [2024]*	-	-	-	0.160	-	-	-	-	-	-
Unspecified generated sections										
Lee et al. [2023]*	0.092	0.046	0.026	0.015	0.162	0.069	0.525	-	-	0.211
Wu et al. [2023a]*	0.128	-	-	-	-	-	-	-	-	-
Liu et al. [2021a]	0.344	0.217	0.140	0.097	0.218	0.133	-	-	-	-
Liu et al. [2021c]	0.350	0.219	0.152	0.109	0.283	0.151	-	0.352	0.298	0.303
Liu et al. [2021b]	0.360	0.224	0.149	0.106	0.284	0.149	-	-	-	-
Li et al. [2023d]	0.360	0.231	0.162	0.119	0.298	0.153	0.217	-	-	-
Lin et al. [2023]	0.362	0.227	0.155	0.113	0.283	0.142	-	-	-	-
Zhang et al. [2023b]	0.362	0.229	0.157	0.113	0.284	0.153	-	0.380	0.342	0.335
Yang et al. [2022]	0.363	0.228	0.156	0.115	0.284	-	0.203	0.458	0.348	0.371
Wang et al. [2023c]	0.363	0.235	0.164	0.118	0.301	0.136	-	-	-	-
Liu et al. [2021d]	0.369	0.231	0.156	0.118	0.295	0.153	-	0.389	0.362	0.355
Xue et al. [2024]	0.372	0.233	0.154	0.112	0.286	0.152	-	-	-	-
Wang et al. [2024a]	0.374	0.230	0.155	0.112	0.279	0.145	0.161	0.483	0.323	0.387
Zhang et al. [2023a]	0.376	0.233	0.157	0.113	0.276	0.144	-	-	-	-
You et al. [2021]	0.378	0.235	0.156	0.112	0.283	0.158	-	-	-	-
Qin and Song [2022]	0.381	0.232	0.155	0.109	0.287	0.151	-	0.342	0.294	0.292
Wu et al. [2023b]	0.383	0.224	0.146	0.104	0.280	0.147	-	-	-	0.758
Yang et al. [2023]	0.386	0.237	0.157	0.111	0.274	-	0.111	0.420	0.339	0.352
Wang et al. [2023b]	-	-	-	0.119	0.286	0.158	0.259	-	-	-
Wang et al. [2023d]	0.386	0.250	0.169	0.124	0.291	0.152	0.362	0.364	0.309	0.311
Liu et al. [2023c]	0.391	0.249	0.172	0.125	0.304	0.160	-	-	-	-
Huang et al. [2023]	0.393	0.243	0.159	0.113	0.285	0.160	-	0.371	0.318	0.321
Wang et al. [2022b]	0.395	0.253	0.170	0.121	0.284	0.147	-	-	-	-
Jin et al. [2024]	0.398	-	-	0.112	0.268	0.157	-	0.501	0.509	0.476
Hou et al. [2023]	0.407	0.256	0.172	0.123	0.293	0.162	-	0.416	0.418	0.385
Wang et al. [2022e]	0.413	0.266	0.186	0.136	0.298	0.170	0.429	-	-	-
Kong et al. [2022]	0.423	0.261	0.171	0.116	0.286	0.168	-	0.482	0.563	0.519